



Design, Fabrication and Preliminary Uncertainty Analysis of a Primary Humidity Measurement Standard

By B.Sc. (Hons) Conor FitzGerald (C.F)

A thesis submitted to Dublin City University for the
degree of Master of Science in the School of Physical
Sciences

Under the supervision of,

Dr. Paul Swift, Dublin City University

Mr. Dubhaltach Mac Lochlainn, National Standards Authority of Ireland

July 2019

Declaration of Authorship

I hereby certify that this material, which I now submit for assessment on the programme of study leading to the award of MSc. is entirely my own work, and that I have exercised reasonable care to ensure that the work is original, and does not to the best of my knowledge breach any law of copyright, and has not been taken from the work of others save and to the extent that such work has been cited and acknowledged within the text of my work.

Signed:

I.D. Number: 16213344

Date:

Acknowledgments

I would like to acknowledge the DCU engineering department, particularly Dean McLoughlin for the work performed in the machining of the final saturator of the new NML dew point generator. A&A Engineering Ltd. particularly Peter Anderson for the work done in fabricating the pre-saturator and humidifier of the new generator. Dairytube Engineering Ltd. particularly Norman Shekleton for the fabrication of the heat-exchanger used in the generator. Willowchem Ireland Ltd. particularly Billy Curtain for the welding and electropolishing performed on the lid of the final saturator. Silchrome Plating Ltd. particularly Austen Thwaite, for the finishing of the final saturator base. I would also like to thank all the firms mentioned for the advice and guidance given based on their many years of experience, without which this work would not be possible.

This project was in part thanks to the European Metrology Programme for Innovation and Research (EMPIR) for their funding of the HUMEA project (no. 15RPT03) which among other things, aims to improve capabilities in the field of dew point measurements and which NSAI is a partner in. I would like to thank the Institute of Metrology of Bosnia and Herzegovina (IMBiH) and the University of Ljubljana, Laboratory of Metrology and Quality (LMK) who are also partners in the HUMEA project, for hosting training workshops where I gained knowledge from experts in the field of primary humidity metrology. I would particularly like to thank Nedžadeta Hodžić for coordinating the project, Slaven Ranogajec for his advice on multiple occasions and Radek Strnad for travelling to our laboratory in Ireland to advise on the operation and validation of our system.

I would like to thank Stephanie Bell of the National Physical Laboratory (NPL) in London, for meeting with me and giving me detailed information about their humidity metrology facilities and research currently being undertaken in the humidity section of NPL as well as answering my questions and discussing my proposed design. I would also like to thank MBW calibration for organising a technical visit giving me information on their operations and ongoing research, a detailed tour of their facilities for production and calibrations, and for answering my questions regarding uncertainty analysis and MBW equipment. I would particularly like to thank Daniel Mutter, Sascha Wettstein and Robin Farley for their hospitality and advice.

I would especially like to thank Dubhaltach Mac Lochlainn and Paul Hetherington, managers at NML, for their invaluable support and for trusting me to complete this project and frequently advising me on aspects of the project as well as providing me with extensive training and the new equipment needed to complete the project. I would like to thank Dr. Paul Swift, my academic supervisor, for supervising my progress, providing guidance and supporting the

academic elements of this project as well as sourcing resources available through DCU. I would also like to thank Plunkett Cromwell for providing advice and training in humidity metrology and providing the humidity measurement equipment needed for the development of the new generator. I would also like to thank Sam Boles for providing the temperature measurement equipment needed to operate the generator and maintaining quality of the equipment as well as Duré Basit and Brian Malone who also maintained this system and shared the resources used by the laboratory.

Finally, I would like to thank my family and friends for supporting me throughout my studies and making my downtime never boring.

Contents

Declaration of Authorship.....	i
Acknowledgments.....	ii
Abstract.....	1
1. Introduction	2
2. Fundamentals of humidity measurement	5
2.1. Humidity as a quantity and its importance to industry	5
2.2. Description of humidity in relation to thermodynamics	6
2.3. Practical humidity measurement and empirical reference functions	10
2.4. Units of mass flow.....	14
2.5. Humidity instrumentation	15
3. Primary dew point generation	18
3.1. Overview	18
3.2. Types of dew point generators	19
3.2.1. Single pressure (1-P) generator	19
3.2.2. Two pressure (2-P) generator	24
3.2.3. Divided flow generator	25
3.3. Primary dew point generator designs used in different NMIs.....	27
3.4. Theory	32
3.4.1. Calculating dew/frost point for a known pressure drop.....	32
3.4.2. Calculating dry air flow for a given output (wet air) flow	33
3.4.3. Calculating the pressure correction due to the difference in altitude of the final saturator and the digital pressure meter.....	35
4. Design and simulation of the new NML saturator	36
4.1. Overview	36
4.2. Calculations and modelling	38
4.2.1. Mass transport of H ₂ O, latent heat and rate of evaporation	38
4.2.2. Reynolds number	39
4.2.3. Rayleigh number	39
4.3. Simulations using Ansys	41
4.4. Brief description of the CFD models used.....	43
4.5. Design and simulation of final saturator.....	48
4.5.1. Spiral design	52
4.5.2. Square design.....	56
4.5.3. Circular design.....	58
4.5.4. Results of final saturator comparison.....	61
4.6. Design and simulation of pre-saturator.....	62

4.6.1.	Spiral pre-saturator	62
4.6.2.	Square pre-saturator	63
4.6.3.	Circular pre-saturator	65
4.6.4.	Results of pre-saturator comparison	67
4.7.	Final saturator flow rate range determination	68
5.	The new NML 1-P dew point generator	70
5.1.	Overview	70
5.2.	Humidifier	70
5.3.	Pre-saturator	72
5.4.	The heat exchanger	73
5.5.	Final saturator	77
5.6.	Full system	83
6.	Initial characterization	87
7.	Uncertainty analysis of the new NML primary dew point generator for the calibration of chilled mirror hygrometers	90
7.1.	Propagation of uncertainty	91
7.2.	Uncertainty due to formulations	92
7.3.	Saturator efficiency	93
7.4.	Adsorption and desorption effects	99
7.5.	Leaks	100
7.6.	Temperature conditioning in the outlet tube and hygrometer	101
7.7.	Repeatability of the generator and chilled mirror hygrometer	103
7.8.	Effect of varying the bath water level	104
7.9.	Water Contamination	105
7.10.	Other uncertainties related to the UUT	105
7.11.	Uncertainties relating to the measurement of the saturator temperature	106
7.11.1.	Standard deviation of the measured saturator temperature	106
7.11.2.	Calibration uncertainty of the PRT	106
7.11.3.	Repeatability and hysteresis of the PRT	106
7.11.4.	Drift of PRTs	107
7.11.5.	Uncertainty due to PRT self-heating	107
7.11.6.	Non-linearity of the resistance measurement bridge	108
7.11.7.	Resistance measurement bridge resolution	108
7.11.8.	Standard resistor calibration	108
7.11.9.	Standard resistor drift	108
7.11.10.	Standard resistor temperature coefficient	109
7.11.11.	Temperature gradients in the final saturator	109

7.11.12.	Bath stability	109
7.12.	Uncertainty of the measured final saturator pressure	110
7.12.1.	Standard deviation of the measured final saturator pressure	110
7.12.2.	Tolerance of the pressure transducer	110
7.12.3.	Drift of the pressure transducer	111
7.12.4.	Hydrostatic head correction	111
7.12.5.	Resolution of the digital pressure meter	111
7.12.6.	Repeatability and hysteresis of the pressure transducer	111
7.12.7.	Pressure stability in the final saturator	112
7.13.	Uncertainty of the hygrometer measuring head pressure	112
7.13.1.	Standard deviation of the measured head pressure	113
7.13.2.	Tolerance associated with the calibration correction	113
7.13.3.	Drift associated with the calibration correction	113
7.13.4.	Drift of the integrated head pressure transducer	113
7.13.5.	Hydrostatic head pressure difference associated with the correction	113
7.13.6.	Resolution of the correction	114
7.13.7.	Resolution of the measured hygrometer head pressure	114
7.13.8.	Non-linearity, repeatability and hysteresis of the hygrometer head pressure transducer	114
7.13.9.	Temperature coefficient of the integrated transducer	115
7.13.10.	Stability of the hygrometer head pressure transducer	116
7.14.	The complete uncertainty budget	117
8.	Changes to the uncertainty budget at -40 °C frost point	119
8.1.	Saturation efficiency	120
8.2.	Adsorption and desorption	121
8.3.	Effect of varying the bath liquid level	121
8.4.	The effect of leaks	122
8.5.	Temperature conditioning in the outlet tube and hygrometer	123
8.6.	Effect of purging the pressure measurement tube	123
8.7.	UUT flow rate dependency	124
8.8.	UUT measuring head temperature dependency	125
8.9.	UUT repeatability	127
8.10.	Uncertainties relating to the measurement of the final saturator temperature .	127
8.11.	Uncertainties relating to the measurement of the final saturator pressure	128
8.12.	Uncertainties relating to the measurement of the UUT head pressure	128
8.13.	Full uncertainty budget at -40 °C fp	129
9.	Calibration of a chilled mirror hygrometer	131

10.	Conclusion and further work	133
11.	References	136

Abstract

Conor FitzGerald

Design, Fabrication and Preliminary Uncertainty Analysis of a Primary Humidity Measurement Standard

This thesis describes the design and implementation of a new primary humidity standard in the National Metrology Laboratory of Ireland. In this thesis the basic principles of humidity metrology and primary dew point generation are explained. A number of existing designs of primary humidity standards are discussed. Useful equations relating to humidity metrology and particularly humidity generation as a primary measurement standard are given and in some cases derived. Several new designs of the components of a primary humidity standard are proposed and the benefits of each design is compared based on theory, cost of fabrication and simulations using computational fluid dynamics. From this comparison the individual components are chosen, and the complete design is given. A new type of corrosion resistant plating that has previously not been used with other primary dew point generators was chosen and its merits are discussed. The design was fabricated, and a number of modifications were made in order to improve the performance of the generator based on initial testing of the system. Finally, a preliminary uncertainty budget was developed for the calibration of chilled mirror hygrometers using the new primary humidity standard. This uncertainty budget covers the range from $-40\text{ }^{\circ}\text{C}$ frost point (fp) to $90\text{ }^{\circ}\text{C}$ dew point (dp) and gives an uncertainty of $\pm 0.060\text{ }^{\circ}\text{C}$ fp at $-40\text{ }^{\circ}\text{C}$ fp and $\pm 0.038\text{ }^{\circ}\text{C}$ dp at $90\text{ }^{\circ}\text{C}$ dp both with a coverage interval of 95 %. A calibration of a chilled mirror hygrometer was performed, and the results are compared to the calibration results obtained at an external metrology laboratory. The results obtained at NML were found to agree with the external laboratory to within $\pm 0.009\text{ }^{\circ}\text{C}$ dew/frost point. Future work involving the generator is outlined.

1. Introduction

The National Standards Authority of Ireland (NSAI) is Ireland's official standards body. The NSAI works to improve the performance of Irish businesses by developing new standards and applying existing standards. The NSAI National Metrology Laboratory (NML) is a department within the NSAI that provides traceability to the International System of Units (SI) for Irish industry and science. The validity of the calibration certificates issued by the NML are internationally recognised by the International Committee for Weights and Measures (CIPM) Mutual Recognition Agreement (MRA). This ensures that the uncertainties of measurement published on certificates are within the Calibration and Measurement Capabilities (CMCs) of the NML and that the NML's calibration systems and CMCs are peer reviewed and approved by experts from other National Metrology Institutes (NMIs). This provides international equivalence of measurement standards in BIPM member states across the world.

A central role of NMIs is to maintain the seven base units from which all other units are derived. This involves maintaining the definition, realisation and dissemination of SI base units (as well as other SI units). Realisation refers to how the definition of the unit is brought about (or realised) in practice. Dissemination is how the definition of a unit is extended to science, industry and the general public. The seven SI base units are; the ampere, the candela, the kelvin, the kilogram, the metre, the mole and the second. Units such as the second and the metre are defined based on quantum phenomena. This makes their definitions repeatable throughout the universe and precise realizations are possible. Until recently the definition of the kilogram has been based on an artefact and the definition of the kelvin has been based on the triple point of water with a specified isotopic content. These definitions are less repeatable than those based on quantum phenomena as they are susceptible to physical changes in the material and rely on the make-up of the material being controlled and very well known. In 2018 the definitions of the kilogram and the kelvin were changed to define the units based on the Planck constant and the Boltzmann constant respectively.

All other SI units are derived from these seven base units. For example, humidity is the presence of water vapour in air, so it can be measured as moles water vapour with respect to moles air, moles vapour with respect to total volume (traceable via the mole and the metre) or mass of vapour to mass of dry air (traceable via the kilogram). As will be discussed, humidity can also be measured in terms of dew point temperature (the temperature at which the air is saturated with water vapour). The dew point depends on the water vapour mole content and pressure of the gas being measured. If the pressure and dew point are known, then the mole fraction of water vapour with respect to dry air can be calculated. Therefore, humidity can be

traceable to the SI via the kelvin and the pascal, or equivalently; the kelvin, the kilogram, the meter and the second.

Not all NMIs are as involved in maintaining the definitions of fundamental units. Many, including the NML, are focused on the practical dissemination of the units to industry allowing companies to achieve the measurement accuracies they need to progress their businesses and technologies and ensuring international measurement equivalence.

The NML temperature and humidity laboratory is responsible for providing traceability to the kelvin temperature scale and for performing humidity calibrations that are traceable to the SI via a reference hygrometer which is calibrated once a year by a Designated Institute of Metrology (DI) in Switzerland. The humidity laboratory currently has two Thunder Scientific 2500 humidity generators. The Thunder Scientific 2500 is a two-pressure humidity generator combined with a climatic chamber of very stable temperature. They are used to create a stable medium in which to calibrate state of the art relative humidity sensors. The laboratory also has a Rotronic HygroGen humidity generator used for some lower accuracy calibrations and a Votch chamber sometimes used to reach humidities above 95% relative humidity (rh) and below 10% rh. The reference standards currently in use include two MBW 373HX chilled mirror hygrometers (-50 to 95 °C dew/frost point), one MBW DP30 chilled mirror hygrometer (-30 to 80 °C dew/frost point) and one MBW 473 chilled mirror hygrometer (-20 to 70 °C dew/frost point). With this system an uncertainty as low as ± 0.8 % rh can be achieved at 30 °C and 50 % rh.

The calibration system is reliant on one of the MBW 373HX reference hygrometers being externally calibrated each year and calibrating the other chilled mirror hygrometers by comparison, with increased uncertainty. The reference hygrometer is not immune to drift and a greater uncertainty component for drift is used because of the long calibration interval. The hygrometer is out of service for several weeks when it is being calibrated and the calibration is significantly expensive. Customers commonly request lower calibration uncertainties and with continuing improvement in relative humidity sensors the conformance of instruments within their specification often cannot be determined. These are all good reasons to reduce the uncertainties of the humidity calibration system.

Presented in this thesis is the design and implementation of a primary humidity generator which will progress the capabilities of the NML humidity laboratory. This is in line with the goals of the project entitled; "Expansion of European research capabilities in humidity measurement," which NSAI is a contributor to. This project is funded by the European Metrology Program for Innovation and Research. A primary dew point generator is a humidity

standard which provides traceability to the SI via temperature and pressure measurements. This will greatly reduce the minimum uncertainty of measurement achievable by the humidity laboratory at the NML. This will in turn reduce the uncertainty in secondary calibrations by reducing the calibration uncertainty of the reference instruments at NML that are calibrated by means of a secondary comparison and reducing the drift uncertainty component of the reference instruments by increasing monitoring. This will also be a new service that will be provided by the NML to Irish organizations, several of which operate chilled mirror hygrometers and send them overseas for calibration.

Similar work has been carried out by a number of other NMIs, which this work has been influenced by. The design of the humidity generators used by other NMIs are described in section 3.3.

The fundamentals of humidity measurement will be discussed. The concept of humidity generation as a primary measurement standard will be discussed and the operating principals of different types of humidity generators are given as well as a description of several humidity generators used in different NMIs. The design process of the new primary humidity standard at NML will be described and a number of useful equations used in the design and operation of the generator will be given and, in some cases, derived. A brief description of the initial tests performed on the generator will be given. A detailed description of a preliminary uncertainty analysis carried out at 90 °C dew point and -40 °C frost point is given. The results of a calibration of a chilled mirror hygrometer are given and compared to the results obtained by an external laboratory.

2. Fundamentals of humidity measurement

2.1. Humidity as a quantity and its importance to industry

Humidity is a measure of the amount of water vapour in a gas. It can be measured in absolute terms, for example, in units of moles water vapour per moles gas, or it can be measured by the dew point of the gas, which is the temperature at which the gas is saturated with water vapour. It can also be measured as relative humidity, which is the percentage that the gas is saturated with respect to complete saturation at its temperature.

Most materials can absorb and desorb some amount of water vapour. This can affect the humidity of the surrounding environment and can also change the qualities of the materials. For example, if a product is being sold on the basis of mass, such as timber, the moisture content can have a significant effect on the price. It is especially important during the packaging of some pharmaceuticals that the humidity of the surroundings is controlled as absorption of water vapour can degrade certain antibiotics. Pharmaceuticals and medical devices industries typically require humidity control of $\pm 2\%$ rh [1]. Humidity can affect clean room environments in a number of ways including bacterial growth, personal comfort, static charge build up, metal corrosion, condensation, photolithographic degradation and absorption. Some of these applications requiring humidity control to less than $\pm 1\%$ rh [2]. As these industries modify their processes to increase efficiency and reduce variability these specifications for humidity control will also have to be improved.

In order to maintain conformity with national standards, all measurements made in industry that affect processes need to be calibrated. This involves calibrating the measuring instrument against an instrument that is traceable to national standards. Ideally, the instrument used for calibration should have at least four times greater accuracy than the unit under test (UUT). In the highest accuracy scenario, the reference instrument will then need to be calibrated against a primary standard. Every step in this calibration chain includes a significant drop in accuracy. This makes a humidity tolerance of $\pm 2\%$ rh at an industrial level very difficult to achieve, especially considering that the calibration uncertainty of the measuring instrument is only one component of the final uncertainty for the process. Humidity metrology is therefore an important area for some industries, with many industries desiring lower uncertainties.

2.2. Description of humidity in relation to thermodynamics

Humidity is the presence of water vapour in air. When water or ice is in contact with air or empty space H_2O is evaporated or sublimated into the air or empty space as water vapour. Water vapour may also condense, returning to the liquid or solid state. When the air is saturated the number of H_2O molecules entering the gaseous state by evaporation is equal to the number leaving by condensation [3]. Therefore, at saturation, the number of H_2O molecules in each phase remains constant so the two phases are in equilibrium. The partial pressure of water vapour under these conditions is called the saturation vapour pressure. If the temperature of the condensate/vapour system increases, more H_2O molecules have enough energy to leave the water/ice surface and the saturation vapour pressure increases. Relative humidity is a measure of the water vapour content of air relative to complete saturation at ambient temperature. Figure 2.1 shows the relationship between the saturation vapour pressure and the temperature of a liquid/vapour system.

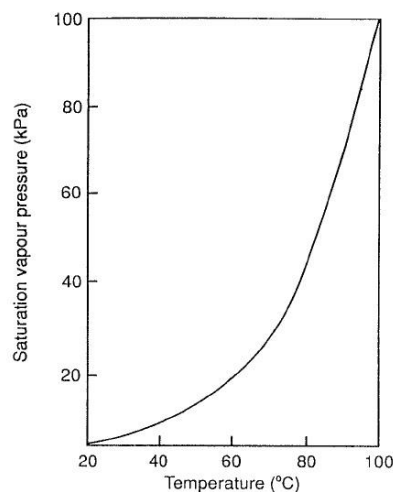


Figure 2.1: Saturation vapour pressure over water as a function of temperature [4].

From approximately $-40\text{ }^{\circ}\text{C}$ to $0\text{ }^{\circ}\text{C}$ pure water can exist in a super-cooled liquid or solid state or a combination of both. At equal vapour pressures the super-cooled dew point temperature (for liquid condensate) is lower than the frost point temperature (for solid condensate) since it requires more energy for molecules to leave the solid surface than a liquid surface. The presence of salts or other ionic or polar covalent molecules has a significant effect on the vapour pressure over the water or ice surface. This is due to the stronger intermolecular bonds requiring more energy for molecules leave the water or ice surface. This is important in relation to humidity as ions are a common impurity in water.

When an amount of H_2O is in an enclosed volume the H_2O may be in the solid, liquid or gas phase or a combination of these phases. If the enclosed volume is partially filled with H_2O in its

liquid or solid phase some of the highest energy molecules will have enough energy to leave the surface of the liquid/solid and enter the vapour phase. This results in a reduction of the temperature of the condensed phase due to it losing its most energetic molecules. The molecules entering the vapour phase will also lose some kinetic energy due to the energy required to break the intermolecular bonds of the condensed phase. The amount of energy required to convert a unit mass from solid or liquid into vapour is the latent heat of sublimation or vaporization. The vapour molecules may also collide with the liquid/solid and return to the condensed phase. The rate at which molecules return to the condensed phase depends upon the pressure of the vapour. The vapour pressure will therefore increase until as many H₂O molecules are condensing as those that are evaporating. At this point the system is in equilibrium and the vapour pressure under these conditions is termed by the saturation vapour pressure. The rate at which molecules enter the vapour state depends on the temperature of the condensate, since higher thermal energy results in more molecules having enough energy to break free from the condensed phase into the vapour phase. Therefore, the saturation vapour pressure depends on the temperature of the system.

Thermodynamic equilibrium is defined as the point at which all infinitesimal changes are reversible; meaning that there is no net increase in entropy for the system [5]. The change in entropy S for a reversible change is given by [5],

$$dS = \frac{\delta q}{T}, \quad (2.1)$$

where δq is heat flow and T is the absolute temperature.

The work done w on a system after expansion into its surrounding at constant pressure is given by [5],

$$\delta w = -P dV, \quad (2.2)$$

where P is pressure and dV is change in volume.

If a system performs work only in the form of expansion work against its surroundings then from the first law of thermodynamics the change in internal energy dU will be equal to the heat flow to the system plus the work done on the system (for a reversible process) therefore [5];

$$dU = TdS - PdV. \quad (2.3)$$

The Gibbs free energy G is given by [5],

$$G = H - TS = U + pV - TS$$

or

$$dG = dU + PdV + VdP - TdS - SdT, \quad (2.4)$$

where H is the enthalpy.

Combining Eqs. 2.3 and 2.4 gives [5],

$$dG = VdP - SdT. \quad (2.5)$$

This relates the change in the Gibbs free energy with changes in temperature and pressure.

This is useful for describing the situation above where two phases of H_2O are in equilibrium

with each other. A similar function is the Helmholtz function F [5];

$$F = U - TS$$

or

$$dF = dU - TdS - SdT. \quad (2.6)$$

Combining this with previous gives,

$$dF = -PdV - SdT. \quad (2.7)$$

This can be used to derive a function for the rate of change of pressure with respect to temperature by first differentiating,

$$\left(\frac{\partial F}{\partial T}\right)_V = -S$$

and

$$\left(\frac{\partial F}{\partial V}\right)_P = -P.$$

And taking the second derivative with respect to V and T ,

$$\frac{\partial^2 F}{\partial T \partial V} = -\left(\frac{\partial S}{\partial V}\right)_T = \frac{\partial^2 F}{\partial V \partial T} = -\left(\frac{\partial P}{\partial T}\right)_V. \quad (2.8)$$

For a reversible change;

$$\frac{\partial S}{\partial V} = \frac{\Delta S}{\Delta V}.$$

Therefore combining Eqs. 2.1 and 2.8 gives;

$$\left(\frac{\partial P}{\partial T}\right)_V = \frac{\Delta S}{\Delta V} = \frac{q}{T \Delta V}. \quad (2.9)$$

Since ΔS is the difference in entropy between the condensed and vapour state; q is the latent heat of vaporization so the equation can be written as [5],

$$\frac{\partial P}{\partial T} = \frac{\Delta H}{T \Delta V}, \quad (2.10)$$

where ΔH is the latent heat of vaporization.

Equation 2.10 is the well-known Clausius Clapeyron equation and it relates the rate of change of pressure with respect to temperature to the latent heat and the change in volume of a system of two phases in equilibrium, at temperature T . If ΔH is the molar latent heat and ΔV is the change in molar volume going from one phase to the other, then assuming the vapour is an ideal gas,

$$\Delta V = \frac{V_{vapour}}{n} - \frac{V_{condensed}}{n} = \left(\frac{RT}{P} \right)_{vapour} - \frac{V_{condensed}}{n},$$

where $\frac{V_i}{n}$ is the molar volume in phase i , and R is the universal ideal gas constant.

$V_{condensed}/n \ll V_{vapour}/n$ so $V_{condensed}/n$ can be considered negligible giving,

$$\Delta V = \left(\frac{RT}{P} \right)_{vapour}. \quad (2.11)$$

Combining Eq. 2.11 with the Clapeyron equation (Eq. 2.10) and integrating to give an expression for P ;

$$\int_{P_0}^P \frac{1}{P} \partial P = \frac{\Delta H}{R} \int_{T_0}^T \frac{1}{T^2} \cdot \partial T,$$

$$P = P_0 \exp \left[\frac{\Delta H}{R} \left(\frac{1}{T_0} - \frac{1}{T} \right) \right]. \quad (2.12)$$

Using P_0 and T_0 as a reference point, the vapour pressure can be calculated as a function of temperature and molar latent heat. However, latent heat depends on temperature so to give a reliable result the function of molar latent heat with respect to temperature would have to be well known with a reliable uncertainty. For practical determination of saturation vapour pressure an empirical function that relates saturation vapour pressure to temperature with a well characterized uncertainty should be used. Equation 2.12 can be used with such a reference function to calculate the latent heat for different temperatures, knowing the vapour pressure from the empirical reference function.

2.3. Practical humidity measurement and empirical reference functions

An empirical reference function which relates the vapour pressure to the saturation temperature of a gas was given by Wexler in 1971 [6] and was updated by Sonntag in 1990 [7] for the International Temperature Scale (ITS-90) revision in 1990. For a given temperature, it gives the pure vapour pressure over water or ice.

The uncertainties given are based on a confidence interval of 99.7% however the accepted usage is to overestimate the uncertainty by assuming the confidence interval given is 68% and multiplying by two to get a 95% confidence interval [8]. The equation for pure saturation vapour pressure $e(T)$ as given by Sonntag is [6],

$$e(T) = \exp \left[\sum_{i=1}^4 (a_i (T + 273.15)^{i-2}) + a_5 \ln(T + 273.15) \right], \quad (2.13)$$

where T is the saturation temperature ($^{\circ}\text{C}$) and a_i are the coefficients listed in table 2.1 and the uncertainties of the reference function are given in table 2.2.

Table 2.1: Coefficients for Sonntag equation [8]

	Over Ice $-100\text{ }^{\circ}\text{C} < T < 0.01\text{ }^{\circ}\text{C}$	Over Water $-50\text{ }^{\circ}\text{C} < T < 100\text{ }^{\circ}\text{C}$
a_1	$-6.024\,528\,20 \times 10^3$	$-6.096\,938\,50 \times 10^3$
a_2	$2.932\,707\,00 \times 10^1$	$2.124\,096\,42 \times 10^1$
a_3	$1.061\,386\,80 \times 10^{-2}$	$-2.711\,193\,00 \times 10^{-2}$
a_4	$-1.319\,882\,50 \times 10^{-5}$	$1.673\,952\,00 \times 10^{-5}$
a_5	$-4.938\,257\,70 \times 10^{-1}$	$2.433\,502\,00 \times 10^0$

Table 2.2: Uncertainty associated with Sonntag formula [8]

$\pm (0.01 - 0.005\, T) \%$	for $-100\text{ }^{\circ}\text{C} < T < 0.01\text{ }^{\circ}\text{C}$
$\pm 0.005 \%$	for $0.01\text{ }^{\circ}\text{C} < T < 100\text{ }^{\circ}\text{C}$

When the vapour over water is mixed with another gas it affects the vapour pressure.

Therefore, in the presence of air the partial pressure of water vapour is not necessarily equal to the saturation vapour pressure given by Sonntag (Eq. 2.13) at that temperature. This is due to three effects; firstly, the chemical potential of the condensed phase increases due to the increase in the total pressure of the gas; secondly, if the gas is soluble in the condensate then the chemical potential of the condensate changes; and thirdly, the chemical potential of the vapour changes due to interactions with the gas [9].

This effect is accounted for in humidity calculations by multiplying the pure phase vapour pressure by a so-called water vapour pressure enhancement factor $f(T, P)$ where P is pressure. The effect is small for near ambient pressures and becomes significant at higher pressures so it is possible to omit the enhancement factors at near ambient pressures depending on the application. The corrected vapour pressure e' in a vapour-air mixture is given by [4],

$$e' = e(T) f(T, P), \quad (2.14)$$

The water vapour pressure enhancement factor formulation for water vapour mixed with air is;

$$f(T, P) = \exp \left[\alpha(T) \left(1 - \frac{e(T)}{P} \right) + \beta(T) \left(\frac{P}{e(T)} - 1 \right) \right], \quad (2.15)$$

$$\text{where } \alpha(T) = \sum_{i=1}^4 b_i T^{i-1} \text{ and } \beta(T) = \exp \sum_{i=1}^4 b_{i+4} T^{i-1},$$

and where b_i are the coefficients listed in the table 2.3 and T is in °C and P is in Pa.

Table 2.3: Coefficients for water vapour pressure enhancement factor formulation [8].

	Over Ice -100 °C < T < 0 °C	Over Super Cooled Water -50 °C < T < 0 °C	Over Water 0 °C ≤ T < 100 °C
b_1	$3.644\ 49 \times 10^{-4}$	$3.621\ 83 \times 10^{-4}$	$3.536\ 24 \times 10^{-4}$
b_2	$2.936\ 31 \times 10^{-5}$	$2.605\ 53 \times 10^{-5}$	$2.932\ 28 \times 10^{-5}$
b_3	$4.886\ 35 \times 10^{-7}$	$3.865\ 01 \times 10^{-7}$	$2.614\ 74 \times 10^{-7}$
b_4	$4.365\ 43 \times 10^{-9}$	$3.824\ 49 \times 10^{-9}$	$8.575\ 38 \times 10^{-9}$
b_5	$-1.072\ 71 \times 10^1$	$-1.076\ 04 \times 10^1$	$-1.075\ 88 \times 10^1$
b_6	$7.619\ 89 \times 10^{-2}$	$6.397\ 25 \times 10^{-2}$	$6.325\ 29 \times 10^{-2}$
b_7	$-1.747\ 71 \times 10^{-4}$	$-2.634\ 16 \times 10^{-4}$	$-2.535\ 91 \times 10^{-4}$
b_8	$2.467\ 21 \times 10^{-6}$	$1.672\ 54 \times 10^{-6}$	$6.337\ 84 \times 10^{-7}$

The relative uncertainty of the enhancement factor $u_r(f)$ can be found as a percentage (%) from [8],

$$u_r(f) \leq (1.68 \times 10^{-9}P - 10^{-5}) \times \exp[(2.2 \times 10^{-5} \ln(P) - 0.0139).T]. \quad (2.16)$$

Equation 2.16 is valid for $-90\text{ °C} \leq T \leq 100\text{ °C}$ and $5 \times 10^4\text{ Pa} \leq P \leq 2 \times 10^6\text{ Pa}$.

All of the random and systematic uncertainties effecting the enhancement factor calculated using Eq. 2.15 were expressed in tabular format and Eq. 2.16 was developed to represent those uncertainties conveniently.

The water vapour mole fraction x is the ratio of the number of moles of water vapour to the total number of moles in a volume of gas and is given by;

$$x = \frac{n_w}{n_w + n_{air}} = \frac{n_w}{n_T}, \quad (2.17)$$

where n_w is number of moles of water vapour, n_{air} is number of moles of dry air (or other gas) and n_T is total number of moles of the gas-vapour mixture.

Assuming an ideal gas,

$$\frac{P_T}{n_T} = \frac{RT}{V} = \frac{P_w}{n_w},$$

so that,

$$\frac{n_w}{n_T} = \frac{P_w}{P_T} = x ,$$

where P_w is the water vapour pressure, P_T is the total pressure, R is the universal ideal gas constant and V is volume.

Since the partial pressure of water vapour can be found from the saturation temperature (from Eq. 2.14), the water vapour mole fraction x is [8];

$$x = \frac{e(T) \cdot f(T, P)}{P} , \quad (2.18)$$

Therefore, if the saturation temperature and the pressure of the gas are known the Sonntag formula (Eq. 2.13) and the vapour pressure enhancement factor formula (Eq. 2.15) can be used to calculate the water vapour mole fraction.

The dew point is the saturation temperature over water, and frost point is the saturation temperature over ice. This is a measure of humidity because it is related to the water vapour pressure (by Eq. 2.14) which is directly related to the number of moles of water vapour in the gas. At a given pressure air with a specific mole fraction has only one dew point. This has a major advantage over relative humidity which is strongly temperature dependant. It is important to differentiate between dew point and frost point as large errors could occur if a dew point temperature is assumed to be a frost point temperature or vice versa. The dew point of a gas is pressure dependant and can be corrected for changes in pressure (as described in section 3.4.1).

Relative humidity is a measure of the vapour content of a gas with respect to complete saturation and is therefore strongly dependant on temperature. The relative humidity, h , can be expressed as [8];

$$h = \frac{x_0}{x_s} \cdot 100\% , \quad (2.19)$$

where x_0 is the mole fraction and x_s is the mole fraction at saturation at the ambient temperature.

This can be combined with Eq. 2.18 and rearranged to give [10],

$$h = \frac{e(T_d) \cdot f(T_d, P_0) \cdot P_c}{e(T_c) \cdot f(T_c, P_c) \cdot P_0} \cdot 100\% , \quad (2.20)$$

where $e(T_d)$ is the vapour pressure, T_d is the dew point of the gas, P_0 is the pressure at the point of measurement, $e(T_c)$ is saturated vapour pressure, T_c is ambient temperature and P_c is the ambient pressure.

If the pressure of the gas is equal to the pressure at the point of measurement the enhancement factors will also be nearly equal and relative humidity can be given by [4];

$$h = \frac{e(T_d)}{e(T_c)} \cdot 100\% . \quad (2.21)$$

Equation 2.21 can be used to calculate relative humidity based on a dew point measurement and ambient temperature measurement.

2.4. Units of mass flow

The mass flow of a fluid is the quantity of mass of that fluid passing a point in the fluid's path in a given time interval. The SI unit for mass flow is the kilogram per second (kg/s). Another commonly used unit for mass flow is the standard litre per minute. This is the number of litres of fluid, at a standard temperature and pressure, passing a point in the flow path every minute. Since the volume corresponds to the fluid's volume only at a fixed temperature and pressure this is a unit of mass flow, not volumetric flow.

The mass flow controller that will be used to operate the humidity generator described in this thesis is a measuring instrument that is sensitive to changes in mass flow and controls the mass flow through the system. It is calibrated in units of litres standard per minute (ls/min) where the standard temperature is 20 °C and the standard pressure is 1013.25 hPa.

In this thesis the fluid of concern is assumed to be an ideal gas and the mass flow in ls/min can be converted to molar flow or mass flow in kg/s using the ideal gas equation and knowing the molar mass of the fluid in question (humid air). This is described further in 3.4.2.

2.5. Humidity instrumentation

Humidity can be measured in a number of different ways. An instrument for humidity measurement should be selected on the basis of accuracy and the response of the instrument to the humidity quantity been measured. For example, if the quantity of interest is relative humidity for the purpose of maintaining human comfort, preventing moisture absorption or preventing or encouraging drying, an electrical impedance based RH sensor could be an appropriate measuring instrument. This is due to the fact that electrical impedance RH sensors respond mainly to changes in relative humidity rather than dew point or mole fraction. If the quantity of interest is the water vapour content of the gas in question, for the purpose of electrical insulation, frost prediction, or for the most accurate metrological applications, then a chilled mirror hygrometer could be the best measurement option due to the fact that it measures dew point directly which, at constant pressure, is directly related to the mole fraction of a gas. Listed below are several measurement methods in order of relation to this project.

Optical Chilled Mirror Hygrometer:

A chilled mirror hygrometer measures the temperature at which dew or frost forms in a gas. It achieves this by passing the gas over a reflective surface which is cooled, usually by Peltier coolers and possibly a refrigeration system (depending on the range of measurement). When the mirror is cooled below the dew/frost point temperature of the gas a dew or frost begins to form on the mirror and is detected by an optical system.

The goal of the chilled mirror hygrometer is to maintain zero net mass transfer between water vapour and condensed states [11]. Under these conditions the system is in equilibrium and the vapour pressure over the condensate is the saturation vapour pressure (in that gas) at the temperature of the condensate-vapour interface (these ideal conditions will not be perfectly met in reality). If this temperature (the dew point) is measured it can then be related to the pure phase vapour pressure and the mole fraction using the reference equations given in the previous section.

The dew point temperature is measured by one or two thermometers, usually platinum resistance thermometers (PRTs) in thermal contact with the mirror. The accuracy of the dew point measurement will depend on the heat transfer between condensate-vapour interface and the PRTs as well as other common measurement errors such as PRT self-heating, calibration uncertainty and drift. Due to the difficulty in measuring the temperature of the

condensate-vapour interface; chilled mirror hygrometers are used as secondary measurement standards and are calibrated against a primary humidity standard.

Another potentially large source of error when using a chilled mirror hygrometer is in the determination of the state of the condensate. If the condensate is assumed to be solid (frost) when it is actually liquid (dew) the resulting vapour pressure calculated will be lower than it is in reality due to the change in chemical potential of the condensate. Errors greater than 1 °C (dew/frost point) could occur due to super-cooled dew been mistaken as frost [12]. A further complication is the possibility of phase transitions and non-equilibrium states existing on the mirror [11]. These errors can be accounted for by both calculating the potential dew/frost error and including this as an uncertainty and by “forcing frost” on the mirror below a certain temperature. To force frost, the mirror is brought to a low temperature (below -40 °C) before returning to the frost point temperature. This ensures that all of the condensed H₂O on the mirror is in the solid state and it cannot return to a liquid state unless the mirror is brought above 0 °C since the solid state is at a lower energy level.

Laser Absorption Spectroscopy:

Absorption spectroscopy can be used to measure the H₂O content of a gas. This involves passing light at wavelengths that are absorbed by H₂O through the sample gas and measuring the absorption. It is possible to scan the isolated absorption lines giving absorption measurements for H₂O with very little cross sensitivity with other molecules. The number density is related to the absorption and path length of laser light through the sample [13], so the system can then be calibrated against a primary standard to give accurate measure of H₂O number density of the sample gas. The number density can then be related to partial pressure of water vapour by the ideal gas law. Unlike chilled mirror hygrometers; since the number density of H₂O molecules is measured directly, this method does not need to rely on the ranges and data of empirical reference functions and is independent of the uncertainty related to them. Laser absorption spectroscopy enables precise measurements of extremely low concentrations of water vapour (as low as a few parts per billion). Spectroscopic methods have the added benefit over other methods of hygrometry of been able to determine the presence of impurities in the gas. They also have a faster response time compared to chilled mirror hygrometers which is beneficial for some applications [13].

Electrical Impedance Based Relative Humidity Meters:

There are two main types of electrical impedance based humidity sensors; capacitive and resistive sensors. Both contain a hygroscopic material, that is, a material that absorbs and desorbs water vapour depending on the relative humidity of the environment. The resistance and the dielectric constant of the material changes depending on the moisture content due to the mobility of the water molecules in the material. Measuring the resistance or the capacitance across such a material and calibrating against a reference humidity instrument gives a practical measure of relative humidity with possible accuracies as low as 0.5 % rh.

The mobility of water molecules in the hygroscopic material increases with temperature giving impedance based sensors a strong temperature dependence [11]. Resistance and dielectric constant also depends on temperature but does not have as large an effect on RH sensors as the hygroscopic temperature dependence [14]. Polynomial coefficients can be used to correct for the temperature dependence. This also requires that the instrument be calibrated at different temperatures to monitor and correct for the drift in the temperature dependence, however this is expensive and many owners of RH meters choose to limit the operating range of the instrument to reduce the number of temperatures that the instrument needs to be calibrated at. Figure 2.2 shows the temperature dependence for a typical impedance based relative humidity meter.

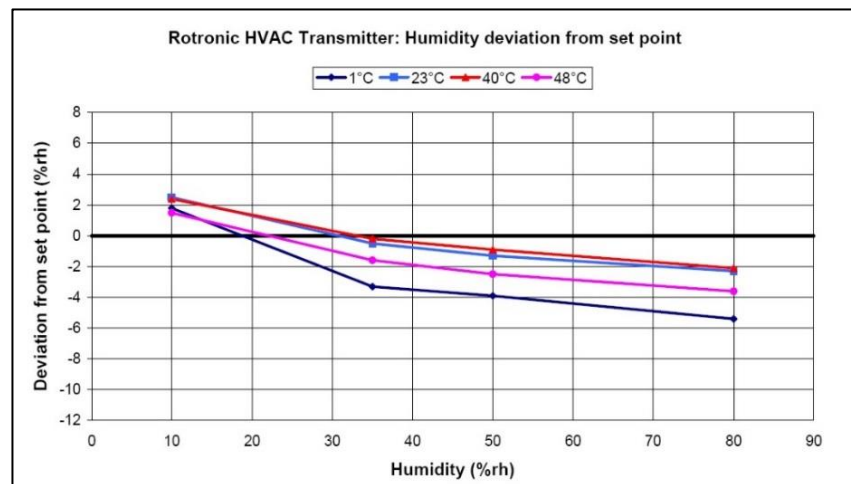


Figure 2.2: Temperature dependence and linearity of a state of the art RH meter [14].

Impedance based sensors also suffer from a significant long term drift. The bonding of water molecules in the hygroscopic material depends on the molecular structure of the material and the presence of other gas molecules and impurities. Because of this and that surface interactions in the material are often irreversible, the sensors experience significant long term drift [11]. Impedance based RH sensors also have a significant uncertainty due to hysteresis and a number of other factors.

3. Primary dew point generation

3.1. Overview

In order to maintain traceability to the SI base units a primary measurement or realization of humidity must be made. According to [16] a primary measurement standard is a measurement standard established using a primary reference measurement procedure. [16] states that a primary reference measurement procedure is a reference measurement procedure that is used to obtain a measurement result without a relation to a measurement standard of the quantity of interest. To achieve this for humidity, the mass of dry gas can be measured and compared to the mass of H_2O in order to determine the water vapour mass fraction. This is very difficult to achieve in practice. The equipment required is very costly and the process is very time consuming. A calibration using this method could take several months. Because of this the most common primary realization of humidity is achieved using a primary humidity generator.

A primary humidity generator or primary dew point generator is a device that ensures complete saturation of air with water vapour over a plane water or ice surface. Since these conditions are similar to the conditions for the saturated vapour pressure given in the Sontag equation then if the temperature of the condensate-vapour interface and the total pressure above the condensate are well known then the vapour pressure in the gas can be determined from Eqs. 2.13 and 2.15 and the mole fraction of the gas can be determined from Eq. 2.18. This is therefore a primary realization of humidity, traceable to the SI via temperature and pressure measurements, and needs no higher link in the humidity calibration chain. In order to maintain traceability to the SI it is also required that all uncertainty contributions are accounted for and the uncertainty budget is peer reviewed and inter-comparisons of the primary realizations must be made with other NMIs, a costly and time-consuming process. Since most NMIs have the highest accuracy temperature and pressure measurement capabilities in their countries, this makes primary dew point realizations a practical primary humidity standard for NMIs.

However, the ideal conditions of the vapour pressure formulations are not completely met by a primary dew point generator with some of the problems encountered as follows: The water vapour is mixed with air, changing the saturated vapour pressure from the pure saturation vapour pressure, which is corrected for with Eq. 2.14. The water may have a lower saturation vapour pressure if it contains impurities especially ones that are polar or polar-covalent. This problem is minimised by using water with known levels of impurities and using filtered air and polished stainless steel parts. The gas is not necessarily in equilibrium with the water or ice since it is flowing past the water or ice surface rather than being stationary, as is in the

definition of water vapour saturation pressure. Because of this, the air may not become completely saturated with respect to the saturator temperature. An uncertainty component must be determined to account for the non-ideal saturation efficiency. This is not a straight forward task and there is no single way to do it. It must be determined from experimental and theoretical knowledge of the dew point generator.

3.2. Types of dew point generators

3.2.1. Single pressure (1-P) generator

In a single pressure generator, gas is saturated at near atmospheric pressure and is then directed to the UUT with only a small drop in pressure from the saturator to the UUT [17]. The mole fraction or dew point of the gas is varied by changing the temperature of the saturator. Figure 3.1 is a schematic diagram of a possible arrangement for a single pressure (1-P) dew point generator.

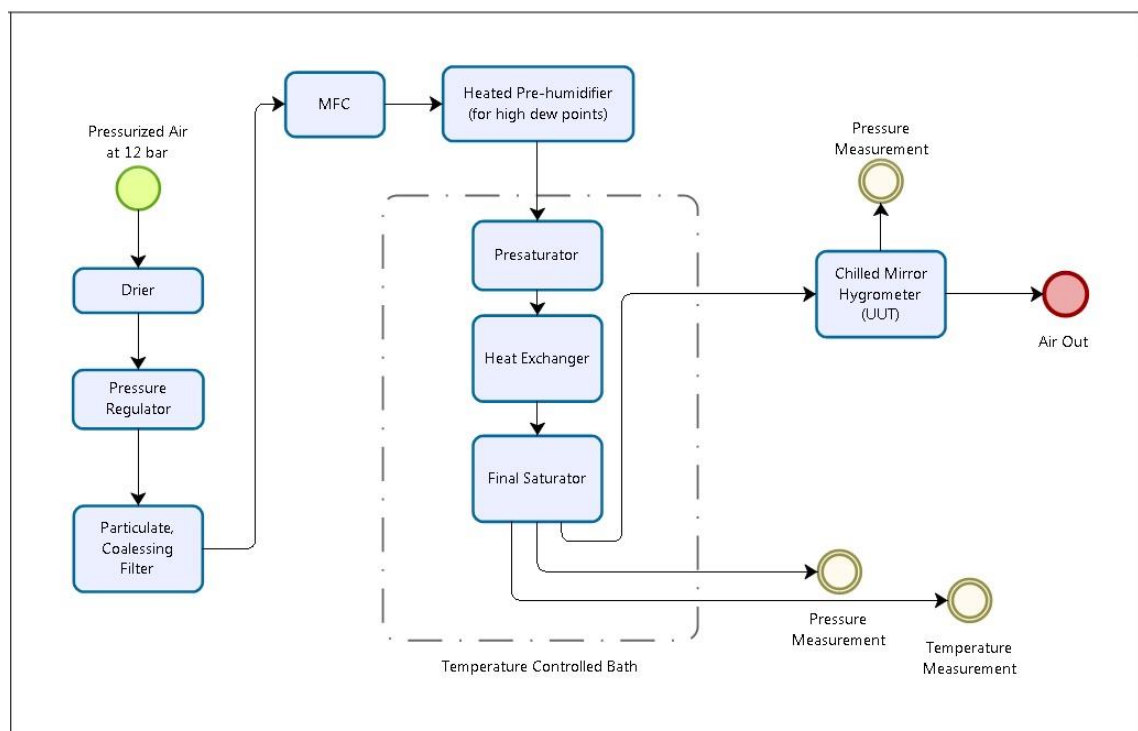


Figure 3.1: Single pass single pressure (1-P) generator.

With this arrangement it is not necessary to make pressure measurements every time the generator is used. Instead the pressure drop between the saturator and the UUT can be characterized throughout the measurement range and can be factored into measurements as an uncertainty or as a correction. The accuracy of the pressure measurements or characterization contributes to the overall uncertainty of the generated dew point. A 1-P

generator allows greater accuracy pressure measurements to be made since the range of the pressure measuring instruments is much smaller and the pressure stability in the saturator will be greater. Wide diameter tubing can also be used to minimise pressure drop between the saturator and the UUT, so depending on the overall uncertainty of the system the pressure drop may be considered negligible. However, it should still be included as an uncertainty component.

For the case of a single pass dew point generator gas is passed over the liquid or solid surface just once before being sent to the hygrometer and expelled to the atmosphere. This means that the dry air supplied to the generator must be completely saturated by the dew point generator. If dry air is saturated to 95 °C dew point at an output mass flow rate of 1 ls/min, evaporative cooling will occur at a rate of 26 W (as can be determined from Eq. 4.4). This is a very large rate of heat loss in the saturator. In the design shown in figure 3.1 the pre-saturator will reduce the latent heat loading on the final saturator, allowing the final saturator to be more efficient and produce a more accurate dew point realization. However, a pre-humidifier may also be placed before the pre-saturator at a similar temperature to the pre-saturator, further reducing the latent heat loading in the system and reducing the overall uncertainty of the system.

The saturators are maintained at a very stable temperature by a temperature controlled liquid bath. The uncertainty of the generated dew point will depend on the stability of the temperature controlled bath. A heat exchanger is used to ensure that the air temperature is very close to the bath temperature before reaching the final saturator. The dew point temperature of the gas leaving the saturator is equal to the temperature of the condensate-vapour interface in the final saturator. This temperature can be approximated by measuring the temperature of the gas leaving the saturator, assuming that the gas and condensate are in thermal equilibrium. This temperature can also be approximated by measuring the temperature of the bath liquid surrounding the final saturator, however this will have a greater uncertainty due to the temperature difference between the bath liquid and the condensate-vapour interface. At set points with little latent heating in the system this difference is expected to be small.

The gas is filtered before entering the system to remove any particulates that may have been introduced by the compressor or the compressed air tubing that may contaminate the system. The gas is also filtered by a coalescing filter to remove any liquid droplets from the gas which if not removed, may travel to the hygrometer and give an inaccurate dew point measurement.

While the accuracy of the mass flow control is not critical it is important that the mass flow can be controlled to a known flow rate with reasonable repeatability since the saturator efficiency depends on the mass flow rate. The response of the chilled mirror hygrometer also depends on the flow rate, meaning mass flow at the chilled mirror must be kept constant at a specified value.

An alternative to the single pass operation of a 1-P dew point generator is the full recirculation mode of operation [18] as shown in figure 3.2. In this arrangement of a dew point generator the gas exhausted from the chilled mirror hygrometer is recirculated back to the inlet of the generator. In this mode of operation, the system is initially purged with clean air from the compressed air source before being recirculated by the pump. Recirculation significantly reduces the mass transfer of H_2O in the saturators and therefore greatly reduces the latent heat loading at high dew points. This requires that the pump and recirculation lines be heated well above the dew point temperature of the gas to prevent condensation. The pressure drop across the pump may also cause condensation but sufficient heating will prevent this. The pump should be made of a material that has a reasonably low water vapour permeability, however, small losses of water vapour will not impact the performance of the system since the air will be passed through the generator again before reaching the UUT.

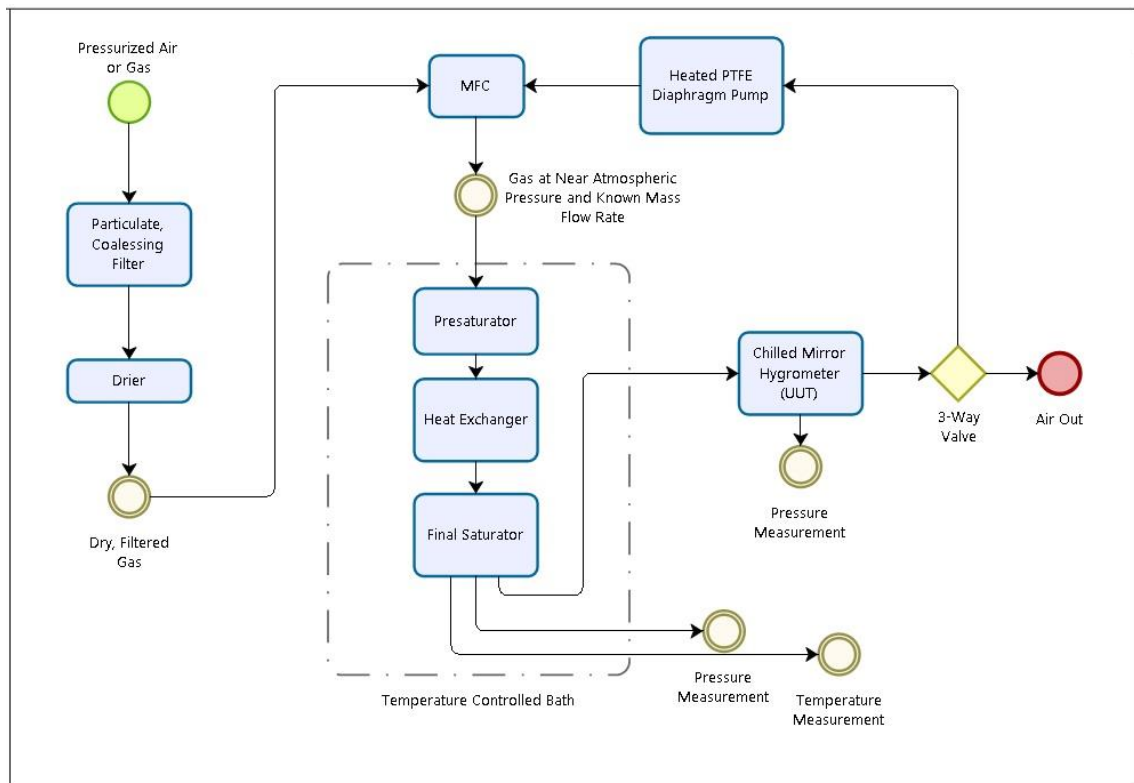


Figure 3.2: Full recirculation 1-P dew point generator.

A suitable pump for this application could be relatively expensive and the system is more complicated than that for single pass operation. Another disadvantage is that any contaminants in the UUT that may be picked up by the gas will be passed to the generator to the point of realization where it may affect the output dew point of the generator.

Another mode of operation used in primary 1-P dew point generation is the partial recirculation mode [17] as shown in figure 3.3. This involves pumping air through the saturators at a high flow rate (possibly 30 ls/min or more depending on the geometry of the saturators) while drawing off air to the UUT at the usual flow rate (usually 0.5 ls/min). The humidity of the air should not change in the recirculation loop so the flow rate through the saturators may be high but the mass transfer in the saturators should be the same as it would be for the draw off flow rate to the UUT. The air that is drawn off is replaced by dry filtered air or pre-humidified air or recirculated air from the UUT.

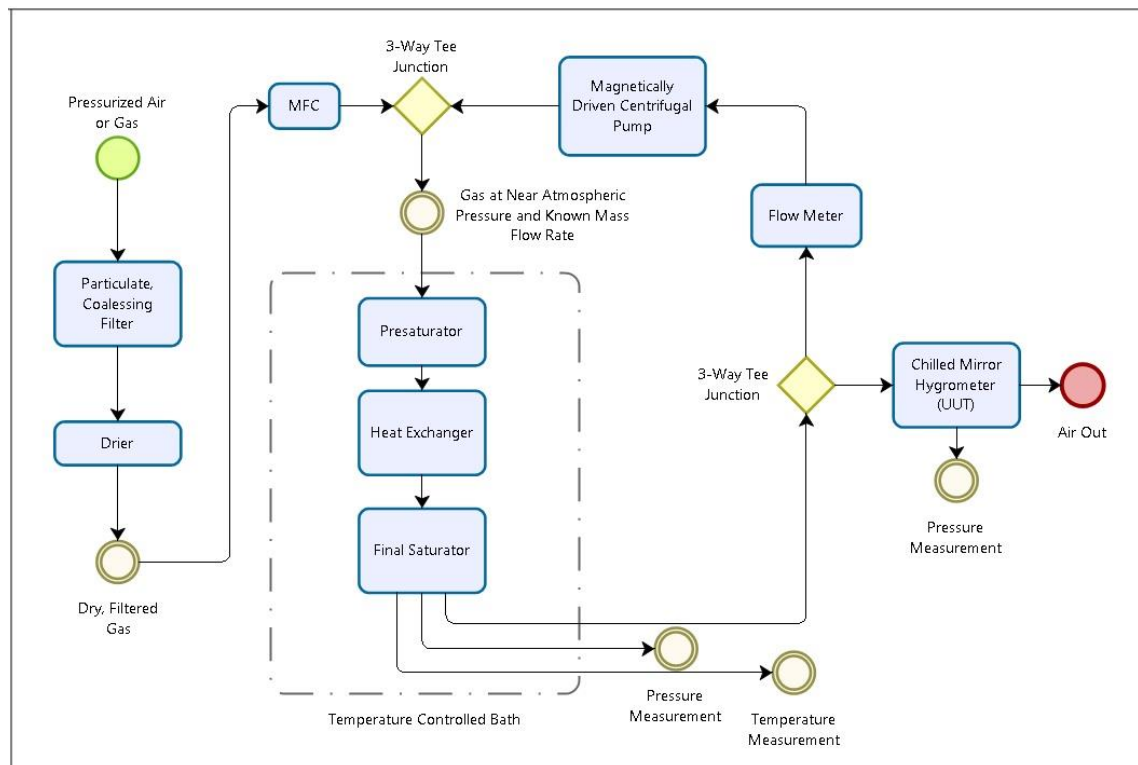


Figure 3.3: Partial recirculation dew point generator.

The benefit of this method is that the higher flow of air through the saturators increases the flow speed and therefore increases the Reynold's number of the flow. If the Reynold's number is high enough turbulence is created and increased mixing of wet and dry air occurs, increasing the saturator efficiency [19].

This method requires a pump with a very low pressure drop (to prevent condensation) and very high degree of leak tightness so that it does not disturb the mole fraction of the gas. Any disturbance of the mole fraction in the recirculation path has the potential to impact significantly the performance of the generator due to the high flow rate. It is also required that the pump be oil free and the bearings in the pump may need to be degreased so that the gas and saturators are not contaminated. To achieve these requirements a magnetically driven centrifugal pump can be used with modifications made to it to achieve the mentioned requirements. A mechanically driven pump can be used if special seals are used that will not contaminate the generator. This is expensive and far more complicated than the single pass or full recirculation modes and it also requires a detailed knowledge of the lubricants, bearings and bushings used in the pump. However in many cases partial recirculation can increase saturator efficiency.

3.2.2. Two pressure (2-P) generator

In a two pressure generator the gas is saturated at an elevated pressure, as shown in figure 3.4.

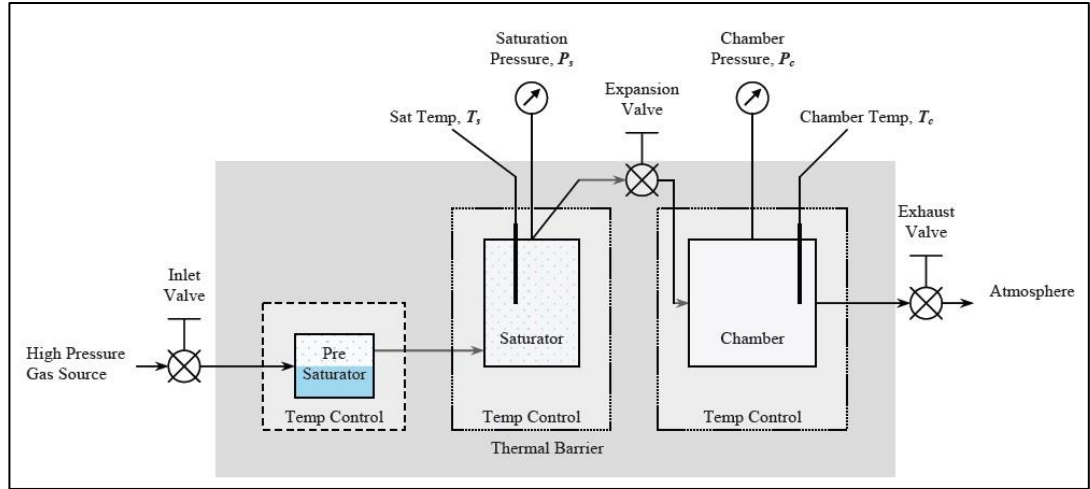


Figure 3.4: Schematic diagram of a two pressure (2-P) generator with independent temperature control [20].

The mole fraction at the saturator can be calculated from Eq. 2.18 using the saturator temperature T_s and pressure P_s . The gas is then expanded, usually to atmospheric pressure, where its humidity is measured by the instrument under test. The mole fraction at the point of measurement will be equal to the mole fraction in the saturator, provided that no water vapour is added to or removed from the gas between the two points. The relative humidity can then be found from Eq. 2.19, using the mole fraction at the saturator and the saturated mole fraction at the point of measurement of the UUT. The saturated mole fraction can be found from Eq. 2.18, using the temperature T_c and pressure P_c at the point of measurement. Combining these equations gives an equation for relative humidity in a two pressure generator [20],

$$h = \frac{e(T_s) \cdot f(T_s, P_s) \cdot P_c}{e(T_c) \cdot f(T_c, P_c) \cdot P_s} \cdot 100\% . \quad (3.1)$$

Two Pressure Humidity generators have a very limited working range. A system with a pressure drop of about 10 bar might only have a range from 10% rh to 100% rh. The advantage of this system is that pressure can be changed very quickly, whereas changes in temperature could take several hours to stabilize. A hybrid system where the temperature and pressure of the saturator can be controlled independently of the calibration chamber is beneficial as it retains the maximum stability and range of a single pressure generator but also with the option of moving between set points quickly and extending the lower range.

3.2.3. Divided flow generator

A divided flow generator mixes a dry steam of gas with a wet stream, both of known mole fraction, at a known mixing ratio. This is generally used as a secondary humidity generation method (traceable via a calibrated reference instrument) but it can also be used as a primary method, provided that the flows are precisely metered and controlled. The main application for this method is in reaching low frost points. It has the benefit of being able to operate the saturator at a convenient temperature (where the uncertainties of the generated dew point and vapour pressure formulations are low) and then precisely mixing the wet stream and dry stream to obtain a low frost point. The mole fraction x of the output gas is given by [21];

$$x = \frac{\dot{n}_w x_w + \dot{n}_d x_d}{\dot{N}}, \quad (3.2)$$

where \dot{n}_w and \dot{n}_d are the molar flow rates of the wet and the dry streams, x_w and x_d are the mole fractions of the wet and dry streams and \dot{N} is the total molar flow rate.

The low uncertainty of the strategically chosen saturator temperature then propagates through Eq. 3.2 to the output mole fraction uncertainty and is combined with the uncertainty of the metered mass flow rates and the mole fraction of the dry stream.

A practical realization of humidity using this method would require a gas multiplexer similar to the one used in [21], shown in figure 3.5.

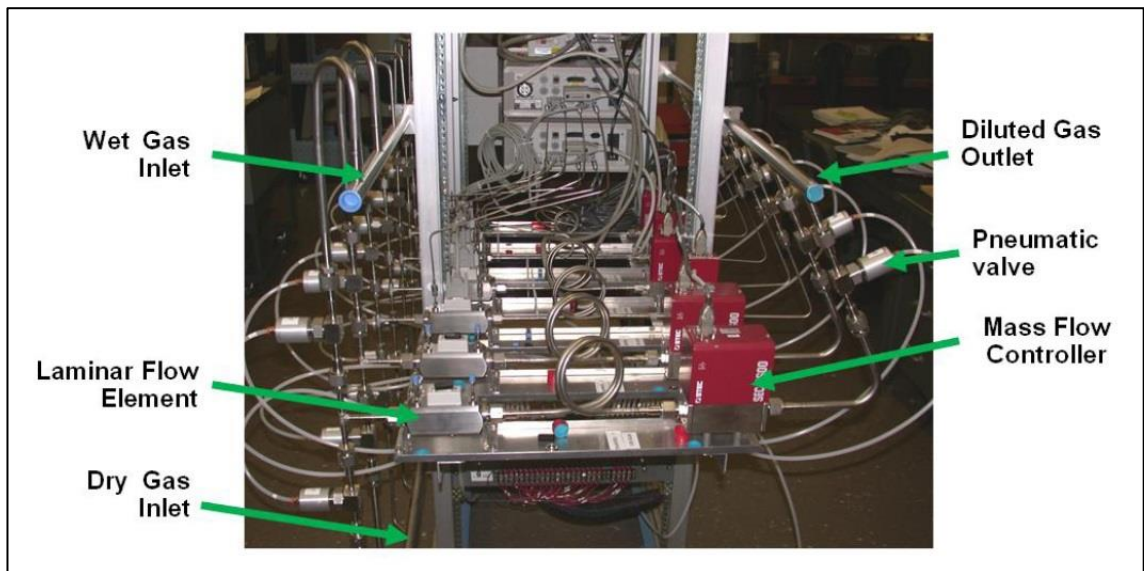


Figure 3.5: Gas multiplexer used by the National Institute of Standards and Technology (NIST) in their primary hybrid humidity generator [21].

This includes an array of precise mass flow controllers and corresponding laminar flow elements to precisely measure and control different flow rates. The measurement range of the

meters used in [21] vary from 10^{-3} L/min to 100 L/min. Pneumatic valves are used to select which controllers/meters are used for the wet and dry streams. The flow meters are calibrated by NIST Fluid Metrology Group with dry air. It is assumed that the change in calibration due to the change in mole fraction of wet air is negligible [21].

The divided flow method can also be used in conjunction with the two pressure method as in the case of the NIST hybrid humidity generator in [21]. In this system the two pressure method is used for dew/frost points above $-15\text{ }^{\circ}\text{C}$ while the divided flow method is used for lower frost points benefiting from the low propagation of uncertainty to the low humidities. This also means only one water bath is needed for the saturator as it does not need to be operated below $0\text{ }^{\circ}\text{C}$.

A primary realization of humidity using the divided flow or hybrid method involves using an expensive and complicated system. It is reliant on initial primary humidity generation with low uncertainty. It also requires knowledge of the best practises of mass flow measurement and is most practical for organizations with existing experience and calibration facilities in mass flow measurement. It is however a good method for achieving low humidities with a low propagated uncertainty.

3.3. Primary dew point generator designs used in different NMIs

In this section a number of dew point generators used in different NMIs are described in relation to journal papers that have been published detailing their design and performance. Some of the benefits of each design are pointed out. Many of the humidity standards in these laboratories have changed since these papers have been published and the laboratories may now have; additional generators, modified operating conditions, wider range of operation and improved uncertainties. However the principals and philosophies of most designs are largely the same.

National Physical Laboratory (NPL), United Kingdom:

The NPL primary dew point generator described in [22] is a single pressure generator that uses the partial recirculation method described in chapter 3.2. It consists of a pre-saturator and saturator in separate temperature controlled baths. The pre-saturator is used for humidities above -50 °C frost point. The temperature of the pre-saturator is sufficiently greater than the temperature of the final saturator in order to compensate for the pre-saturator inefficiency. Pressure is controlled at the dry gas inlet and the mass flow rate is monitored using a mass flow meter. The saturator consists of a $\frac{3}{4}$ " coiled stainless steel tube that acts as a heat exchanger and contains horizontal sections which are half filled with water or ice. This method of saturation is beneficial as a long saturation path can be used and saturation occurs in separate sections which are reasonably thermally isolated, thereby reducing the latent heat loading on each subsequent section. The saturator efficiency can be determined by adding length to the saturation path and observing the difference in the generated dew point. The output dew point temperature is determined from the pressure and temperature at the output of the saturator. The temperature at the output is measured by a platinum resistance thermometer (PRT) placed in the air stream at the output of the generator. This assumes that the air and the liquid/solid surface are in thermal equilibrium. A minimum diameter of $\frac{1}{2}$ " is used for all tubing to minimise pressure drop throughout the system.

Centre for Metrology and Accreditation (MIKES), Finland:

The MIKES primary dew point generator, described in [23] is a single pressure generator. It uses partial recirculation and has the option to also use full recirculation as described in section 3.2. The full recirculation system was developed for use with low temperatures to prevent the build-up of frost in the pre-saturator. The full recirculation pump and the UUT are

in a thermally enclosed area above the rest of the generator. The generator consists of a pre-saturator, heat exchanger and final saturator. The pre-saturator consists of two vertical cylinders one of which is partially filled with water and the incoming air is allowed to bubble up through the water. When the system is operated below 0 °C the pre-saturator is dry. The main saturator consists of a stainless steel horizontal tube with an inner diameter of 26 mm and a vertical outlet cylinder. The saturator is half filled with water or ice. The saturation temperature is measured by two 100 Ω platinum resistance thermometers (PRTs). One PRT measuring the water or ice temperature and the other measuring the air temperature in the exit cylinder. Measuring both the air and water/ice temperature gives valuable information about the state of equilibrium. The two temperatures with associated uncertainties can be used to give a better estimate of the saturation temperature and to estimate the saturator inefficiency.

Van Swinden Laboratory (VSL), the Netherlands:

The primary dew point generator used at VSL, described in [19] is a single pressure (1-P) dew point generator that uses partial recirculation. It consists of a high and low temperature saturator, each in separate thermostatic baths for the low and high temperature ranges (-60 °C to 20 °C and 5 °C to 82 °C respectively). The low temperature unit consists of a copper heat exchanger and a gold plated copper saturator. The high temperature unit consists of a pre-saturator, a heat exchanger and a final saturator. The pre-saturator is made from stainless steel and glass and uses a piezo-driven oscillator to fill the pre-saturator with tiny water droplets that readily evaporate causing the gas to become nearly saturated with respect to the pre-saturator temperature. The final saturator is of a similar design to the low temperature saturator. The dry gas flow rate is controlled by a mass flow controller and the recirculation flow rate is measured by a mass flow meter. The pump is a centrifugal pump with three propellers driven by a shaft that is inserted into the housing by a vacuum tight seal that has been found to operate at high temperatures (above 100 °C) without breaking down or outgassing its components. The bearings in the pump use a relatively chemically inert lubricant. A number of ball valves are used for ease of operation. The valves are designed for use at high temperatures (rated to 290 °C), the wetted parts are made from stainless steel and the seat and stem are made from polyetheretherketone (PEEK) which is quite impenetrable to water vapour. In order to allow automation pneumatic actuators are used which can withstand temperatures up to 200 °C.

In 2009 the gold plated copper saturator was disassembled for inspection and dark spots on the gold surface were observed indicating corrosion [24]. This could be due to the original plating being too thin for the number of years of operation used, possibly due to the dimensions of the unit and the placement of the electrodes during electroplating. It could also be due to the expansion and contraction of the plating, under-plating and substrate, weakening the under-plating and/or the plating over the years of operation. After the inspection it was decided to machine a new saturator from stainless steel [24].

Bundesamt für Eich (BEV) / E+E Elektronik, Austria:

The Austrian national standard for humidity is maintained by E+E Elektronik on behalf of BEV, the national metrology institute of Austria [25]. The dew point generator described in [25] is a two pressure humidity generator. It consists of a pre-saturator with independent temperature control, a heat exchanger and two main saturation units. The saturation units and heat exchanger function as a condenser. In the pre-saturator the sample gas is supersaturated with respect to the condenser or final saturators. The condenser is at the temperature of the desired dew point and causes net condensation of water vapour until the gas is saturated with respect to the condenser temperature and the water vapour and condensate phases are in equilibrium. The saturators can also be used in an evaporative mode of operation and the pre-saturator can be bypassed for low frost points. Each saturator is machined from a single piece of stainless steel and contains a serpentine path and fins to encourage condensation. The saturators can be operated at a maximum pressure of 9400 hPa. The gas is then expanded using a heated needle valve which can also be bypassed in order to use the generator in a single pressure mode of operation.

Laboratory for Process Measurement (LPM), Croatia:

The LPM uses a high range dew point generator capable of generating humidities from 1 °C to 60 °C dew point and a low range generator with a range from -70 °C to 5 °C frost point, as described in [26]. The saturators were designed by MIKES and implemented in cooperation with LPM. Both generators are single pressure, single pass systems. Both systems consist of an initial humidifier, a pre-saturator, a heat exchanger and a final saturator. In the case of the low range generator the humidifier is at ambient temperature (usually 20 °C). A valve is used to allow the humidifier to be bypassed for low frost points where it's not necessary. The humidifier is connected in parallel with a coiled tube that provides enough resistance to flow so that roughly 50% dry air passes through the humidifier. The pre-saturator is a vertical

cylinder partly filled with water or ice. It is partially immersed in the liquid bath resulting in the pre-saturator being at an elevated temperature to the final saturator, resulting in gas that is supersaturated with respect to the final saturation temperature. Water vapour is either condensed or evaporated in the pre-saturator depending on the range of use. The gas is then cooled to the final saturation temperature in the coiled tube heat exchanger, causing excess water vapour to condense in the tube so that when it reaches the final saturator it is close to the desired output humidity. The final saturator is a box shaped vessel with a baffle plate inside it to increase the path length of the air flowing through it. It ensures final saturation of the gas with respect to the temperature of the saturator. The saturation temperature is measured by two platinum resistance thermometers (PRTs), one of which is inserted through a tube into the saturation chamber and measures the water or ice temperature. The tube has a small outwards air flow to minimize the stem conduction effect of the PRT. The other PRT measures the liquid bath temperature near the final saturator. The outlet tube which draws gas from the saturator to the UUT contains a coil so that any vapour that condenses in the outlet tube does so at a temperature near the saturation temperature making the output dew/frost point still near to the saturator temperature.

The high range generator is similar to the low range generator with some exceptions: The humidifier is located in a temperature controlled enclosure above the bath containing the dew point generator. Unlike the low range generator 100% of the dry stream of air flows through the humidifier and it is used throughout the range (with no option to bypass it). The heated enclosure heats the humidifier to a sufficient temperature to ensure that it saturates air to well above the final generated dew point temperature. Since the pre-saturator is now mainly used as a condenser it is fully immersed in the liquid bath. The heat exchanger continues to cool the gas to the final saturation temperature and as it does so excess water vapour condenses. The final saturation temperature is measured by two PRTs immersed in the liquid bath near the final saturator. Gas is drawn off from the high range saturator to the UUT by a straight vertical tube (with no coil).

Laboratory for Metrology and Quality (LMK), Slovenia:

The two primary dew point generators described in [17], designed and used at LMK, are single pressure generators with the option to be used in single pass, partial recirculation or full recirculation modes of operation. The system consists of a low range generator capable of generating dew/frost points from -50 °C to 20 °C and a high range generator for the 20 °C to 95 °C range. The high temperature generator consists of a pre-saturator a heat exchanger and

a final saturator while the low temperature generator consists of just a heat exchanger and saturator. The pre-saturator allows gas to bubble up through water bringing it closer to the saturation temperature. The final saturators are cylindrical and contain a path that moves inwards towards the centre of the cylinder. The path length of the low temperature saturator is approximately 0.8 m and 1.2 m for the high temperature saturator. Both units are made from brass and gold plated to prevent contamination of the water or ice and corrosion of the brass. The lid of each unit is made from stainless steel to allow welding of other stainless steel components to the unit, and is polished to prevent corrosion. Brass has significantly better thermal conductivity and more thermal mass than stainless steel which could potentially increase the performance of the saturator depending on the conditions of use.

The pump used for full recirculation is a diaphragm pump with a stainless steel body which reduces the main water vapour leakage area to the diaphragm itself. The diaphragm is made of ethylene propylene diene monomer (EPDM) which has a low water vapour transmission rate. The pump used for partial recirculation is a magnetically coupled centrifugal pump. The pump contains an impeller which is magnetically coupled to the driving motor rather than being directly driven by the motor via a shaft. This has the advantage of improved leak tightness and less risk of contamination since it avoids the use of seals where the shaft enters the pump housing. Different bushings and bearings for use in the centrifugal impeller were studied in order to avoid the use of lubricants which could contaminate the generator. The bearings used have been treated with an aggressive solvent to remove any lubricants and after two months of continuous operation the bearings showed no signs of wear. The pressure drop across the pump was found to be less than 100 Pa at different flow rates. All the inner parts were electropolished to reduce adsorption and desorption effects and were thoroughly cleaned with solvents to prevent contamination.

3.4. Theory

3.4.1. Calculating dew/frost point for a known pressure drop

The mole fraction of the gas in the saturator (at higher pressure than the UUT) can be calculated using Eq. 2.18 in terms of the saturator temperature T_s and pressure P_s ,

$$x = \frac{e(T_s) \cdot f(T_s, P_s)}{P_s}. \quad (3.3)$$

In a 2-P generator the gas is then expanded before reaching the UUT. In a 1-P generator a small pressure drop will occur between the saturator and UUT. The mole fraction will be equal to the mole fraction in the saturator if no water vapour is added to or removed from the gas between the saturator and UUT. The mole fraction can also be expressed in terms of the dew point at the point of measurement,

$$x = \frac{e(T_d) \cdot f(T_d, P_{uut})}{P_{uut}}, \quad (3.4)$$

where T_d is dew point temperature at the point of measurement and P_{uut} is pressure at the point of measurement.

For a 1-P generator; $T_s \approx T_d$ and $f(T, P)$ is not sensitive to small changes in temperature so assuming that the mole fraction at the point of realization is equal to the mole fraction at the point of measurement, Eqs. 3.3 and 3.4 can be combined to give;

$$e(T_d) = \frac{e(T_s) \cdot f(T_s, P_s) \cdot P_{uut}}{f(T_s, P_{uut}) \cdot P_s}.$$

In the case of a two pressure generator where $T_s \neq T_d$ the following arrangement of the formula can be used,

$$e(T_d) \cdot f(T_d, P_{uut}) = \frac{e(T_s) \cdot f(T_s, P_s) \cdot P_{uut}}{P_s}, \quad (3.5)$$

which takes into account the difference in the enhancement factors at the different pressures and saturation temperatures of the saturator and the point of measurement. The component $e(T_d) \cdot f(T_d, P_{uut})$ can be solved for T_d iteratively from Eq. 2.13 and 2.15. This is the equation that will be used to correct for pressure differences in the NML 1-P dew point generator as it is more correct than the previous approximated form and can continue to be used if the generator is operated in a two-pressure mode. Equations 2.13 and 2.15 are used and iteratively solved because their uncertainty is lower than other equations used to calculate dew point from water vapour pressure.

3.4.2. Calculating dry air flow for a given output (wet air) flow

The flow rate through a dew point generator is controlled at the dry air input to the generator so that the conditions of use for the mass flow controller are similar to the calibration conditions in dry air and to provide the necessary pressure drop across the mass flow controller. The mass flow rate after saturation is greater than the mass flow rate at the input due to the water vapour that is added to the gas. For low frost points this effect will be negligible. However, for high dew points the effect is significant. It is important that the flow rate through the reference hygrometer remains constant since its response is flow dependant. Therefore, the change in mass flow before and after saturation will be quantified.

The mass flow rate will be set at the dry air inlet by a mass flow controller which is calibrated for use with dry air, in units of ls/min. This is the number of litres of air passing per minute, at 293.15 K and 101.325 kPa, so if the gas being controlled is an ideal gas then the standard volumetric flow at the input $\Delta V_{stp\ In}$ can be converted to input molar flow rate $\Delta n_{T\ In}$ with the following equation,

$$\Delta n_{T\ In} = \frac{\Delta V_{stp\ In} P_{stp}}{R T_{stp}}, \quad (3.6)$$

where T_{stp} is standard temperature (293.15 K), P_{stp} is standard pressure (101.325 kPa) and R is the universal gas constant.

The output mass flow rate will be defined based on the number of chilled mirror hygrometers been supplied with air from the generator and the defined mass flow rate through each hygrometer. For the hygrometers used at NML the flow rate through each hygrometer is defined to be equal to 1 ls/min for frost points and 0.5 ls/min for dew points. This is ambiguous since 0.5 ls/min dry air has a different mass flow rate to 0.5 ls/min humid air, since the molar mass is not standardized as the temperature and pressure are. Additionally, the flow meter used to set the flow rate through the hygrometer during calibration will likely be calibrated for dry air and produce an error when used with humid air. This is of little importance, provided that the mass flow through the hygrometer stays approximately constant and an uncertainty is applied to measurements based on the variation of flow through the hygrometer. For calculations made in this thesis the discrepancy in mass flow rate due to the change in the molar mass of humid air is not significant. Additionally, the flow rate through the hygrometers is user-defined so for this work it will suffice to define the flow rate at the output based on a flow rate through each hygrometer of 0.5 ls/min regardless of the water vapour mole fraction. This results in the following equation for the molar flow rate at the output $\Delta n_{T\ Out}$,

$$\Delta n_{T \text{ Out}} = \frac{\Delta V_{stp \text{ Out}} P_{stp}}{R T_{stp}}, \quad (3.7)$$

where $\Delta V_{stp \text{ Out}}$ is the standard volumetric flow rate at the output.

The molar mass M of humid air is found from,

$$M = x \cdot M_{H_2O} + (1 - x) \cdot M_{air}, \quad (3.8)$$

where M_{H_2O} is the molar mass of H_2O .

The mass flow rate at the output $\Delta m_{T \text{ Out}}$ can then be found from,

$$\Delta m_{T \text{ Out}} = \Delta n_{T \text{ Out}} (M_{H_2O} \cdot x_{Out} + M_{air} (1 - x_{Out})). \quad (3.9)$$

Knowing the total output molar flow rate $\Delta n_{T \text{ Out}}$ and knowing the output mole fraction x_{Out} from Eq. 2.18, the molar flow rate of water vapour at the output $\Delta n_{w \text{ Out}}$ can be found from,

$$\Delta n_{w \text{ Out}} = x_{Out} \cdot \Delta n_{T \text{ Out}}. \quad (3.10)$$

The molar flow rate of dry air entering the saturator is equal to the molar flow rate of dry air exiting the saturator, so;

$$\Delta n_{air \text{ In}} = \Delta n_{air \text{ Out}} = \Delta n_{air}.$$

The molar flow rate of dry air Δn_{air} is found from,

$$\Delta n_{air} = \Delta n_{T \text{ Out}} - \Delta n_{w \text{ Out}}. \quad (3.11)$$

Knowing the molar flow rate of air entering the saturator and the mole fraction of air entering the saturator x_{In} , Eq. 2.17 can be rearranged to give an expression for the molar flow rate of water vapour entering the saturator $n_{w \text{ In}}$,

$$\begin{aligned} x_{In} &= \frac{n_{w \text{ In}}}{n_{w \text{ In}} + n_{air}}, \\ \frac{1}{x_{In}} &= 1 + \frac{n_{air}}{n_{w \text{ In}}}, \\ \Delta n_{w \text{ In}} &= \frac{\Delta n_{air} \cdot x_{In}}{1 - x_{In}}. \end{aligned} \quad (3.12)$$

Now the total molar flow rate at the input $\Delta n_{T \text{ In}}$ can be found,

$$\Delta n_{T \text{ In}} = \Delta n_{air} + \Delta n_{w \text{ In}}. \quad (3.13)$$

Equations 3.10, 3.11, 3.12 and 3.13 can now be combined to give an expression for input molar flow rate as a function of output molar flow rate,

$$\Delta n_{T In} = \Delta n_{T Out} \left(1 - x_{Out} + x_{In} \frac{1 - x_{Out}}{1 - x_{In}} \right). \quad (3.14)$$

This equation can now be combined with Eqs. 3.6, 3.7 to give the same expression in terms of standard volumetric flow,

$$\Delta V_{stp In} = \Delta V_{stp Out} \left(1 - x_{Out} + x_{In} \frac{1 - x_{Out}}{1 - x_{In}} \right). \quad (3.15)$$

Equation 3.15 can therefore be used to calculate input mass flow rate for a given output mass flow rate, provided that the input and output mole fractions are known. In many cases x_{In} is very small and can be considered negligible. If dry air is supplied to the input then Eq. 3.15 simplifies to,

$$\Delta V_{stp In} = \Delta V_{stp Out} (1 - x_{Out}). \quad (3.16)$$

The equation can be used to calculate the dry air mass flow for a given output mass flow rate.

3.4.3. Calculating the pressure correction due to the difference in altitude of the final saturator and the digital pressure meter

This difference in air pressure due to small changes in height ΔP is given by,

$$\Delta P = \rho g h, \quad (3.17)$$

where ρ is density, g is acceleration due to gravity and h is the difference in height.

The density will be calculated from the ideal gas law as,

$$\rho = \frac{PM}{RT}. \quad (3.18)$$

The molar mass of the humid air in the pressure measurement tubing is found from Eq. 3.8.

4. Design and simulation of the new NML saturator

4.1. Overview

The new NML primary dew point generator is intended to operate as a single pressure, single pass dew point generator with the possibility to modify it to operate in complete recirculation and/or partial recirculation. It is also intended that the generator will be capable of being used at pressures above atmospheric pressure so that in the future the generator could be tested at pressures up to five bars to determine the maximum pressure range that it could be operated at whilst maintaining suitable precision. However, it will initially be used only at near atmospheric pressure as a single pressure (1-P) generator.

The initial temperature range of operation is limited by the range of the chilled mirror hygrometer used to characterize the generator. The hygrometer is an MBW 373 HX with a range from -50 °C fp to 95 °C dp and is calibrated over a range from -40 °C fp to 90 °C dp. The thermostatic bath has a temperature range from -90 °C to 130 °C so the lower range of the generator can be extended to -90 °C fp in the future. The design considers effects that limit the precision at frost points as low as -100 °C as well as dew points approaching 100 °C in order to maximise the precision of the instrument and allow the widest operating range to be achieved in the future.

The generator consists of a pre-humidifier, pre-saturator, heat exchanger and final saturator, as shown in figure 4.1.

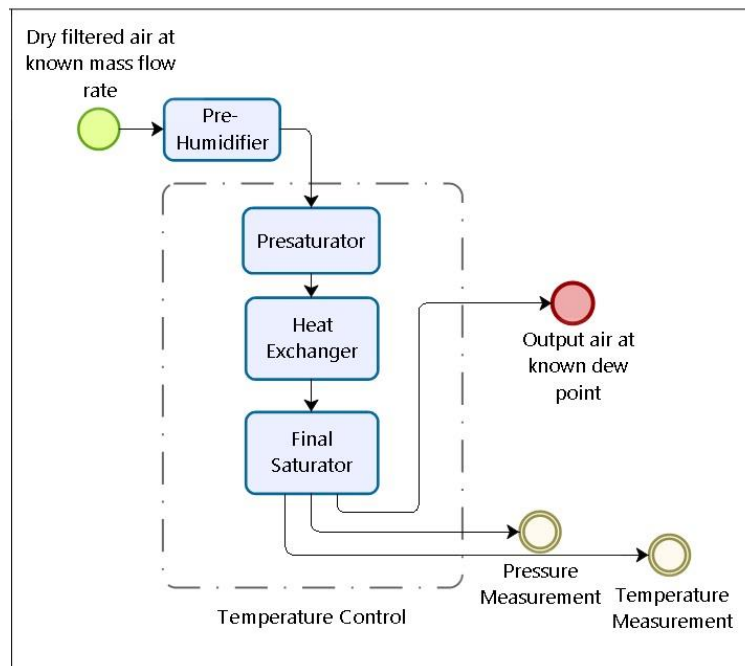


Figure 4.1: NML dew point generator overview schematic.

The pre-humidifier is heated for high dew points and can be bypassed for low dew/frost points. It conditions the air to be close to the final output dew point in order to reduce the latent heat loading on the pre-saturator and final saturator. The pre-saturator is immersed in the temperature controlled bath and conditions the air to be very near to the final dew point. The heat exchanger ensures that the temperature of the pre-saturated air is very close to the bath temperature. Final saturation of the gas occurs in the final saturator and the temperature and pressure of the gas is measured at this level of saturation in order to determine the output dew point temperature.

The design of a saturator should be such as to maximise the planar surface area of water or ice and to have the maximum path length of air flowing through the saturators. They are also designed to hold enough liquid so that they can be operated at dew points as high as 95 °C for a convenient amount of time without needing to be refilled. Since it is very important for the gas and condensate to be in thermal equilibrium and the temperature inside the saturator will be affected by thermal and latent heat loading; the saturator design should be optimized to provide sufficient heat exchange with the temperature controlled liquid bath. To investigate the proposed saturators' performance as heat exchangers each proposed design was simulated in order to analyse the thermal performance and flow properties. The saturator is designed to allow accurate temperature and pressure measurements to be made, in order to determine the dew point of the output gas. This should be achieved without compromising the leak tightness of the system. The validity of temperature measurement at different locations in the saturators, the temperature difference between the water/ice surface and the gas, and the temperature homogeneity in the saturators was investigated by computer simulation.

Several saturators were designed and compared in respect of the desired qualities mentioned. The cost of manufacture, the material properties and the implication of different combinations of saturators and pre-saturators was investigated. The reason for modelling different saturator designs is not just to determine the most potentially accurate saturator but also to find the design that will cause the least problems during fabrication and will be cost effective, without compromising the quality of measurements produced.

4.2. Calculations and modelling

4.2.1. Mass transport of H₂O, latent heat and rate of evaporation

An expression for the evaporation rate of H₂O can be used to find the rate of mass transport of H₂O, the rate of heat loss due to the latent heat of vaporization and the rate of volumetric water loss from the saturator. It will be necessary to determine these quantities in the designing of the saturator to ensure that the saturator will be fit for purpose. Some of these quantities will be needed for CFD simulation of the saturators.

The molar flow rate of water vapour at the output can be found from Eq. 3.10 and the molar flow rate of dry air can be found from Eq. 3.11. Knowing the molar flow rate of dry air and the mole fraction at the input, the molar flow rate of water vapour at the input can be found using Eq. 3.12. The rate at which moles of H₂O leave the saturator by evaporation $\Delta n_{w\text{ Sat}}$ is equal to the number of moles of H₂O leaving the saturator minus the number of moles of H₂O entering the saturator,

$$\Delta n_{w\text{ Sat}} = \Delta n_{w\text{ Out}} - \Delta n_{w\text{ In}}. \quad (4.1)$$

This can be combined with Eqs. 3.10, 3.11 and 3.12 to give an expression for $\Delta n_{w\text{ Sat}}$,

$$\Delta n_{w\text{ Sat}} = \Delta n_{T\text{ Out}} \left(x_{\text{Out}} - x_{\text{In}} \frac{1 - x_{\text{Out}}}{1 - x_{\text{In}}} \right). \quad (4.2)$$

The rate of mass of H₂O evaporated $\Delta m_{w\text{ Sat}}$ can be calculated by multiplying the rate of moles of H₂O evaporated by the atomic mass of H₂O,

$$\Delta m_{w\text{ Sat}} = M_{H_2O} \Delta n_{T\text{ Out}} \left(x_{\text{Out}} - x_{\text{In}} \frac{1 - x_{\text{Out}}}{1 - x_{\text{In}}} \right). \quad (4.3)$$

The rate of water volume lost from the saturator can be found by dividing the rate of mass evaporated by the density of water. This will be used to determine the volume of water needed in the saturators to allow continuous operation for a sufficient time.

The rate of heat absorbed due to evaporation in the saturator P_{latent} can be calculated by multiplying the rate of mass of H₂O evaporated by the latent heat of vaporization ΔH_{vap} of H₂O at the saturator temperature,

$$P_{\text{latent}} = \Delta H_{\text{vap}} M_{H_2O} \Delta n_{T\text{ Out}} \left(x_{\text{Out}} - x_{\text{In}} \frac{1 - x_{\text{Out}}}{1 - x_{\text{In}}} \right). \quad (4.4)$$

The latent heat of vaporization of water at different operating temperatures can be found using Eqs. 2.10 and 2.13.

4.2.2. Reynolds number

The Reynold's number is a dimensionless quantity and is the ratio of inertial to viscous forces in a fluid. It relates the fluid flow speed u , the characteristic length L (e.g. the diameter of a pipe), the density ρ and the dynamic viscosity μ of a fluid to the Reynold's number Re which can be used to predict the occurrence of turbulences in a fluid [27],

$$Re = \frac{uL\rho}{\mu}. \quad (4.5)$$

If the flow is in a circular tube the characteristic length L is equal to the inner diameter of the tube. For a square tube the hydraulic diameter can be calculated from the following equation [27];

$$L = \frac{4A}{p}, \quad (4.6)$$

where A is the cross sectional area and p is the perimeter of the square.

Combining Eqs. 4.4 and 4.5 gives;

$$Re = \frac{4uA\rho}{\mu p}. \quad (4.7)$$

For air at 20 °C the dynamic viscosity is approximately equal to $1.846 \times 10^{-5} \text{ kg m}^{-1} \text{ s}^{-1}$ and the density is approximately equal to 1.177 kg m^{-3} [28]. Equation 4.6 will be used to predict the existence of turbulence in the proposed saturator designs which is of interest as turbulence can be used to provide mixing which is necessary for efficient saturation.

4.2.3. Rayleigh number

The Rayleigh number, Ra , is a dimensionless quantity and it is the ratio of buoyancy forces to viscous forces and thermal diffusivity and is given by [29];

$$Ra = \frac{\beta \Delta T g d^3}{\nu \alpha_{th}}, \quad (4.8)$$

where β is the thermal expansion coefficient, ΔT is the temperature gradient, g is acceleration due to gravity, d is the layer thickness, ν is the viscosity of the fluid and α_{th} is the thermal diffusivity.

For fluids with a high thermal expansion coefficient, high temperature gradient and low viscosity, the Rayleigh number is high. If the fluid has a Rayleigh number above the critical value of approximately 1708 [29], the buoyancy forces are large enough that convective flow will occur. This equation can be used to predict the existence of convective flow in the final saturator which is of interest as it could provide mixing which is necessary for efficient saturation.

4.3. Simulations using Ansys

In order to test the performance of the proposed saturator designs they will be simulated in Ansys using a computational fluid dynamics (CFD) conjugate heat transfer (CHT) model, a model that is used to simulate heat transfer between solids and fluids.

The goal of the saturator is to output air that is completely saturated with water vapour at a stable measured temperature with known uncertainty. The uncertainty of the output dew point is directly related to the temperature stability within the saturator. The performance of the saturator as a heat exchanger and the temperature homogeneity within the saturator is therefore a very good indication of how well the saturator will perform as part of a dew point generator. Each saturator design will therefore be simulated to determine how well it conducts heat between the air flowing through it and the surrounding thermostatic liquid bath. The temperature homogeneity in the final section of the saturation path and the temperature difference between the air and the ice will also be investigated as these factors also directly affect the uncertainty of the output dew point.

Different temperature measurement methods will be investigated. A common method to determine the air temperature in the saturator is to measure the temperature in the liquid bath near the outlet of the final saturator. This method requires that the temperature difference between the output air and the liquid bath be characterized and incorporated into the uncertainty calculation. A more accurate method to measure the air temperature is to place a temperature probe directly in the stream of air leaving the saturator. This will require the probe wiring to be fed through a leak tight seal somewhere in the saturator or the outlet tubing. Another method will be tested which avoids the use of leak tight seals: A thermal well will be welded to the saturator near the outlet so that a temperature probe can be inserted into the thermal well to determine the output air temperature. The relative accuracy of each of these methods will be investigated through simulation.

A further complication in outputting air at a stable temperature near the bath temperature is due to the fact that net evaporation is occurring in the saturator resulting in heat loss from the saturator. In order to simulate evaporation a multiphase model would have to be used which would significantly complicate the simulation. Instead of simulating evaporation the latent heat resulting from saturation of air from the input dew point to the output dew point will be included as a negative heat flux on the surface of the water or ice inside the saturator. The simulation of evaporation will not be necessary as it would not be metrologically accurate enough to be meaningful for a primary humidity standard. In the following simulations the thermal performance will be investigated, which is directly related to the precision of the

humidity output of the saturators. It is unknown where in the saturation path most of the evaporation will occur. It is possible that an equal amount of evaporation will occur throughout the saturation path. It is also possible that more evaporation will occur at the input of the saturator since the less humid air at the input will cause an increased rate of evaporation and as the air travels along the path and approaches full saturation the rate of evaporation decreases relative to condensation. This will be assumed to be true for these simulations and will be investigated further by experiment with the final design. It is not known at what gradient the rate of evaporation will occur over. This will also be investigated by experiment with the final design but to simplify the model the latent heat loading due to evaporation will take place over an area of the saturation path near the input. This area will be kept constant throughout the comparison of the different designs so even though it is not identical to the situation in reality, it should still serve as a suitable comparison assuming that most of the saturation takes place over some area at the input of the saturator.

Another important factor is that sufficient mixing occurs within the saturator. If mixing does not occur, then the air closest to the water surface will be saturated while the air further from the water may not become saturated resulting in incomplete saturation of the output gas. Mixing can be increased by using recirculation (described in section 3.2) which causes an increase in the Reynolds number of the flow within the saturator. If the Reynolds number is high enough then the flow will become turbulent and mixing will be increased, thereby increasing the saturation efficiency. Another method to provide sufficient mixing is by using convective flow within the saturator. If the flow speed is low and the convective force is large, then the Rayleigh number for the flow will be high and turbulence will occur. However even without convective turbulence the presence of convection will still cause mixing of the gas. In each of the proposed saturator designs it is not expected that mechanical turbulence will occur due to the low flow speed of air and the large dimensions of the saturation path. However a Reynolds averaged Navier Stokes k- ω shear stress transport model (SST) will be used to test if any turbulence is created due to the geometry of the saturators. Streamlines will be plotted for each simulation to test if convective forces will provide sufficient mixing of air in the saturators at the desired flow rate. The range of flow rates at which mixing is sufficient will also be investigated for the selected final design.

4.4. Brief description of the CFD models used

Computational fluid dynamics is based on three fundamental principles: Conservation of mass, Newton's second law of motion and conservation of energy. CFD is based on experiments and theory and can also be used to validate experiment and theory so the three disciplines are interlinked. The fundamental principles that CFD is based on must be applied to a suitable model of flow which breaks down the overall flow into a number of different volumes or elements. This can be achieved using a finite control volume or an infinitesimal fluid element. A finite control volume can either be fixed in space with different molecules passing through it or moves with the fluid and always contains the same molecules of fluid. The fluid flow equations that are obtained by applying the fundamental principles to the volume are in integral form which can be manipulated to give the preferred partial differential form. If the equations are describing the control volume that is fixed in space the equations are said to be in the conservation form and if they describe the control volume that moves with the flow they are the non-conservation form of the governing equations. An infinitesimal fluid element is an infinitesimally small volume that is still large enough to contain a huge number of molecules so that it can be modelled as a continuous medium. By applying the fundamental principles to this model of flow, the governing equations are obtained directly in partial differential form and can be given in conservation or non-conservation forms as before.

The substantial derivative $\frac{D}{Dt}$ is frequently used in aerodynamics, it is the same as the total derivative with respect to time in calculus and is defined as [30];

$$\frac{D}{Dt} \equiv \frac{\partial}{\partial t} + \vec{V} \cdot \nabla = \frac{\partial}{\partial t} + u \frac{\partial}{\partial x} + v \frac{\partial}{\partial y} + w \frac{\partial}{\partial z}, \quad (4.9)$$

where t is the time elapsed, \vec{V} is the velocity vector and u , v and w are the velocity components along the x , y and z axes, respectively.

In Eq. 4.9, $\frac{\partial}{\partial t}$ is the local derivative; the time rate of change at a fixed point and $\vec{V} \cdot \nabla$ is the convective derivative; the time rate of change due to the elements motion where flow properties are spatially different.

The three governing equations of fluid dynamics are the continuity equation, the momentum equation and the energy equation. The continuity equation is based on the physical principal

that mass is conserved. By applying this principal to an infinitesimal fluid element that is moving with the flow (non-conservation form) the following equation is obtained [30];

$$\frac{D\rho}{Dt} = \rho \nabla \cdot \vec{V} , \quad (4.10)$$

describing the change in density due the motion of the fluid element.

The momentum equation is based on Newton's second law of motion. All of the forces on the fluid element must be considered. There are two types of force which act on the fluid element, body forces and surface forces. Body forces act at a distance directly on the volumetric mass of the fluid element and surface forces act directly on the surface of the fluid element. Surface forces can be caused by the pressure imposed by the surrounding fluid elements and the shear and normal stress acting on the element imposed by the surrounding fluid by means of friction. By taking account of all the forces acting on a moving infinitesimal fluid element Newton's second law gives [30],

$$\rho \frac{Du}{Dt} = -\frac{\partial p}{\partial x} + \frac{\partial \tau_{xx}}{\partial x} + \frac{\partial \tau_{yx}}{\partial y} + \frac{\partial \tau_{zx}}{\partial z} + \rho f_x , \quad (4.11)$$

where f_x is the body force per unit mass acting on the element, p is the pressure, τ_{xx} is the normal stress in the x-direction, τ_{yx} is the shear stress in the x-direction on a plane perpendicular to the y-axis and τ_{zx} is the shear stress in the x-direction on a plane perpendicular to the z-axis.

Equation 4.11 is the x-component of the momentum equation in non-conservation form. Along with the y and z components these equations are called the Navier-Stokes equations. The normal and shear stresses in Eq. 4.11 can be found from [30];

$$\tau_{xx} = \lambda \nabla \cdot \vec{V} + 2\mu \frac{\partial u}{\partial x} , \quad (4.12)$$

$$\tau_{xy} = \mu \left(\frac{\partial v}{\partial x} + \frac{\partial u}{\partial y} \right) , \quad (4.13)$$

$$\tau_{xz} = \mu \left(\frac{\partial u}{\partial z} + \frac{\partial w}{\partial x} \right) , \quad (4.14)$$

where μ is the molecular viscosity and λ is the bulk viscosity coefficient.

These equations are valid for Newtonian fluids where the sheer stress is proportional to the time rate of strain or velocity gradients. Combining these equations with Eq. 4.11 gives the complete Navier-Stokes equation in the x-direction.

The energy equation is based on the physical principal that energy is conserved [30],

$$A = B + C, \quad (4.15)$$

where A is the rate of change of energy within the fluid element, B is the net flux of heat into the element and C is the rate of work done on the element due to body and surface forces.

The rate of work done by body forces is equal to the product of the forces and the component of velocity in the direction of the force. The rate of work done by surface forces is found by adding all the pressure and stress forces on the element in each direction (x, y and z).

Combining the rate of work done by body forces and surface forces gives [30],

$$\begin{aligned} C = & \left[-\left(\frac{\partial(up)}{\partial x} + \frac{\partial(vp)}{\partial y} + \frac{\partial(wp)}{\partial z} \right) + \frac{\partial(u\tau_{xx})}{\partial x} + \frac{\partial(u\tau_{yx})}{\partial y} + \frac{\partial(u\tau_{zx})}{\partial z} \right. \\ & + \frac{\partial(v\tau_{xy})}{\partial x} + \frac{\partial(v\tau_{yy})}{\partial y} + \frac{\partial(v\tau_{zy})}{\partial z} + \frac{\partial(w\tau_{xz})}{\partial x} + \frac{\partial(w\tau_{yz})}{\partial y} \\ & \left. + \frac{\partial(w\tau_{zz})}{\partial z} \right] dx dy dz + \rho \vec{f} \cdot \vec{V} dx dy dz, \end{aligned} \quad (4.16)$$

The net heat flux into the fluid element is due to volumetric heating such as absorption and emission of radiation, and conductive heating due to heat transfer across the element due to thermal gradients. The net heat flux into the element is found by summing the volumetric and conductive heating in each direction (x, y and z) and rearranging knowing that heat transfer due to thermal conduction is proportional to the local temperature gradient [30],

$$B = \left[\rho \dot{q} + \frac{\partial}{\partial x} \left(k \frac{\partial T}{\partial x} \right) + \frac{\partial}{\partial y} \left(k \frac{\partial T}{\partial y} \right) + \frac{\partial}{\partial z} \left(k \frac{\partial T}{\partial z} \right) \right] dx dy dz, \quad (4.17)$$

where \dot{q} is the rate of volumetric heating per unit mass and k is the thermal conductivity.

The total energy of a fluid element is the sum of its internal energy and its kinetic energy. For a moving fluid element the time rate of change of energy per unit mass is given by the

substantial derivative of the energy per unit mass. Therefore the time rate of change of energy of the fluid element can be given by [30],

$$A = \rho \frac{D}{Dt} \left(e + \frac{V^2}{2} \right) dx dy dz , \quad (4.18)$$

where e is the elements internal energy per unit mass and V is the scalar velocity of the element.

Equations 4.16, 4.17 and 4.18 can be substituted into Eq. 4.15 to give the energy equation in terms of flow field variables, in non-conservation form. Combined with Eqs. 4.10 and 4.11 these are the three fundamental equations of computation fluid dynamics.

The purpose of the simulation of the proposed saturators is to determine their performance as heat exchangers. This involves simulating heat transfer between solid and fluid domains meaning that a conjugate heat transfer model must be used. The heat transfer in a solid is due only to conduction and is modelled by Fourier's law [31],

$$q = -k \nabla T , \quad (4.19)$$

where q is the local heat flux density, k is the thermal conductivity and ∇T is the temperature gradient.

For time dependant problems the heat transfer by conduction through solids can be modelled by the transient form of the heat equation [31],

$$\rho C_p \frac{\partial T}{\partial t} = \nabla \cdot (k \nabla T) + Q , \quad (4.20)$$

where Q is the heat generated.

In a fluid convection can be a significant means of heat transfer as well as conduction. Heat can also be generated by viscous effects or pressure effects as modelled by the following transient equation for heat transfer in a fluid [31],

$$\rho C_p \frac{\partial T}{\partial t} + \rho C_p u \cdot \nabla T = \alpha_p T \left(\frac{\partial p_A}{\partial t} + u \cdot \nabla p_A \right) + \tau : S + \nabla \cdot (k \nabla T) + Q , \quad (4.21)$$

where α_p is the thermal expansion coefficient, p_A is the absolute pressure, τ is viscous stress tensor and S is the strain rate tensor.

Equation 4.21 models heat transfer in a fluid by accounting for the rate of change of temperature, the heat transferred by convection, the heat generated due to changes in

pressure, the heat generated due to viscous heating, the heat transferred by conduction and the heat added to the system, respectively.

Slight temperature differences in a compressible fluid can cause natural convection. This is modelled by accounting for changes in density due to the temperature field in the momentum equation (Eq. 4.11). The pressure and body force components are rewritten as [32],

$$-\frac{\partial p'}{\partial x} + (\rho - \rho_0)g , \quad (4.22)$$

Where ρ_0 is the operating density and $p' = p - \rho_0 g x$.

This model assumes constant density and is suitable if the density gradients are small.

4.5. Design and simulation of final saturator

A number of parameters will be kept constant throughout the simulations of the alternative saturator designs and a number of parameters which give an indication of the performance of the saturators will be measured for each design and compared. Ansys AIM Academic is the software package that will be used to run the simulations. A conjugate heat transfer model as described in section 4.4 will be used. A buoyancy model will also be used as small temperature differences within the saturator are expected to cause mixing due to the buoyancy effect. This effect will be underestimated in the simulation since a further buoyancy effect will take place due to the fact that the humid air at the water surface will be less dense than any less humid air above it and the evaporation of water will not be simulated. A laminar flow model will be used since the Reynolds number for the flow is low, so turbulence is not expected. The run time at 95 °C will also be calculated for each design at a common maximum water level using Eq. 4.3. The value will be a conservative estimate since in reality a pre-humidifier will also be used.

The parameters that will be chosen and remain constant in the comparison of designs for the final saturator are listed in table 4.1:

Table 4.1: Common parameters for CHT comparison of final saturators

Parameter	Symbol	Value
Water level		10 mm (40 mm air path height)
Bath temperature	T_{bath}	95 °C
Input air temperature	$T_{air\ in}$	95 °C
Input air dew point	$T_{d\ in}$	94 °C dp
Latent heat loading per unit time	P_{latent}	-2.32 W
Area of latent heat flux		0.0096 m ² (at the input)
Air flow rate		0.5 ls/min
Air outlet pressure		101325 Pa
Bath flow rate		0.03 kg/s
Bath outlet (ambient) pressure		101325 Pa
Operating density		1.135 kg m ⁻³
Acceleration due to gravity	g	9.8 m/s
Number of elements		1 x 10 ⁶

The number of significant figures given in table 4.1 is inconsistent but the output results are not equally sensitive to all input parameters. Also, the main purpose of the simulations is to give a comparison of different saturator designs and a conservative estimate of performance rather than giving absolute results.

The water level is set at 10 mm in depth out of the total 50 mm of height in the saturation path. For most dew points this water level gives a convenient run time so it is likely to be a commonly used water level during use. When a final design is chosen the effect of varying the water level and flow rate will be further investigated to choose a suitable range of operation.

The bath temperature is set to 95 °C to simulate the generation of dew points of approximately 95 °C. This temperature is chosen as it is the maximum temperature that the generator may operate at and is the most challenging set point to achieve complete saturation. The working range of the generator will be chosen based on tests after

construction and will likely not extend to 95 °C. However 95 °C dew point generation will be simulated to see how the saturator will perform at a demanding dew point for latent heat loading and to choose a design based on these conditions. The bath water will flow from bottom to top to simulate an upwelling bath such as the one that generator will be used in. The direction of the bath liquid flow will have an effect on the temperature gradients, the efficiency of the heat exchanger and possibly on the efficiency of the saturators.

The input air temperature is set to 95 °C since the simulation is of the final saturator so the air will have been passed through the pre-saturator and heat exchanger by this point, making it very close to the bath temperature. This input air will be at 94 °C dew point. This is chosen because according to simulations of the pre-saturator designs; the pre-saturator should saturate the air to within 0.2 °C dp of the final dew point. The pre-saturator may perform worse in reality due to factors that will not be simulated however it should also perform significantly better in reality due to the use of the heated pre-humidifier that was not accounted for in the simulation. Therefore, an input dew point of 94 °C to the final saturator is a reasonably conservative test of the final saturator's performance. The effect of the increase in dew point of 1 °C dp will be simulated by applying latent heat loading (found from Eq. 4.4) to an area of the water surface, as described in section 4.3.

The mass flow rate of air through the saturator will be set to 0.5 ls/min as this will be a common flow rate in operation due to the fact that the reference chilled mirror hygrometers in use usually operate at 0.5 ls/min for dew points, and are calibrated at this flow rate. In order to be simulated this will be converted to units of kg/s using Eqs. 3.6 and 3.9. Different mass flow rates will be simulated in the final design to determine the appropriate range of use.

The air outlet and the bath outlet pressure are set to atmospheric pressure.

The operating density is used to simulate the buoyancy effect and is taken as the density of air near ambient conditions. The density at 95 °C dp differs from this value but since the purpose of the simulation is to provide a comparison this value held constant will suffice. For future simulations the operating density can be found from Eqs. 3.17 and 3.18 from the mole fraction of water vapour at the dew point in question and the temperature and pressure of the gas.

The most important measurements that will be made in each simulation include temperature measurement of a platinum resistance thermometer (PRT) in the circulating air flow at the output of the saturator T_{air} , temperature measurement of a standard platinum resistance thermometer (SPRT) immersed in the liquid bath near the output of the saturator T_{bath} , temperature measurement of a PRT inserted into the thermal well near the output T_{well} , measurement of the temperature uniformity of an area of water surface near the outlet

$\Delta T_{water\ final}$, temperature measurement of different areas of the water surface $T_{water\ 1,2,3}$ where approximately the first $\frac{1}{4}$ of the total surface area is not measured and the final area is divided evenly into $T_{water\ 1,2,3}$ with $T_{water\ 3}$ been the water surface near the outlet. The first $\frac{1}{4}$ of the path is not measured as this is where the latent heating is applied.

The PRTs will be represented by a stainless steel cylinder of 3 mm diameter and 40 mm height, which are the dimensions of the sensing element capsules of the PRTs that will be used. For the simulation, the cylinder will be solid stainless steel while in reality the probe will be a platinum resistive sensing element housed in a stainless steel capsule. Self-heating of the PRTs will not be simulated as the reason for simulating the PRTs is not to analyse temperature measurement uncertainty but to demine the effect of measuring at different locations and the relative difference to the condensate/vapour temperature at different locations. The SPRT will be represented by a stainless steel cylinder of 7 mm diameter and 40 mm height, similar to the diameter of the sheath and the height of the sensing element of the SPRT that will be used. The locations of these measurements will be shown in diagrams for each saturator design.

The temperature T_{air} will be taken to be the most accurate approximation of the output air temperature and so for each simulation its difference from T_{well} and T_{bath} will be found as $\Delta T_{well-air}$ and $\Delta T_{bath-air}$ respectively. The water temperature must also be in equilibrium with the air-vapour mixture, otherwise the saturation efficiency is affected. For example if the water temperature is lower than the air temperature then the air cannot be saturated with respect to the air temperature. Therefore the difference between $T_{water\ final}$ and T_{air} will be found as $\Delta T_{water-air}$ for each simulation. The water surface area A_{water} will also be measured for each design as a greater surface area will increase the likelihood of complete saturation. The temperature of the thermostatic bath water at the output $T_{bath\ out}$ will be measured as it may affect other measured parameters if a large temperature gradient is present and it may indicate if a greater flow rate of temperature controlled bath water is needed.

The mesh resolution will be set to the highest possible value and the number of elements and the number of nodes will be recorded for each simulation.

4.5.1. Spiral design

Figure 4.2 shows a computer-aided design (CAD) model of the saturator design that will be referred to as the spiral design.

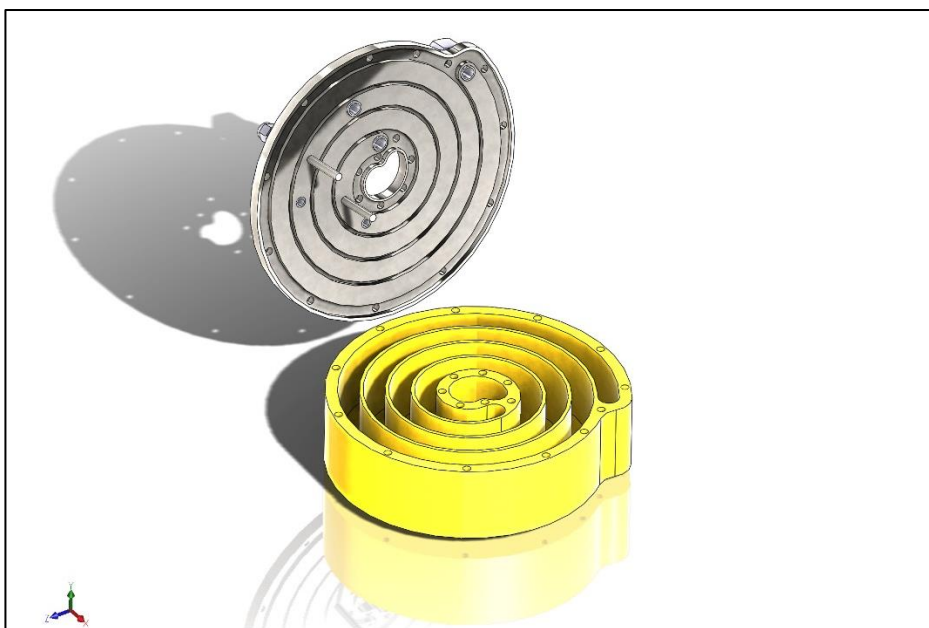


Figure 4.2: Image a of CAD model of the spiral saturator design.

This design consists of a path of approximately 1.9 m in length, in a spiral shape going from the outside to the centre of the saturator. The saturator has a hole in its centre which improves thermal contact with the bath, allows tubing to be fed through it and allows temperature measurements to be made near the outlet of the saturator. The base can be machined from brass and the lid can be machined from 316 stainless steel. Brass is chosen for the base because of its machinability and high thermal conductivity and thermal mass. Brass will corrode in water so must be plated with a corrosion resistant material like gold. 316 stainless steel is used for the lid to allow welds to be made to tubing and other components. The lid will also be electropolished to improve its corrosion resistance and to undo any damage and oxidation that may occur during welding. The lid will be bolted to the base at a number of points around the outside walls of the saturator. An indium gasket made from 0.7 mm diameter indium wire will be used to create a seal between the base and lid. The surface of the lid and base are precision machined so both surfaces are very flat, making a seal with high leak tightness possible. The walls creating the spiral path can be sealed using the same indium gasket material however this is optional since the pressure drop across the saturator is negligible so very little air will pass through the cracks where the lid meets the base due to the tight fitting lid. If the saturator is to be used at significantly higher flows rates and elevated pressures the sealing of the walls of the path may become necessary.

The dimensions and internal structure of the saturator are chosen in order to maximize the path length of the gas flowing through it and also to allow it to fit comfortably in a bath with a cylindrical working volume of diameter 320mm and height 500 mm. The benefit of this design is that the gas is forced to follow a minimum path length of 1.9m and the path is wide and tall enough (17 mm x 50 mm) that for a low flow rate (1 to 3 ls/min) the flow speed will be low allowing convective mixing to occur within the saturation path. The fact that the saturation will occur on a single consistent path means that the temperature and dew point of the gas can be monitored at intermediate points along the path and used to estimate the saturation efficiency. As mentioned previously, the design also includes thermal wells inserted through the lid into the saturation path, at the midpoint of the path and at the end of the path near the outlet of the saturator.

The CAD model was simplified for the simulation. The geometry will be effectively the same without needless complexities that are not expected to affect the simulation results. The model used for simulation is shown in figure 4.3.

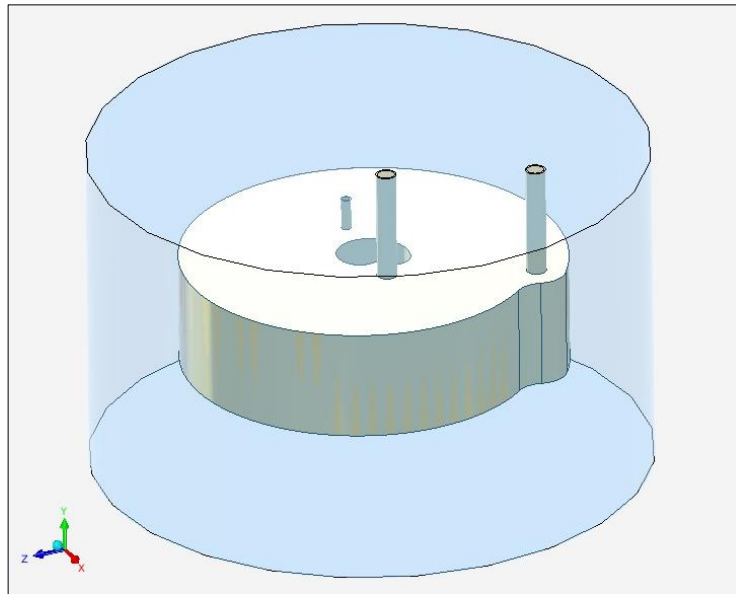


Figure 4.3: CAD model of spiral saturator used for simulations.

The CAD model used for simulations has the same dimensions as the detailed CAD model except that it is a solid part (not a base and lid), there are no holes for fixings and the only attachments on the saturator are two pieces of ½" tubing at the input and output and one thermal well near the output. A specified level of water is also added in the interior of the saturator. Figure 4.4 shows an image of the streamlines in the spiral saturator plotted as a result of the simulation.

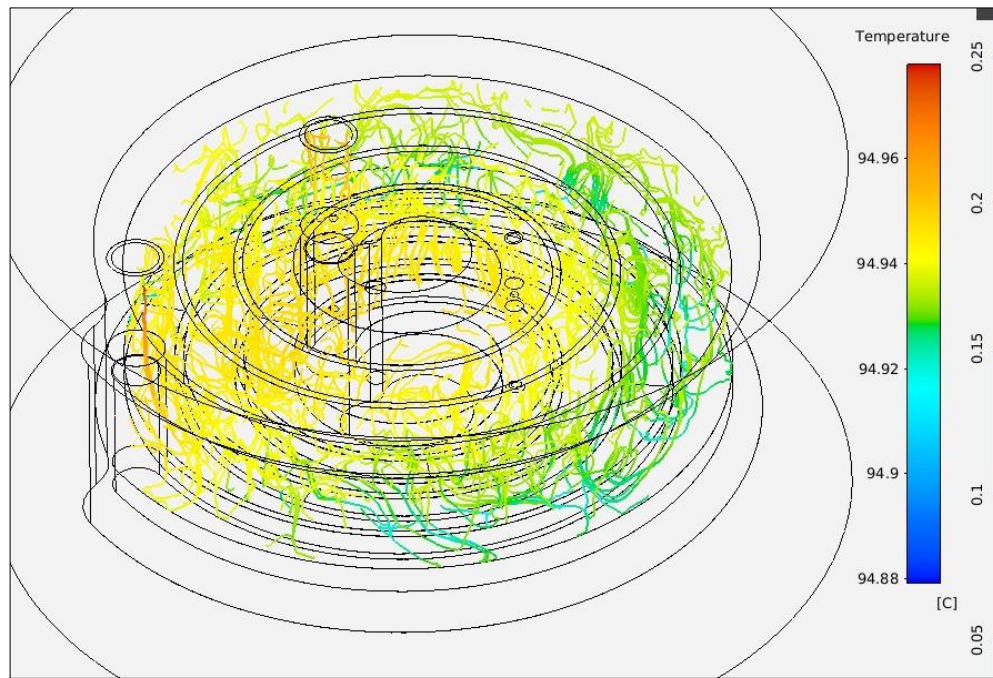


Figure 4.4: Streamlines representing the path taken by air molecules and air temperature within the spiral saturator design when used as a final saturator.

Figure 4.4 shows that sufficient mixing is taking place within the saturator due to the random direction of the streamlines. The streamlines can also be seen to travel from the bottom to the top of the saturator regularly, indicating that sufficient mixing will take place under these conditions. This can also be seen in figure 4.5.

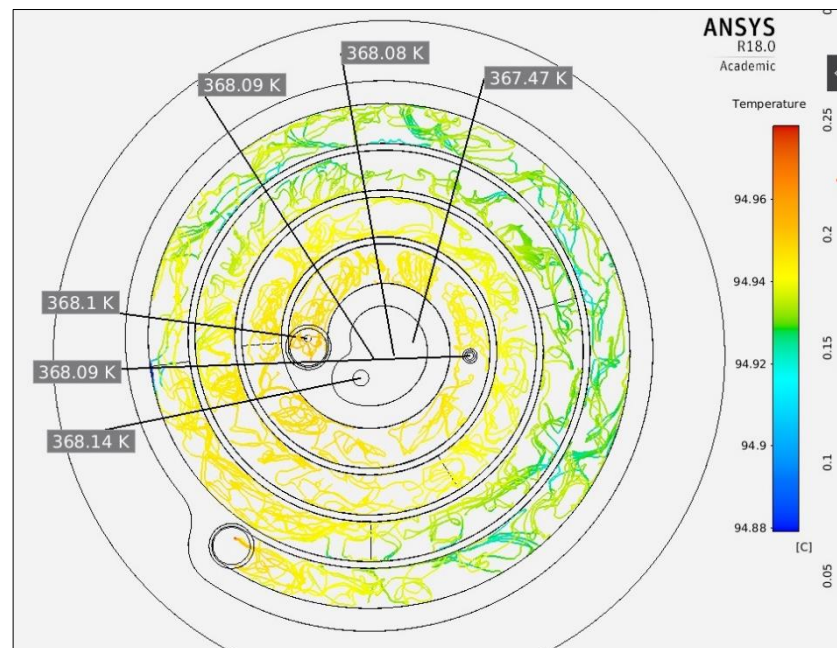


Figure 4.5: Plan view of streamlines in the spiral saturator when used as a final saturator.

Figure 4.5 also shows that no laminar flow occurs in the saturation path and the streamlines follow random directions throughout the flow path. It also shows good temperature

uniformity of the air in the final section of the saturation path with a variation of less than 0.01 °C. The temperature homogeneity of the water surface is shown in figure 4.6.

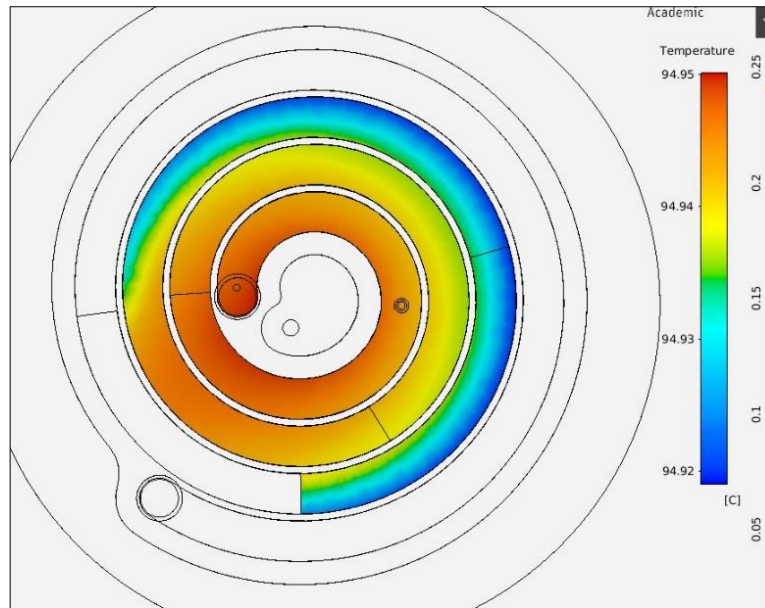


Figure 4.6: Temperature contour of the water surface in the spiral saturator when used as a final saturator.

Figure 4.6 shows that there is high temperature uniformity particularly in the final section of the saturation path. The effect of evaporative cooling can be seen as cold areas on the outside of the spiral. The initial area of the path is not shown in the contour as this is the area where the latent heat loading is placed and it would reduce the resolution of the contour. The temperature increases fairly steadily, however there are some areas where temperature increases and then decreases slightly before continuing to increase. The actual temperature distribution will vary from this contour due to the way that the latent heat of vaporization was included in the model. It is not known where most evaporative cooling will occur or on what gradient it will occur along the saturation path. This can be investigated by experiment with the final design and compared to the simulation.

The measured parameters of this simulation are summarized in section 4.5.4.

4.5.2. Square design

The square design was considered as it was thought that it may be cheaper to produce as it would require less materials and could be fabricated from stainless steel sheet metal, rather than been machined from a single piece of metal. It was also considered that it would fit better inside an alternative thermostatic bath before the bath with circular working volume was chosen. Figure 4.7 shows a CAD model of the square design.

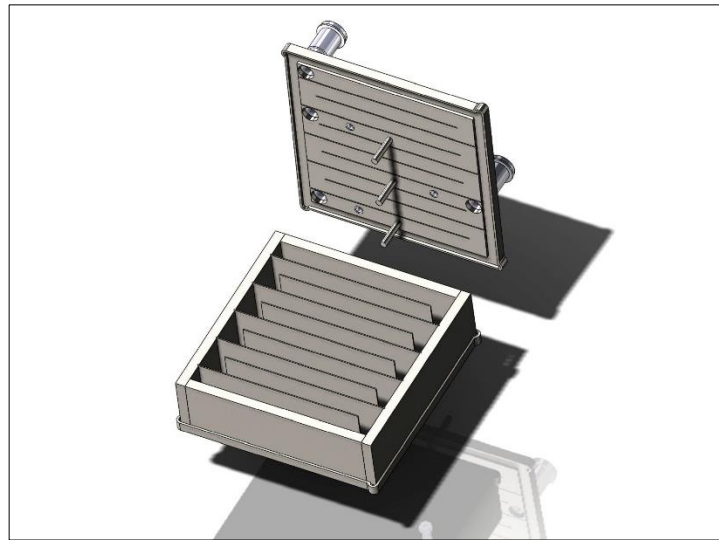


Figure 4.7: Image of a CAD model of the square saturator design.

In this design the walls and the base of the unit can be cut from sheet metal and welded together and the lid and top surface of the base could be machined to produce a flat surface to create a seal. The unit contains a serpentine path creating a path length of approximately 1.9 m.

The CAD model was simplified for simulation and the input parameters were identical to the ones given in table 4.1. The SPRT will not be simulated for the square design as there is no convenient area to place it for accurate measurement of the bath temperature. Instead the liquid bath temperature will be estimated as the input temperature of the bath liquid.

Figure 4.8 shows an image of the streamlines produced by the simulation.

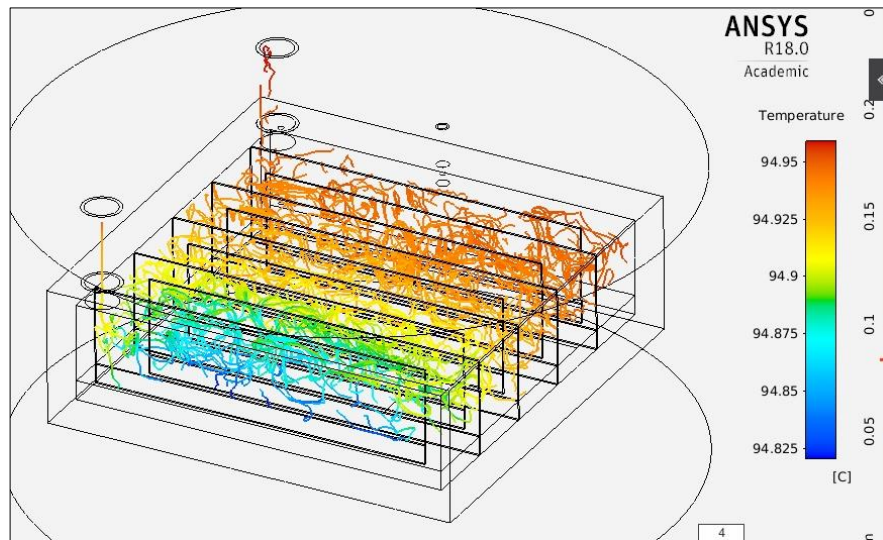


Figure 4.8: Image of streamlines produced by simulation of the square saturator.

It can be seen from figure 4.8 that sufficient mixing occurs and the motion of the streamlines is fairly random. This can also be seen in figure 4.9.

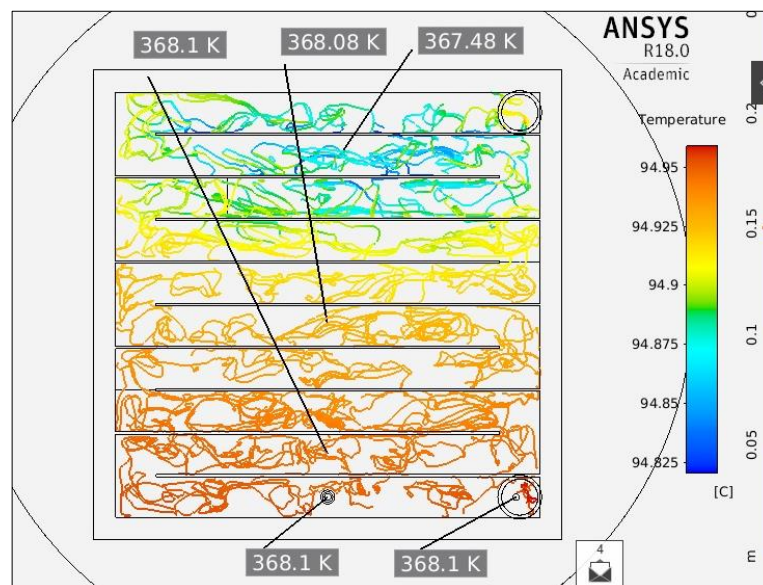


Figure 4.9: Plan view of the streamlines in the square saturator.

Figure 4.10 shows a temperature contour of the water surface inside the square saturator.

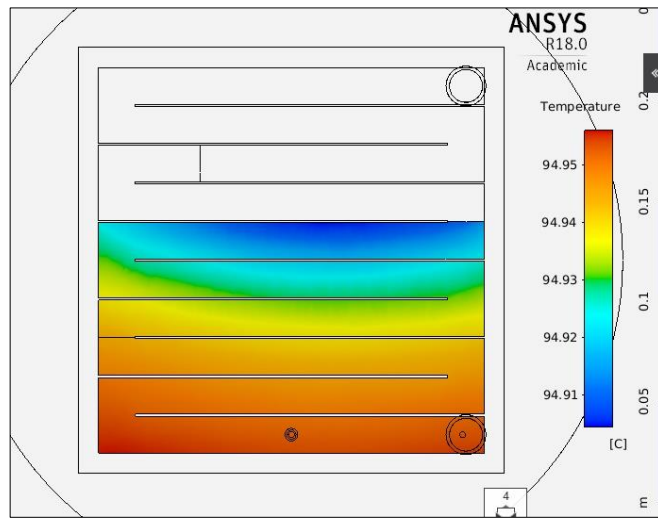


Figure 4.10: Temperature contour of the water surface in the square saturator.

This temperature contour shows good temperature homogeneity of the water surface, comparable to that of the spiral saturator in figure 4.6. The temperature gradient is visible due to the latent heat loading near the input of the saturator and the area near the input is not shown in the contour in order to improve the resolution near the output.

4.5.3. Circular design

The circular saturator was designed as a simplified saturator to be used as a pre-saturator to reduce the cost of fabrication. It will however be simulated as a final saturator as well as a pre-saturator to test how it performs under both conditions. Figure 4.11 shows a CAD model of the pre-saturator.



Figure 4.11: Exploded view of a CAD model of the circular saturator design.

This design can be fabricated from a piece of 8 inch diameter tubing, 80 mm diameter tubing and sheet metal. It has a hole in its centre to allow tubing and a temperature probe to be fed through it. It also contains a baffle plate to prevent laminar streamlines and a thermal well near the output to allow accurate measurement of the vapour/condensate temperature.

The internal volume has a height of 60 mm so the unit will be filled with 20 mm of water during simulation in order to be consistent with the other units which have a height of 40 mm in the airflow path. All other parameters are the same as the ones given in table 4.1.

Figure 4.12 shows the streamlines generated by the simulation.

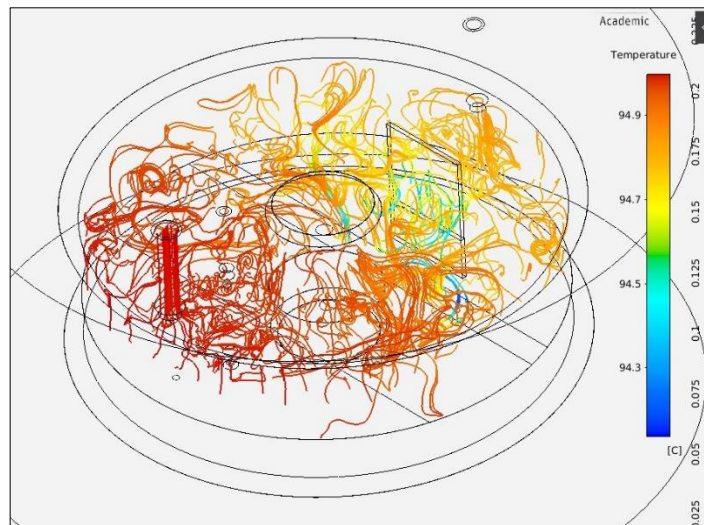


Figure 4.12: Image of the streamlines produced by the simulation of the circular saturator.

Figure 4.12 shows that sufficient mixing occurs in the circular saturator and that the motion of the streamlines is reasonably random as can also be seen in figure 4.13.

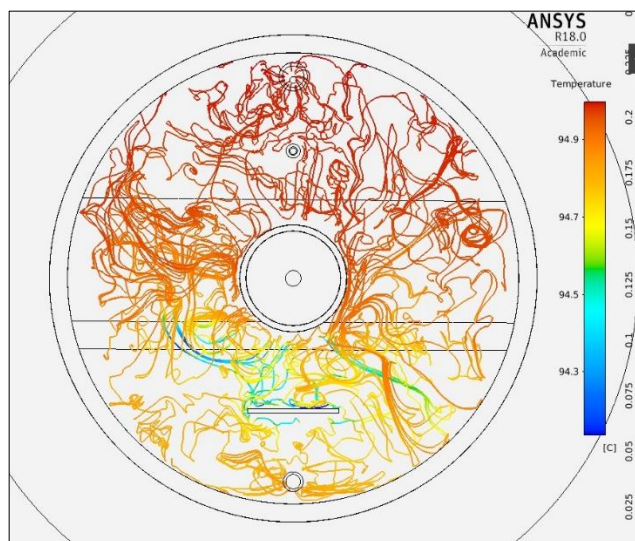


Figure 4.13: Plan view of the streamlines in the circular saturator.

Figure 4.14 shows a temperature contour of the water surface in the final section of the circular saturator.



Figure 4.14: Temperature contour of the water surface in the circular saturator.

Figure 4.14 only shows the temperature contour of the water surface near the output of the circular saturator as due to its geometry the latent heating at the input caused a large temperature gradient at the midpoint of the saturator causing reduced resolution near the outlet where the stability is improved. This contour shows good uniformity in the area near the outlet of the circular saturator. It also shows that the thermal well is in a good position to approximate the temperature at the output. Because there is no path in this design there is no way to guarantee that all of the output air has had sufficient temperature conditioning.

4.5.4. Results of final saturator comparison

A number of calculations were performed as described in section 4.5. Table 4.2 shows a summary of the values calculated in the simulation of the final saturator designs.

Table 4.2: Results of the final saturator comparison

	Square saturator	Spiral saturator	Circular saturator
Quantity	Value (°C)	Value (°C)	Value (°C)
T_{air}	94.952	94.948	94.989
T_{well}	94.948	94.944	94.988
T_{bath}	n/a	94.993	95.000
$T_{water\ 3}$	94.948	94.943	94.988
$T_{water\ 2}$	94.927	94.934	94.894
$T_{water\ 1}$	94.331	94.325	93.308
$\Delta T_{well-air}$	0.004	0.004	0.001
$\Delta T_{bath-air}$	-0.036	-0.045	-0.011
$\Delta T_{water-air}$	0.004	0.005	0.001
$\Delta T_{water\ final}$	0.017	0.014	0.030
A_{water}	0.035269	0.029773	0.030322
$T_{bath\ out}$	94.976	94.983	94.981

The results of the simulation show that the circular saturator is the best heat exchanger of the three saturators as it brings the temperature of the output air closest to the bath temperature. It also has the lowest temperature difference between the air and water surface and thermal well. This could be due to the low flow speed in the flow path. The spiral saturator has the best temperature homogeneity of the water surface near the output. Because the humidity depends on the air/condensate temperature not the bath temperature and the uncertainty of the output dew point depends on the stability of the final saturator this makes the spiral design the best choice for a final saturator, although all of the saturators performed similarly. The spiral saturator also has the advantage over the circular saturator of being able to measure temperature or dew point at different points along the path length in order to determine the saturator efficiency experimentally. It was also found that the square design

would be more expensive to fabricate compared to the spiral design giving it little advantage over the spiral design.

The PRT directly measuring the output air temperature is assumed to be the most accurate estimate of the output dew point temperature. The results show that the maximum temperature difference between the PRT in the thermal well and the PRT directly in the air flow is 4 mK. The temperature difference between the SPRT in the liquid bath and the PRT in the air flow can be as high as 45 mK showing that the thermal well is the best method to estimate the saturation temperature without compromising the leak tightness or simplicity of the saturator.

4.6. Design and simulation of pre-saturator

The pre-saturators will be simulated using the same input parameters as the final saturators shown in table 4.1 except the input air temperature will be set to ambient at 20 °C and the input dew point will be changed from 94 °C dp to -50 °C fp meaning that the latent heat loading will change from 2.32 W to 12.49 W as calculated from Eq. 4.4. In reality at 95 °C dp the pre-humidifier will be used reducing the loading on the pre-saturator for better accuracy however the simulation will be carried out with dry air to observe the worst case scenario and serve as a comparison and validation of the different designs.

4.6.1. Spiral pre-saturator

The design of the spiral pre-saturator is identical to the spiral saturator except some connections to the lid could be removed. If the spiral design is used for the pre-saturator and final saturator then from a manufacturing point of view it would mean that two units would be machined rather than one thereby saving costs, however the materials for the spiral saturator are so expensive that a simplified stainless steel design could still reduce the cost depending on the fabricator used.

The streamlines generated in the simulation of the spiral pre-saturator are similar to that of the spiral saturator and show that sufficient mixing is taking place. Figure 4.15 is a temperature contour of the water surface in the spiral pre-saturator.

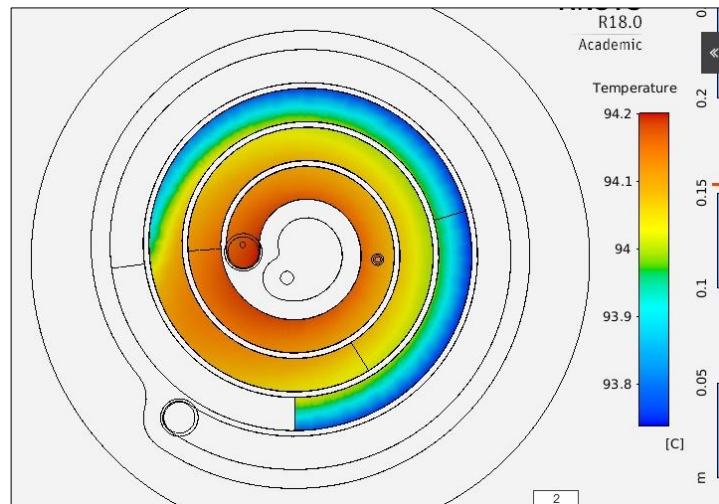


Figure 4.15: Temperature contour of the water surface in the spiral pre-saturator.

This contour is similar to figure 4.6 for the spiral saturator except the inhomogeneity is much larger due to the increased latent heat loading. The inhomogeneity is still reasonable considering that this is just the first stage of saturation and in reality a pre-humidifier will be used before this stage further reducing the latent heat loading on the pre-saturator. Only part of the water surface is shown in order to improve the resolution of the contour near the end of the saturation path.

4.6.2. Square pre-saturator

If the square saturator is used then a similar design will be used for the pre-saturator except it will have to be smaller than the final saturator in order to allow tubing to enter the bath and reach the final saturator. It will also be simplified since it is not the final stage of saturation. Figure 4.16 shows the CAD model of the square pre-saturator.



Figure 4.16: Exploded view of the CAD model of the square pre-saturator.

The square pre-saturator does not contain a path, instead it only contains a baffle plate to prevent laminar streamlines. Figure 4.17 shows the streamlines generated during the simulation.

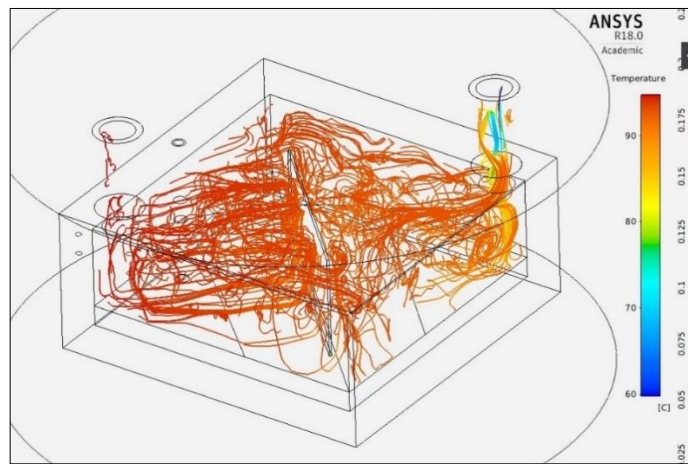


Figure 4.17: Streamlines generated during simulation of square pre-saturator.

Figure 4.18 shows a plan view of the streamlines generated during the simulation.

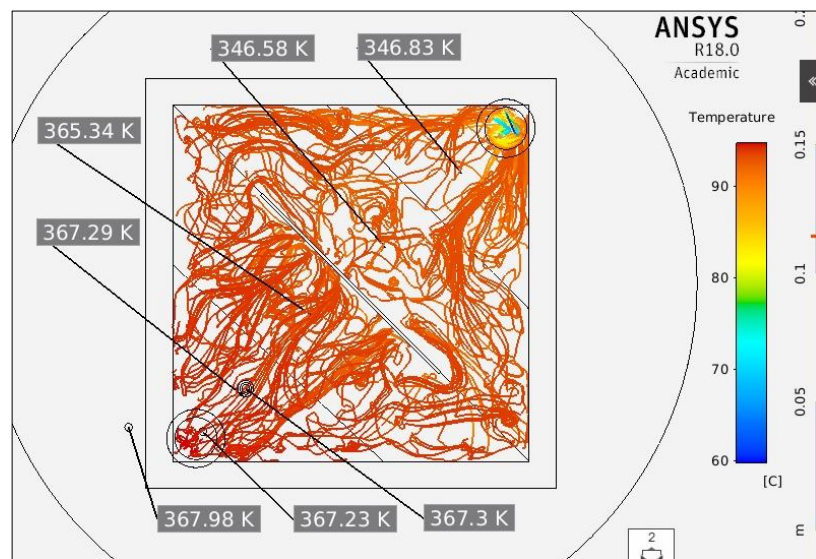


Figure 4.18: Plan view of the streamlines generated during simulation of square pre-saturator.

Figure 4.17 and 4.18 show that sufficient mixing occurs in the square pre-saturator. They also show that some convective mixing occurs in the final section of the saturator probably due to a temperature effect of the baffle plate. Figure 4.19 shows a temperature contour of the water surface in the final section of the square pre-saturator.

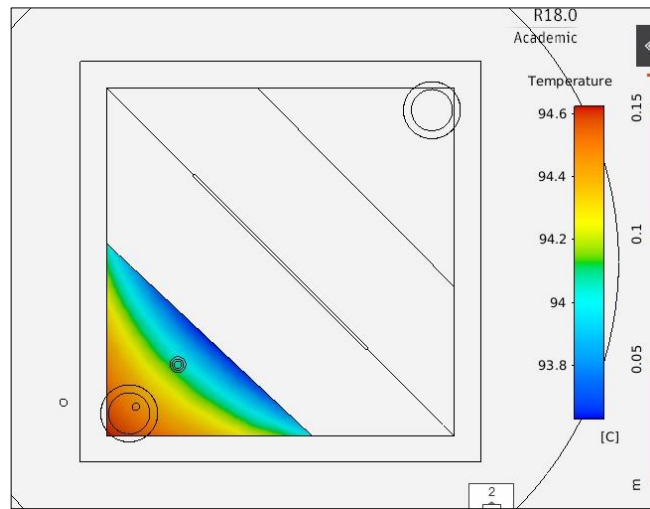


Figure 4.19: Temperature contour of the water surface near the output of the square pre-saturator.

The temperature contour of only the water surface near the output is shown to improve the resolution near the output. This contour shows less temperature homogeneity compared to the spiral pre-saturator due to the smaller size of the square pre-saturator.

4.6.3. Circular pre-saturator

The design of the circular pre-saturator is described in section 4.5.3. Figure 4.20 shows the streamlines generated during the simulation of the circular pre-saturator.

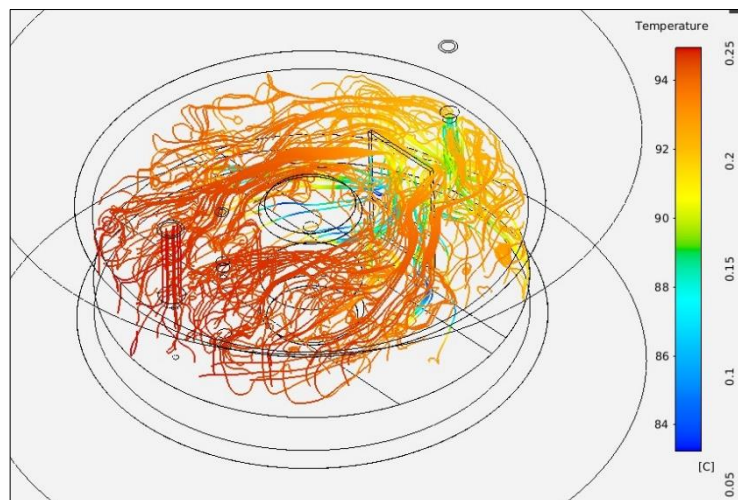


Figure 4.20: Streamlines generated in the simulation of the circular pre-saturator.

Figure 4.21 shows a plan view of the streamlines generated in the simulation.

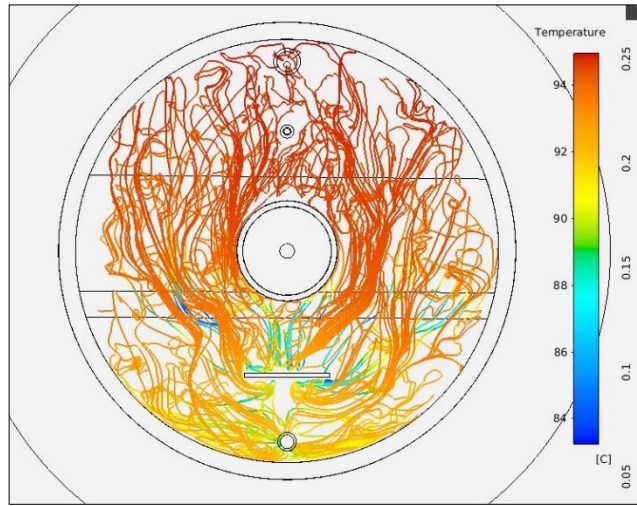


Figure 4.21: Plan view of streamlines generated in the simulation of the circular pre-saturator.

Figure 4.20 and 4.21 show that the flow is more laminar and directional than it was in figure 4.12 and 4.13 where the circular saturator is used as a final saturator (with less latent heat loading). This could be due to the increased pressure gradient, encouraging air to flow towards the hotter, less dense side of the saturator. Sufficient mixing is still observed and while the flow is more directional towards the hotter side of the saturator it is not directed straight to the output so mixing continues at the final stage of the saturator. Also, in practice at high dew points the pre-saturator will be used with the heated pre-humidifier so the latent heating will be reduced and the streamlines will be more similar to those in figure 4.12 and 4.13.

Figure 4.22 shows a temperature contour of the water surface in the final section of the pre-saturator.

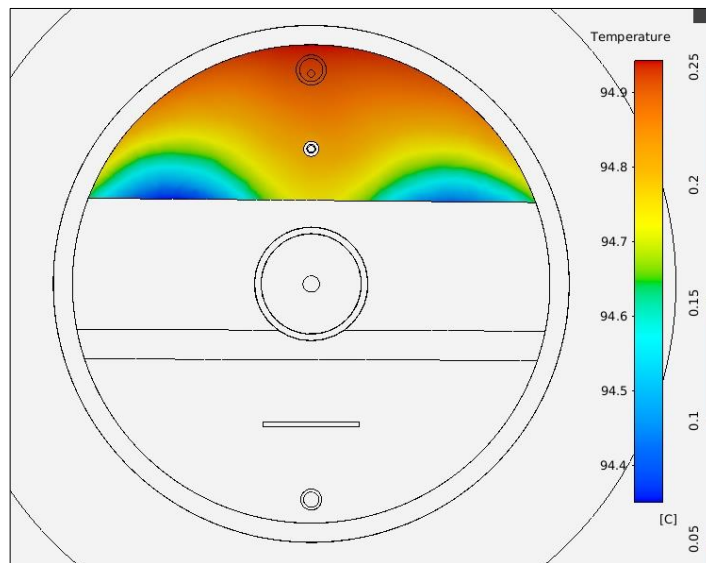


Figure 4.22: Temperature contour of the water surface near the output of the circular pre-saturator.

This contour is similar to 4.14 except with a much higher temperature inhomogeneity due to the added latent heat loading. The inhomogeneity appears to be much greater than that for the spiral pre-saturator, probably due to the geometry of the saturators. Only the final section of the water surface is shown in order to improve the resolution of the contour near the output.

4.6.4. Results of pre-saturator comparison

A number of calculations were performed as described in section 4.5. Table 4.3 shows a summary of the results calculated for the pre-saturator designs.

Table 4.3: Results of the pre-saturator comparison

	Square pre-saturator	Spiral pre-saturator	Circular pre-saturator
Quantity	Value (°C)	Value (°C)	Value (°C)
T_{air}	94.085	94.163	94.785
T_{well}	94.15	94.104	94.795
T_{bath}	94.835	94.892	94.998
$T_{water\ 3}$	94.138	94.095	94.761
$T_{water\ 2}$	92.188	93.954	93.193
$T_{water\ 1}$	73.428	84.641	69.096
$\Delta T_{well-air}$	-0.065	0.059	-0.010
$\Delta T_{bath-air}$	-0.75	-0.729	-0.213
$\Delta T_{water-air}$	-0.053	0.068	0.024
$\Delta T_{water\ final}$	0.993	0.205	0.590
A_{water}	0.019213	0.029773	0.030322
$T_{bath\ out}$	94.646	94.718	94.678

The results show that the circular pre-saturator is a much better heat exchanger than the other pre-saturators as it brings the air temperature much closer to the bath temperature. This is probably due to the low flow speed and increased mixing in the circular pre-saturator. This is important for the pre-saturator since its purpose is to provide most of the saturation needed but not necessarily to saturate the gas accurately. The temperature difference between the air and the water surface was also found to be smallest in the circular pre-saturator. The

temperature homogeneity and stability was significantly better in the spiral saturator, probably due to its geometry and the thermal properties of brass. The square saturator was consistently worse than the circular saturator, probably due to its size. Because the temperature homogeneity and stability are more important for precise saturation and the job of the pre-saturator is to do the bulk of the saturation, this makes the circular saturator most suitable as a pre-saturator.

4.7. Final saturator flow rate range determination

As discussed in section 4.3 the mixing of gas within the saturator is an important characteristic which enables the gas to become uniformly saturated and increases the efficiency of the saturator. The range of flow rates for which sufficient mixing occurs in the final saturator will be investigated in the same manner as the previous simulations. The flow rate range will be tested at 90 °C to correspond with the highest dew point that the generator will initially be tested at. The density of air at 90 °C dp was found from Eqs. 3.8 and 3.18. The latent heating in the saturator due to evaporation will be applied throughout the entire volume of the water in the saturator rather than just a selected area. A latent heating of evaporation will be applied at a rate of 0.06 W. This value was chosen by taking the experimentally determined difference in temperature of the pre-saturator and final saturator at the midpoint of the working range as shown in figure 7.5. This gives a temperature difference of 25 mK so it is assumed that the final saturator must increase the dew point of the gas by approximately 25 mK to the final saturation temperature. From Eq. 4.4 it is found that an increase in dew point of 25 mK at 90 °C dp at a flow rate of 1 ls/min corresponds to latent heating at a rate of 0.06 W. This latent heating is expected to inhibit mixing due to the fact that it will reduce the temperature of air at the bottom of the saturator and reduce convective mixing. The fact that the evaporation at the water surface and vapour pressure gradients are not simulated could make the tests conservative as the humidity gradients within the saturator are expected to increase mixing, however the effect may be small or negligible. Figure 4.23 shows the temperature contoured streamlines generated for the air flow in the saturator at various flow rates.

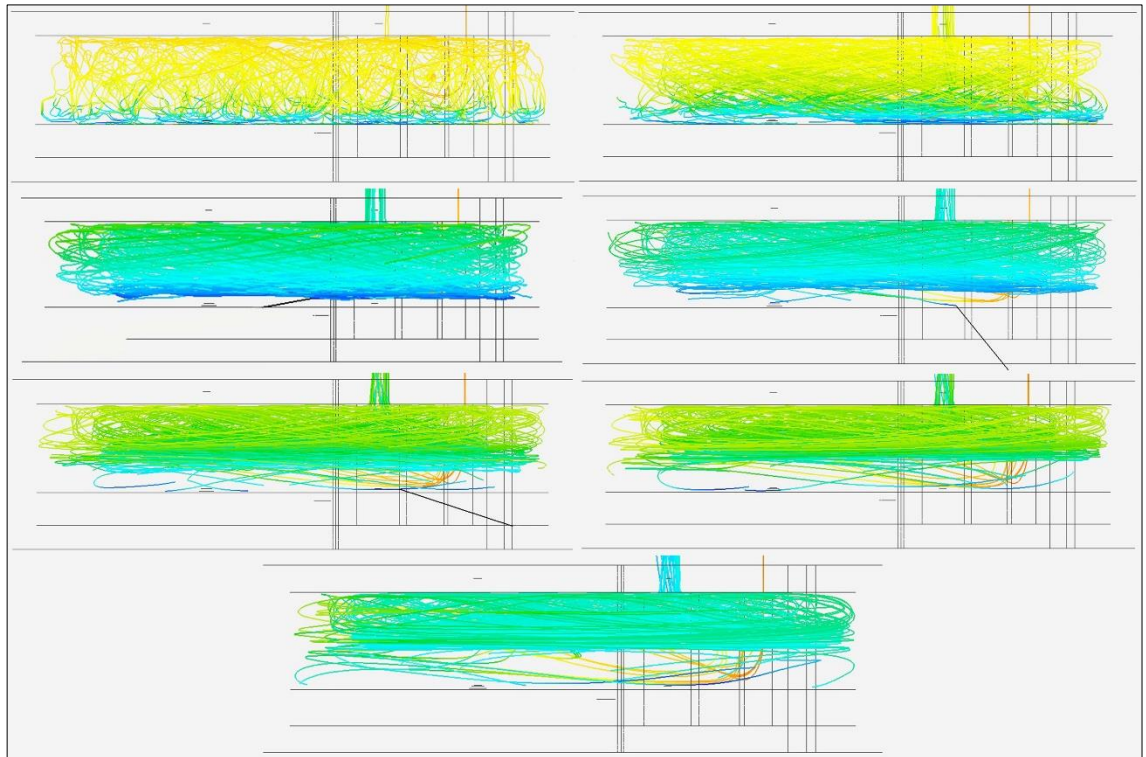


Figure 4.23: Streamlines coloured to represent temperature, in the final saturator at flow rates of 1, 2, 3, 4, 5, 7, and 10 ls/min at 90 °C dp, in order from left to right and descending.

Figure 4.23 shows that at 1 ls/min the flow is random and good mixing occurs in the saturator. At 2 ls/min the flow becomes slightly more directional but mixing still occurs and the streamlines can be seen to go from the top to bottom of the saturator. At 3 ls/min the flow becomes more laminar and the mixing can be seen to drop off. Still some streamlines can be seen to go from top to bottom so complete saturation may still occur over the full path length, but the efficiency is expected to decrease at this flow rate. As the flow rate increases beyond 3 ls/min the flow continues to become more laminar and mixing decreases.

5. The new NML 1-P dew point generator

5.1. Overview

The new NML primary dew point generator will run in a single pressure, single pass mode of operation. It consists of a heated humidifier at an independent temperature to the final saturation temperature and a pre-saturator, heat exchanger and final saturator all immersed in the same thermostatic bath. The thermostatic bath is capable of maintaining temperatures from -90 °C to 130 °C however the initial range which the generator can be used is limited to a range of -50 °C to 95 °C as this is the measurement range of the chilled mirror hygrometers at NML. The design of each of the main components of the new NML humidity generator will be discussed in this chapter.

5.2. Humidifier

The humidifier will be the first stage of saturation. For high dew points the humidifier will be used to reduce the mass transport of H₂O and latent heating in the generator. The air flow can be directed fully or partially through the humidifier or it can be completely bypassed via the operation of two needle valves. At low frost points the humidifier will be completely bypassed since the evaporative latent heat loading is very small and the latent heat of fusion if the humidifier were to be used is quite large. This is because the humidifier cannot be cooled below the room temperature of approximately 20 °C. The humidifier is heated using a constant wattage heat trace and proportional interval derivative (PID) controller. This allows stable operation at temperatures above room temperature.

The humidifier is a closed cylinder made from polished 316 stainless steel with connections for input and output air as shown in figure 5.1.



Figure 5.1: Heated humidifier.

Some dimensions of the humidifier are shown in figure 5.2.

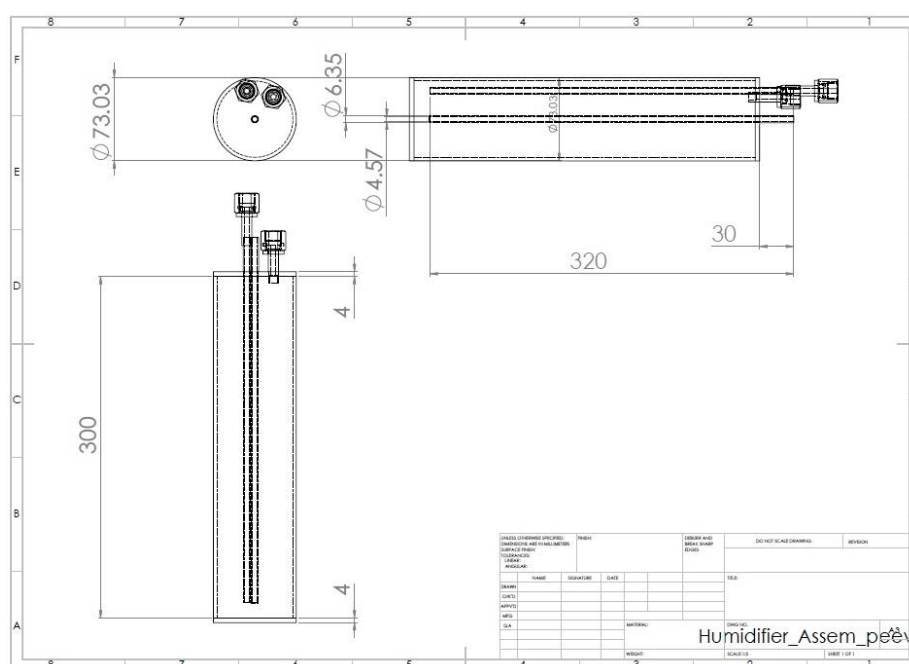


Figure 5.2: Heated humidifier plan elevation and end view with dimensions in millimetres.

It is possible to use the humidifier in an upright position as a bubbler saturator however it is intended that it will operate in a horizontal position where the air is passed over the plane water surface. This prevents water droplets becoming suspended in the airstream and being carried to the chilled mirror hygrometer where they would cause errors in the readings. The input air is brought to the opposite end of the unit via a ¼ inch diameter tube. The input and output connections are made using metal gasket face seal fittings to allow connections to be remade without reducing leak tightness. The unit also includes a thermal well that can be used

to take accurate temperature measurement of the vapour/water inside. The unit is heated using constant wattage heat tracing and controlled using a PID temperature controller. All connections are made from polished 316 stainless steel.

The humidifier can hold 1200 ml of water with enough space remaining for air flow over the water surface. From Eq. 4.3 it can be shown that 1200 ml of water will allow the humidifier to saturate air from -50 °C fp to 95 °C dp for 32 hours in continuous operation at 1 ls/min output flow rate. At a more regular dew point of 30 °C the humidifier can saturate dry air for 26 days in continuous operation.

5.3. Pre-saturator

The pre-saturator is kept at a constant temperature very near the final saturation temperature in the thermostatic bath. The purpose of the pre-saturator is to bring the dew point of the gas close to the final saturation temperature before it reaches the final saturator, thereby reducing the mass transport and latent heat loading on the final saturator. It is a 60 mm tall enclosed cylinder with a hole in the centre to allow tubing and a temperature measurement probe to be fed through it to the final saturator below. It also contains a baffle plate near the input to prevent laminar streamlines from developing in the flow path. Figure 5.3 shows an exploded view of the pre-saturator.

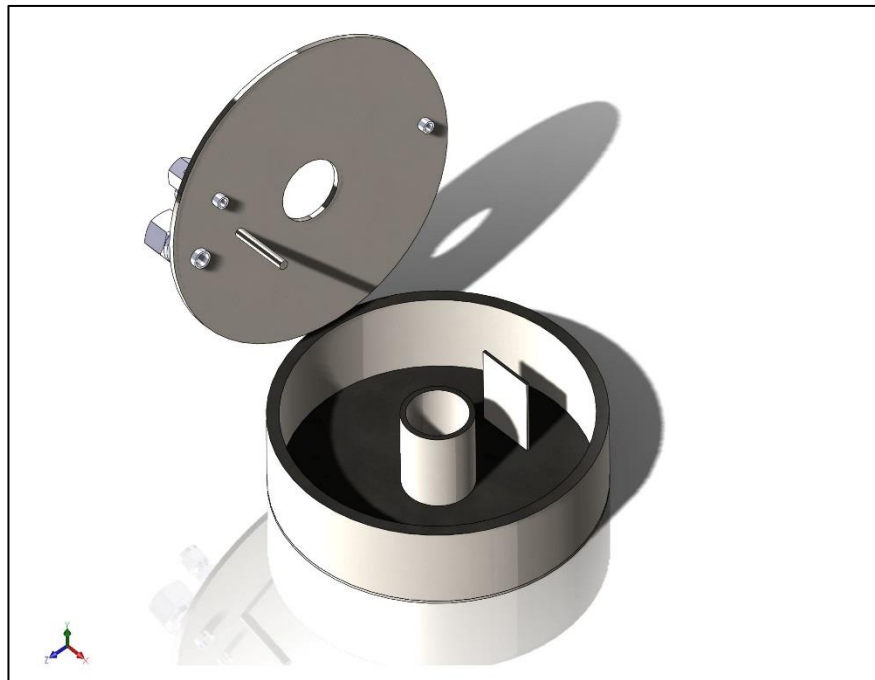


Figure 5.3: Exploded view of pre-saturator.

The large dimensions of the flow path in the pre-saturator result in a very low flow speed within the unit. This prevents laminar streamlines and encourages random motion of the gas and convective mixing due to small temperature and density gradients as described in chapter four. The pre-saturator is made from polished 316 stainless steel. It includes metal gasket face seal fittings for input and output connections and pressure measurement and a thermal well near the output to measure the condensate/vapour temperature. Figure 5.4 shows some dimensions of the pre-saturator.

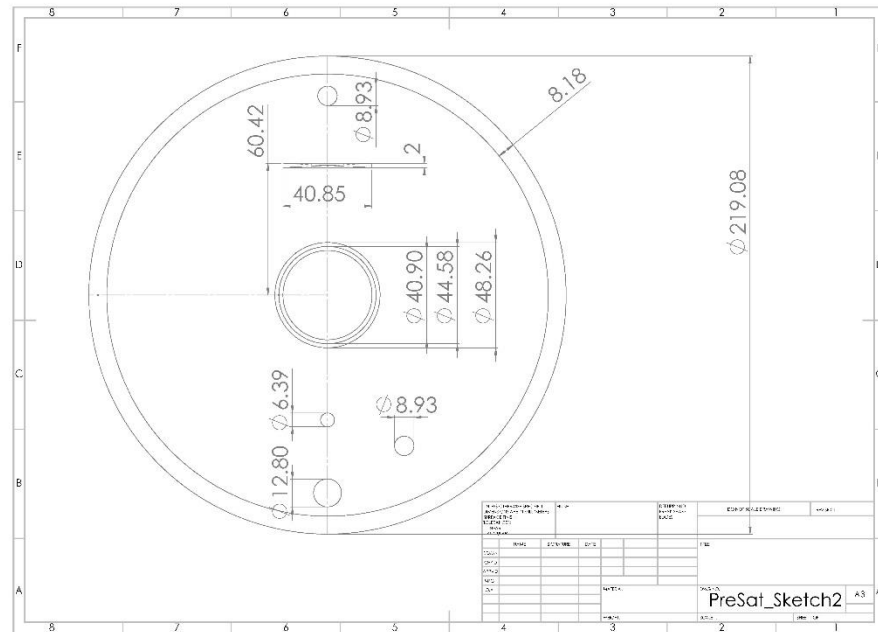


Figure 5.4: Top view of pre-saturator with dimensions in millimetres.

The pre-saturator can hold 600 ml of water with the water level at less than 20 mm high leaving more than 40 mm of height for air flow above it. From Eq. 4.3 it can be shown that 600 ml of water will allow the pre-saturator to saturate air from -50°C fp to 95°C dp at a flow rate of 1 ls/min for 16 hours. However, in practise the heated humidifier will be used to reduce the load on the pre-saturator. If the heated humidifier saturates the gas to within 0.5°C dp of the target dew point and the pre-saturator raises the dew point from 94.5°C to 95°C then it can run for 7 days in continuous operation. At a less extreme dew point of 30°C the pre-saturator can saturate dry input air for 13 days or more than 200 days if the heated humidifier is used.

5.4. The heat exchanger

The heat exchanger connects the pre-saturator to the final saturator and brings the temperature of the gas very near to the final saturation temperature. It is made from

approximately 4.5 meters of 316 stainless steel. The interior of the tube is not polished in order to encourage condensation in the heat exchanger if the gas is over saturated with respect to the liquid bath temperature. This is important if the pre-saturator over saturates the gas or if frost points below the frost point of the input air (-55 °C fp) are generated. The heat exchanger was designed in SolidWorks and fabricated using computer numerical control (CNC) tube bending. It takes the form of a helix with bends at the ends to connect with the pre-saturator and final saturator via metal gasket face seal connections. Figure 5.5 shows a CAD model of the heat exchanger when connected to the models of the pre-saturator and final saturator.

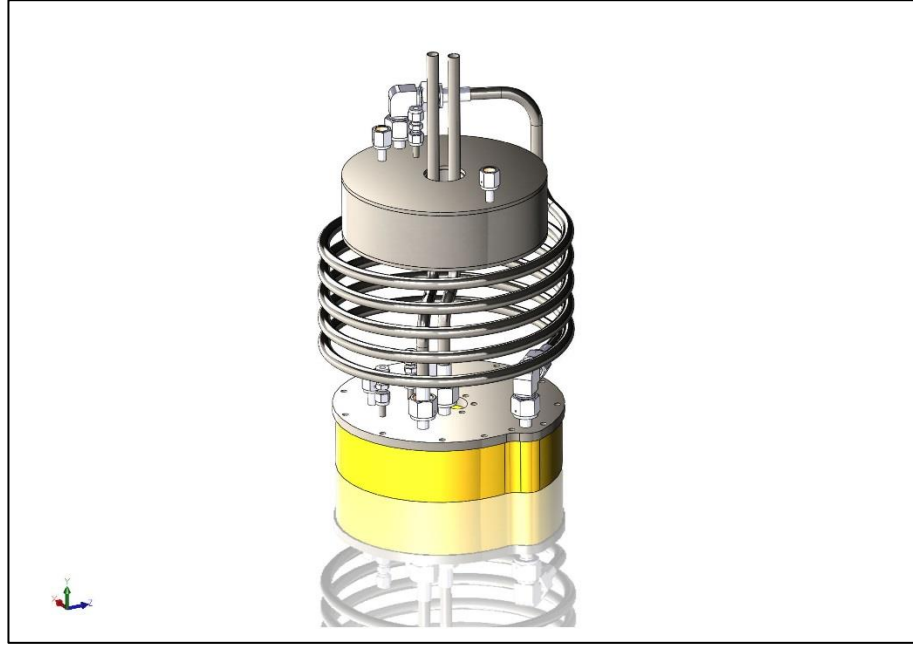


Figure 5.5: CAD model of the heat exchanger connected to the models of the pre-saturator and the final saturator.

The length of tubing needed in order to achieve the maximum desired temperature change can be found by [18],

$$l = \frac{\dot{m} c_p (T_a - T_{s,in})}{\Delta T_{ln}} \left(\frac{1}{\alpha_{out} 2\pi r_{out}} + \frac{1}{\alpha_{in} 2\pi r_{in}} + \frac{d \ln(r_{out}/r_{in})}{\lambda 2\pi (r_{out} - r_{in})} \right), \quad (5.1)$$

where l is the length of the tube, \dot{m} is the mass flow rate, c_p is the specific heat capacity of the gas used, T_a is the input temperature to the heat exchanger, $T_{s,in}$ is the output air temperature from the heat exchanger, ΔT_{ln} is the logarithmic mean temperature difference, α_{out} is the convective heat transfer coefficient of the fluid outside the tube, α_{in} is the convective heat transfer coefficient of the fluid inside the tube, r_{in} is the inner tube radius, r_{out} is the outer tube radius, d is the tube wall thickness and λ is the thermal conductivity of the tube wall.

The mass flow rate will be set to be 1 ls/min as this will be the flow rate needed to supply two chilled mirror hygrometers with 0.5 ls/min in parallel. Equations 3.6 and 3.9 can be used to calculate the mass flow rate in kg/s.

The specific heat capacity will be taken as the specific heat capacity of air at 95 °C dew point as this will be the highest specific heat capacity throughout the intended range of use. The specific heat capacity at a particular mole fraction x can be found from,

$$c_p = x c_{p,w} + (1 - x) c_{p,air} , \quad (5.2)$$

where $c_{p,w}$ is the specific heat capacity of water vapour and $c_{p,air}$ is the specific heat capacity of dry air.

If the specific heat capacity of water vapour is 1996 J kg⁻¹ K⁻¹ and of dry air is 1009 J kg⁻¹ K⁻¹ and the mole fraction at 95 °C dew point is 0.8370 then from Eq. 5.2 the specific heat capacity at 95 °C dew point is 1835 J kg⁻¹ K⁻¹.

The logarithmic mean temperature difference can be found from [18],

$$\Delta T_{ln} = \frac{T_a - T_{s,in}}{\ln \frac{T_a - T_{bath}}{T_{s,in} - T_{bath}}} , \quad (5.3)$$

where T_{bath} is the temperature of the liquid in the thermostatic bath.

Because the temperature of the gas in the heat exchanger will never fully reach the temperature of the surrounding fluid, the bath temperature will be set to be 0.1 mK below the output air temperature of the heat exchanger. The input temperature to the heat exchanger will be set to the ambient temperature of 20 °C and the output temperature of the heat exchanger will be set to -100 °C as this is the largest temperature difference that the heat exchanger will be used over. In reality the air temperature will be quite close to the bath temperature after exiting the pre-saturator and the temperature difference between the air and the bath at this point will be due to latent heat loading in the pre-saturator. Based on simulations (described in chapter 4) the output air temperature from the pre-saturator should be approximately 0.2 °C lower than the bath temperature at 95 °C dew point, 0.5 ls/min and no humidifier used.

The convective heat transfer coefficient of the fluid inside and outside of the tube will be taken as 10 W m⁻² K⁻¹ [18] and 340 W m⁻² K⁻¹ [33] respectively. A range of different values for these coefficients could be possible so the most conservative estimates are chosen.

The thermal conductivity of the tube wall will be taken as 16 W m⁻¹ K⁻¹ [34]. The tube has an outside diameter of 12.7 mm and a wall thickness of 1.5 mm.

Using the data above and Eq. 5.1 it is found that the minimum length of tubing needed for the maximum temperature change required is 1.83 m meaning that the heat exchanger of length 4.5 m exceeds its requirements for the temperature change needed.

The heat generated due to condensation in the heat exchanger must also be considered. In order to do this the rate of heat transfer from the liquid bath to the air in the heat exchanger can be found from [18],

$$U A \Delta T_{ln} = \Delta T_{ln} \left(\frac{1}{\alpha_{out} A_{out}} + \frac{1}{\alpha_{in} A_{in}} + \frac{d \ln(A_{out}/A_{in})}{\lambda(A_{out} - A_{in})} \right)^{-1}, \quad (5.4)$$

where U is the overall heat transfer coefficient, A is the heat transfer area, A_{in} is the inner surface area of the tube and A_{out} is the outer surface area of the tube and the product $U A \Delta T_{ln}$ is the rate at which heat is transferred to or from the fluid inside the tube.

Using the parameters discussed above it is found that heat is transferred between the air and the liquid bath at a rate of 11.5 W.

The heat required to bring about the temperature change discussed above \dot{q} can be found from,

$$\dot{q} = \dot{m} c_p (T_a - T_{s,in}), \quad (5.5)$$

Using the parameters above it is found that the heat needed to bring about the required temperature change is 4.68 W. From Eq. 4.4 it can be found that the latent heat of fusion needed to reduce the frost point of the input gas from -50 °C frost point to -100 °C frost point is 0.001 W at 1 ls/min so this is negligible and the heat transferred to the air from the bath should be sufficient to lower the frost point as low as -100 °C frost point. Throughout the rest of the range it is intended that each stage in the generator is operated in an evaporative mode so no condensation should occur in the heat exchanger. If the air is supersaturated before the final saturator, for example because of bath gradients, at high dew points; the latent heat required to reduce the dew point could be large. From Eq. 4.4 it can be shown that if the dew point is to be reduced from 95.5 °C dp to 95 °C dp at 1 ls/min it would require 3.10 W. This is also well with the capability of the heat exchanger based on the previous calculations. Also, it is not expected that such a large over saturation will occur.

5.5. Final saturator

The final saturator, shown in figure 5.6, is the last stage of saturation in the dew point generator. By this point the gas should already be quite close to the output dew point and the final stabilisation of the dew point should occur in the final saturator.



Figure 5.6: Image of final saturator.

The base of the final saturator is machined from brass for its machinability and high thermal conductivity and thermal mass. The base is plated with 40 μm of high phosphorous electroless nickel plating (ENP) to resist corrosion. A minimum of 25 μm of high phosphorous ENP is needed to ensure that the finished surface is relatively free from pores. The corrosion rate of high phosphorous ENP in deionized water can be as low as 0.5 μm per year [35] or 0.1 μm per year [36] and the corrosion rate is lower in methanol [35]. This means that the unit should last 30 to 150 years in the environment that it will be used before it becomes unfit for purpose. However since the unit will only be used several times a year and will be stored dry this will further reduce the risk of excessive corrosion.

The thermal expansion coefficient of high phosphorous ENP is approximately $8 \times 10^{-6} \text{ K}^{-1}$ to 10^{-5} K^{-1} while the thermal expansion coefficient of brass (the substrate) is approximately $18 \text{ to } 19 \mu\text{m m}^{-1} \text{ K}^{-1}$. This means that there will be internal stress in the plating due to the expansion and contraction of the plating and substrate throughout the maximum foreseen temperature range from -100°C to 95°C . This may cause microscopic cracks in the plating and may increase the porosity of the plating decreasing the corrosion resistance. High phosphorous ENP has relatively high ductility compared to other ENPs. If the ENP is heated to 300°C its ductility is significantly reduced and porosity is significantly increased so it will be ensured that the unit is not brought above 100°C to ensure that no heat treatment occurs. The thickness of the deposit also affects the ductility. Figure 5.7 shows the crack initiation

deflection value for different thicknesses of high phosphorous ENP plated on a 1018 steel substrate, obtained by a three point bending test [37].

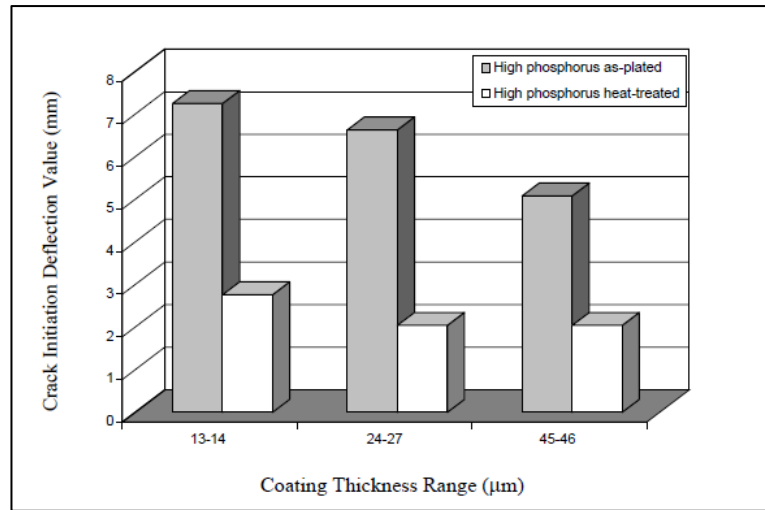


Figure 5.7: Variation of crack initiation deflection value with coating thickness for 1018 steel coated with high phosphorous electroless nickel (EN) coatings [37].

This shows that increasing the coating thickness increases the risk of stress cracking, so a compromise will be made between corrosion resistance and likelihood of stress cracking. It is not known exactly how the temperature range of the generator, from -40 °C to 90 °C will affect the porosity or cracking of the plating so a similar brass sample will be plated identically to the base of the saturator in order to study the change in surface roughness and porosity after temperature cycling across the range of use. Figure 5.8 shows atomic force microscopy (AFM) images taken at random positions on the sample, before and after temperature cycling.

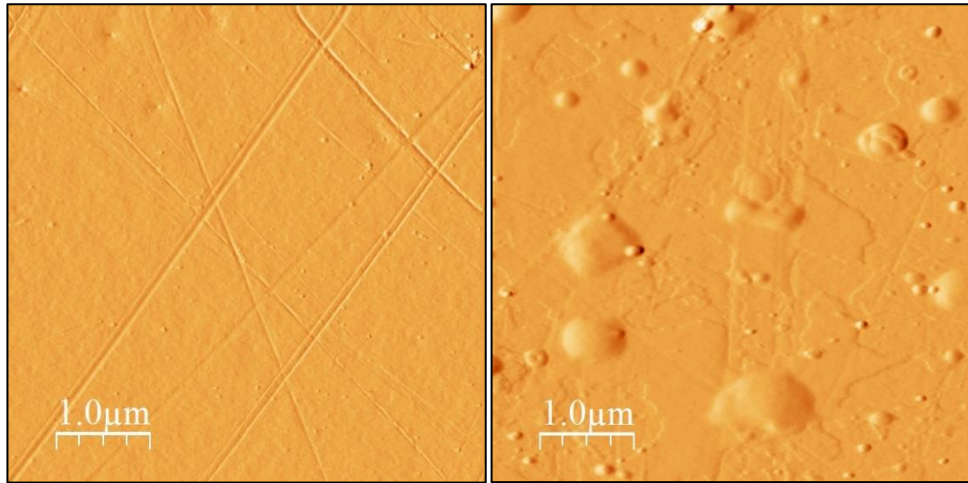


Figure 5.8: AFM images of the ENP plated brass sample before and after temperature cycling, respectively.

The root mean squared (RMS) roughness before temperature cycling was 4 to 6 mV and 12 to 18 mV after temperature cycling. The increase in roughness could be due to a different area been sampled or due to the expansion and contraction of the plating and substrate.

Imperfections observed after temperature cycling are significantly smaller than the plating thickness so it is expected that the corrosion resistance should be maintained. For a higher resolution scan the RMS roughness was found to be 0.71 mV and 0.74 mV before and after thermal cycling, respectively. Figure 5.9 shows some of the pores imaged before thermal cycling took place.

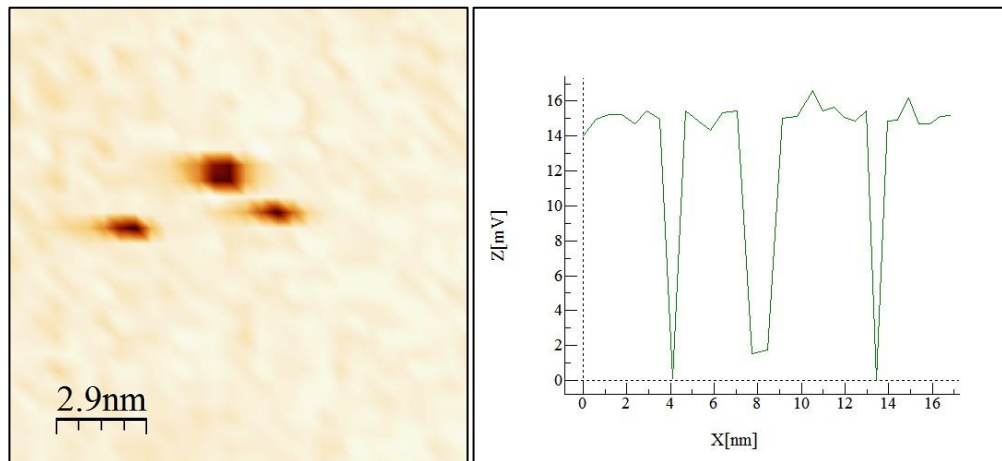


Figure 5.9: AFM image and profile of pores before temperature cycling.

Figure 5.9 was taken from a scan size of 250x250 nm. The scan had other similar sized pores to the ones in figure 5.9. Another scan of the same size showed no visible pores. Figure 5.10 shows a larger pore imaged after thermal cycling.

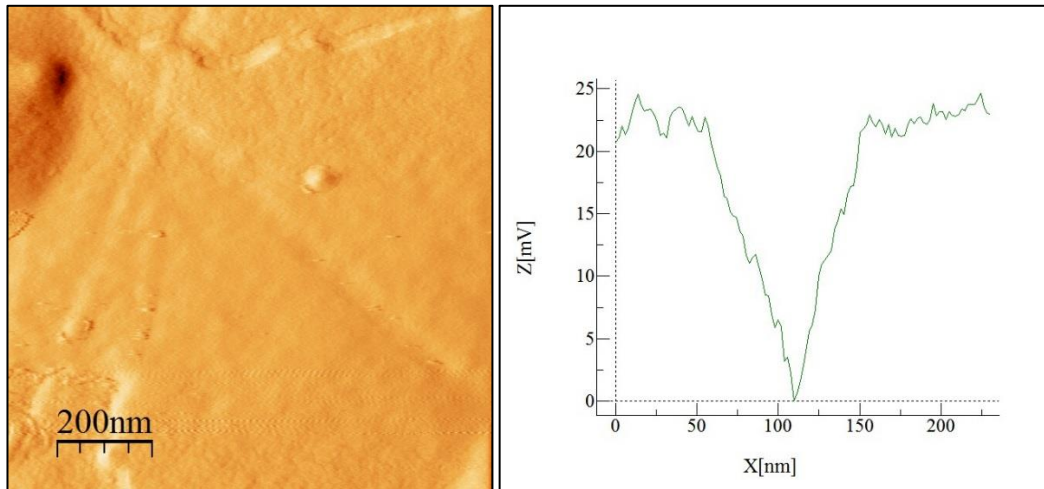


Figure 5.10: AFM image and profile of a pore imaged after thermal cycling.

Figure 5.10 shows a large pore in the top left corner. No other scans taken after thermal cycling showed any visible pores. The number of scans taken were therefore not sufficient to indicate an increase in porosity after temperature cycling of the brass sample however due to the smoothness of the sample and the lack of visible pores is expected the surface is still relatively pore-free and unreactive. It is also expected that due to the plating thickness of 40 μm that none of the pores reach the substrate.

The saturator base shown in figure 5.11 contains a spiral path approximately 17 mm in width and 49 mm in height, with the lid in place. The path is approximately 1.9 meters in length. The fact that the final saturation of the gas occurs along a consistent path allows the temperature to be measured along the path and the dew point to be measured at different locations on the path to determine the saturation efficiency at the output of the saturator. The saturator contains a hole in its centre to improve thermal contact between the air flow path and the liquid bath and to allow a temperature probe to measure the temperature of the bath liquid near the output of the saturator.



Figure 5.11: Base of the final saturator.

The large dimensions of the flow path make the flow speed low enough that the motion of the particles is random and convective mixing occurs due to small temperature and density gradients within the saturator, as shown in simulations in chapter 4. At higher flow rates the flow becomes laminar and prevents mixing. Some dimensions of the saturator are shown in figure 5.12.

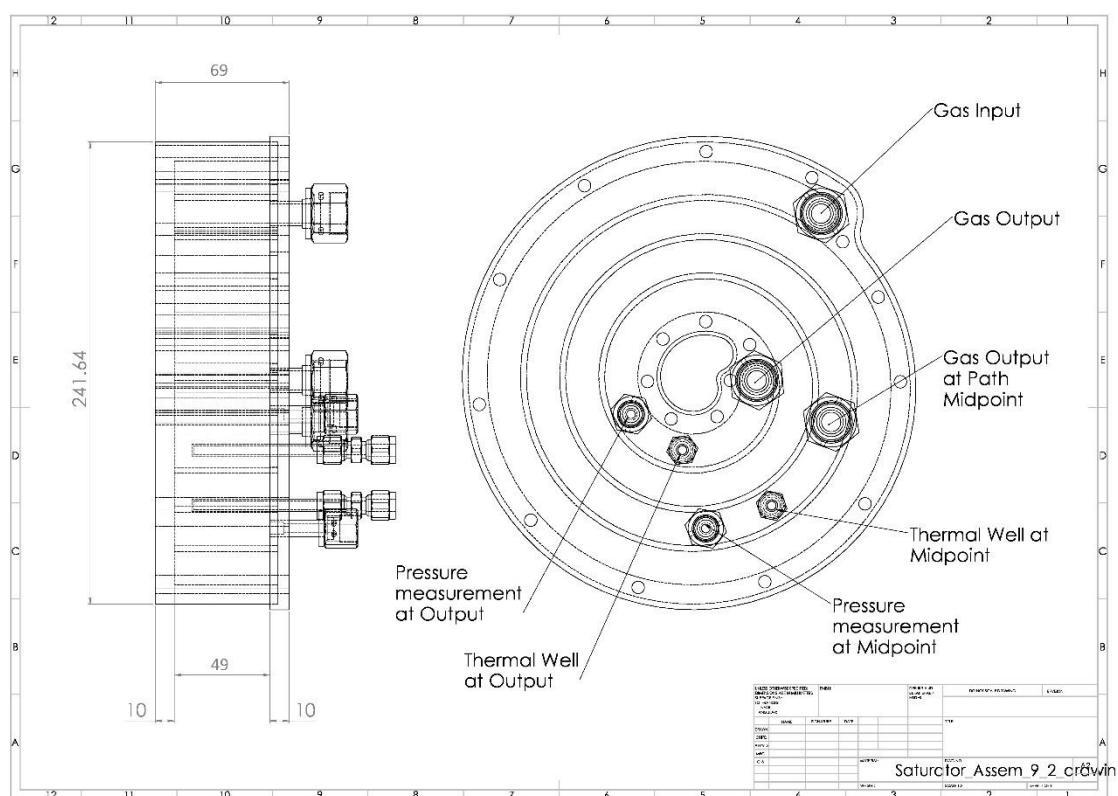


Figure 5.12: Drawing of final saturator with dimensions in millimetres.

The saturator can hold 400 ml of water in 13.5 mm of height leaving 35.5 mm of height in the air flow path. From Eq. 4.3 it can be shown that 400 ml of water will allow the final saturator to saturate air from -50 °C fp to 95 °C dp for 11 hours at 1 ls/min. Based on the simulations discussed in chapter 4 the pre-saturator should be capable of saturating air to within 0.2 °C of 95 °C dp without the use of a pre-humidifier. If the input air to the final saturator is 95 °C dp ± 0.2 °C dp the final saturator could saturate the air to 95 °C dp for 10 days at 1 ls/min. At a more regular dew point of 30 °C the unit could saturate dry air for 9 days or several years if the pre-saturator is used. Based on temperature measurements of the generator in use at 90 °C it is expected that the pre-saturator should saturate air to approximately 0.02 °C dp below the output dew point, meaning that the final saturator could run for more than 200 days without needing to be refilled. The refilling interval is therefore dependant on the pre-saturator which can run for 14 days in continuous operation at 90 °C under normal circumstances. The humidifier can run for 38 hours continuously at 90 °C dp but is not immersed in the thermostatic bath and can be conveniently refilled.

Figure 5.13 shows the underside of the saturator lid.



Figure 5.13: Final saturator lid.

The lid of the saturator is machined from 316 stainless steel in order to allow welds to be made with other stainless steel components. The lid includes welded connections for input, output, pressure measurement and a thermal well near the output to allow accurate temperature measurement of the output air. It was shown in chapter four by simulation that the thermal well is the best measurement location to determine the water vapour/condensate temperature, other than measuring directly in the flow path. The lid also has a second output, pressure measurement and thermal well roughly half way along the path length. This can be used to verify the saturation efficiency by comparing the level of saturation along the path

length. All connections are electropolished metal gasket face seal fittings and the lid was electropolished in order to improve corrosion resistance and undo any damage which occurred during welding.

Since the lid and the base are precision machined, the surfaces that make contact are very flat and create a very good seal. A gasket made from 0.7 mm diameter indium wire is used to create the seal. The lid is secured to the base with 19 M6 stainless steel bolts each fastened with 10 Nm of torque.

5.6. Full system

Figure 5.14 shows a schematic diagram of the new NML dew point generator.

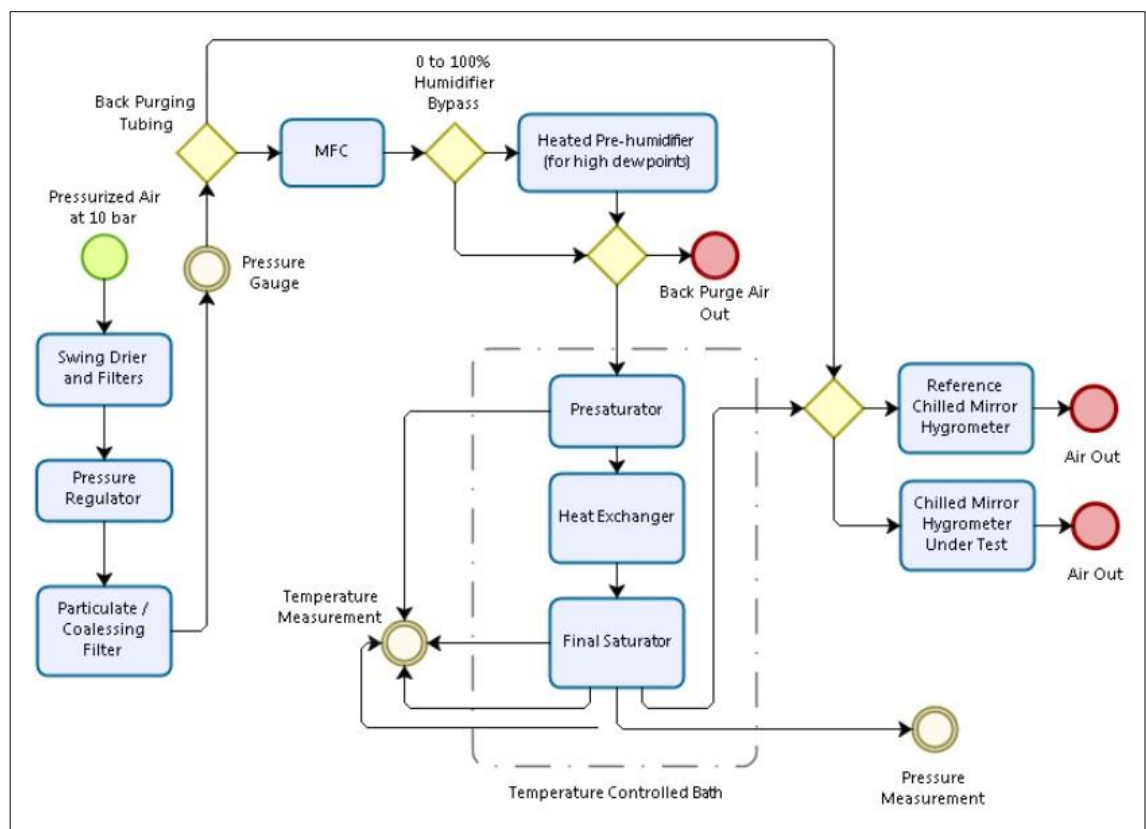


Figure 5.14: Schematic diagram of the new NML dew point generator.

The input air to the generator is taken from a compressed air reservoir that is maintained at 10 bar. The air is then filtered and dried to approximately -50 °C fp by a swing drier. The air is then brought to a pressure regulator through a number of connections and tubing. A particulate and coalescing filter is installed after the pressure regulator to remove any particles that could have been picked up in the connecting lines and to ensure that there are no water droplets suspended in the airstream. After the filter all connections are made using 316

stainless steel tubing. A pressure gauge is installed before the mass flow controller (MFC) so that the pressure regulator can be set to maintain a pressure drop of 2 Barr across the MFC. The MFC has a range from 0 to 10 ls/min which is needed to perform experiments at higher flow rates as well as for maintaining the standard flow rate of 1.0 ls/min for calibrating a chilled mirror hygrometer with an additional reference hygrometer to monitor the output.

The next stage of the generator is the heated humidifier, pre-saturator, heat exchanger and final saturator. These units have been discussed previously in this chapter. The heated humidifier will be set to produce a dew point slightly lower than the temperature of the pre-saturator. This can be controlled by changing the temperature of the humidifier or by changing the percentage of the total airflow through the humidifier via the operation of two needle valves. It can be verified that the dew point output from the humidifier is slightly lower than the pre-saturator temperature by checking that the temperature of the pre-saturator is slightly lower than the temperature of the final saturator, indicating that evaporation is occurring in the per-saturator (provided that the gradient produced is larger than any pre-existing bath gradients and the pre-saturator is colder than the final saturator). The output of the humidifier could also be calibrated with respect to temperature and valve position for mid-range dew points with little latent heat of vaporization. Figure 5.15 shows an image of the pre-saturator, heat exchanger and final saturator.

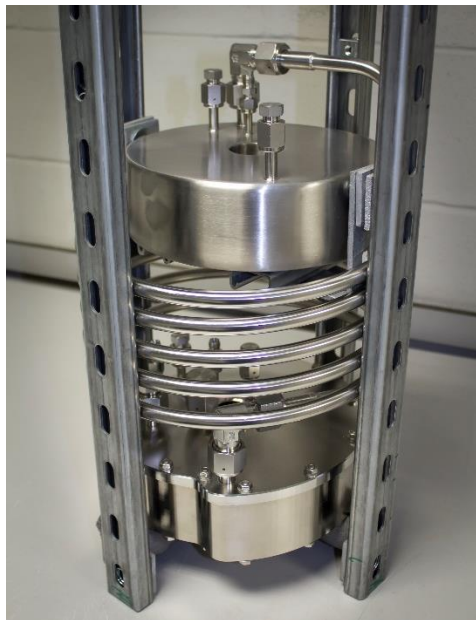


Figure 5.15: Image of pre-saturator connected to heat exchanger and final saturator.

100 Ω platinum resistance thermometers (Pt100s) are used to measure the temperature at the pre-saturator, approximately half way along the path length of the final saturator and near the output of the final saturator. The temperature of the bath liquid near the output of the final saturator is measured using a 25 Ω standard platinum resistance thermometer (SPRT). The

temperature measured using the SPRT will have a significantly lower uncertainty than that of the Pt100s. However based on the simulations described in chapter four the temperature of the bath liquid at this location could be approximately 0.05 °C higher than the temperature of the airstream inside the saturator while the temperature inside the thermal well may be just 0.004 °C higher, for high latent heating within the final saturator. This simulation represents the generation of a 95 °C dp with 1 °C dp deficiency to the final saturator, at 0.5 ls/min. In reality the input to the final saturator will be much closer to the target dew point due to accurate pre-conditioning of the gas, however the thermal well is still expected to be the optimum measurement location due to the latent heating that remains. At lower temperatures latent heating is negligible and the bath liquid will be closer to the temperature of the vapour/condensate inside the saturator. The temperature used to calculate the output dew point can be taken from the SPRT or the Pt100 near the output as long as the corresponding uncertainty due to the difference in the condensate/vapour temperature and temperature at the point of measurement is included. The combined uncertainty may be lower for the SPRT in the low range and for the Pt100 in the high range.

The saturation pressure is measured near the output of the final saturator via internally polished 316 stainless steel tubing with a precision digital pressure meter. The pressure at the point of measurement in the reference chilled mirror hygrometer can be measured using the same pressure meter via a three way ball valve. The pressure in the measuring head of the reference chilled mirror hygrometer is measured by an integrated pressure transducer connected to the flow path directly after the hygrometers sensing element. The transducer is affected by the temperature variation of the measuring head and is corrected for the temperature variation. This makes calibration of the integrated transducer complicated and time consuming so instead the head pressure can be measured by the calibrated pressure meter via an attachment to the head where an endoscope is usually connected. The integrated transducer can then be corrected at each set point where the measuring head temperature differs. If it is not possible to measure the pressure directly at the point of measurement of a UUT then this pressure can be estimated as the midpoint of the saturation pressure and the pressure at the output of the UUT. The uncertainty of this pressure will then be a rectangular distribution with limits from the pressure at output of the UUT to the saturation pressure and the standard uncertainty u_{puut} can be calculated from the following equation,

$$u_{puut} = \frac{\Delta P}{2\sqrt{3}}, \quad (5.6)$$

where ΔP is the pressure drop from the final saturator to the output of the UUT.

The output tube from the saturator is a ½ inch diameter 316 stainless steel tube which is then connected to a ¼ inch tube before being connected to the hygrometers. The ½ inch tube is internally polished but not electropolished, increasing stabilization times and the uncertainty associated with adsorption and desorption effects. It is intended to replace the output tube with a ¼ inch diameter internally electropolished tube going straight from the saturator to the hygrometers. It is expected that due to the electropolished interior surface and reduction of surface area the adsorption and desorption effects should be significantly reduced at low frost points. Since the pressure at the point of measurement will be measured whenever possible the additional pressure drop across the tube should not affect the overall uncertainty. The output tubing is always heated well above the generated dew point temperature by means of a constant wattage heat trace.

All instruments and hardware excluding valves and heat tracing are controlled by a single software package which was developed specifically for this purpose and is capable of been operated remotely and automated. Remote operation is necessary due to the long stabilization times of the system.

6. Initial characterization

The system was pressure tested with a pressure gauge at 2 to 3 bar and found to lose no measurable pressure over a number of days. This test is sufficient to determine that all the connections have been made correctly, a seal has been made between the lid and the base of the final saturator, and that all of the welds throughout the system are leak tight. Only after all of these conditions were met could testing continue.

The generator was initially tested at 10 °C, 60 °C and 90 °C in order to assess its performance and determine what changes need to be made to improve its operation. The output from the humidifier was greater than expected so two valves were added to allow 0 % to 100 % of the flow to by-pass the humidifier. This allows the humidifier to be used for mid-range dew points without causing condensation in the generator which can be more problematic than evaporation. It also allows the input dew point to be adjusted without the long stabilization times needed for temperature changes. It was found that there was a large temperature gradient from the final saturator to the pre-saturator, which could be as high as 1.7 °C at a 60 °C set point. It was found that the temperature gradient of the liquid bath between these points was approximately 2 mK meaning that the difference in temperature of the pre-saturator must be due to conduction from ambient temperature through the connections at the top of the pre-saturator. To reduce this gradient the generator was lowered slightly in the bath and the distance from the pre-saturator to the final saturator was reduced. This provided additional immersion of the pre-saturator bringing it closer to the final saturation temperature. After the change was made the temperature difference from the pre-saturator to the final saturator is 0.08 °C at 60 °C with no latent heating effects.

When the generator was lowered a ½ inch diameter tube was connected to the final saturator to allow it to be filled without being removed from the bath. When the generator was tested after the modifications it was found that it outputted a dew point up to 0.02 °C lower than the expected value at a 60 °C set point (as measured by a chilled mirror hygrometer). It was also noticed that when the bath water level varied it caused a large change in the output. When the bath water level dropped significantly the output could be up to 0.4 °C below the expected dew point. The same effect was observed at 10 °C output dew point. The fill tube which was installed could have contributed to this deficiency due to the dead volume that it introduces. The high sensitivity to the bath water level could be due to condensation occurring in the outlet tube when the bath water level drops and the heating of part of the outlet tube decreases. The outlet tube reduces from ½ inch to ¼ inch diameter before it reaches the chilled mirror. The different diameter tubes and the connections used have different thermal

masses and should be temperature controlled by separate PID controllers to maintain consistent temperature along the tube, however only one PID control unit was used. When the bath water level dropped, part of the tubing and heat tracing would have been wet and exposed to ambient air, possibly causing it to drop slightly below the dew point temperature of the output gas causing condensation in the output tube. The bath stability and gradients were also found to be affected by the reduced water level and could have caused condensation in the output tube. For these reasons the output tube was replaced with a single ¼" internally electropolished stainless steel tube. Extra care was taken when heat tracing was applied to the tube to ensure that the area where the tube enters the liquid bath is well heated with slightly more power than the rest of the tube. Two thermocouples were attached to the heated input and output tubes to monitor their temperature above and slightly below the bath liquid. The tube will be more uniformly heated since the thermal mass is more consistent along its length. The temperature will be controlled by varying the voltage across the heat tracing rather than using a PID controller in order to ensure that the power of the heat tracing is never fully off, thereby preventing areas of different thermal mass dropping below the output dew point. The electropolished interior and reduced internal surface area will reduce the likelihood of condensation and significantly reduce adsorption and desorption effects (which will be necessary for low frost points). The likelihood of condensation occurring may also be reduced by the pressure drop due to the Bernoulli effect when the air flow goes from the large internal dimensions of the final saturator to the small internal dimensions of the ¼ inch output tubing. The drop in pressure can be found from [38],

$$P_1 + \frac{1}{2}\rho v_1^2 + \rho g y_1 = P_2 + \frac{1}{2}\rho v_2^2 + \rho g y_2 , \quad (6.1)$$

where P_1 is the pressure in the saturator, P_2 is the pressure in the outlet tubing, v_1 is the flow speed in the saturator, v_2 is the flow speed in the outlet tubing, y_1 is the height of the saturator flow path and y_2 is the height of the outlet tube flow path.

Using Eq. 6.1 it was found that the drop in dew point will be negligible for the flow range used for the generator with a maximum drop of 7 mK dp for 4 ls/min at 95 °C output dew point. This may have a small effect of preventing condensation near the outlet of the final saturator but over the length of the tube; is insignificant compared to other effects.

After the new outlet tube was fitted and the fill tube was removed, the output dew point measured by the chilled mirror hygrometer was 6 mK higher than the expected output of the generator at 60 °C, which is negligible considering the typical uncertainties of the two systems.

When the bath was set to 90 °C it failed to reach the set point due to the amount of evaporation occurring at its surface. The bath was covered with insulation with low water

vapour permeability to reduce evaporation and heat loss at the surface of the bath. After the bath was insulated it was found to be capable of maintaining a stability of ± 1 mK with a square probability distribution (or a standard deviation of 0.5 mK) for ten minutes at 90 °C. The gradient from the saturator to the pre-saturator reduced to 0.04 °C at 90 °C when insulation was used.

A flexible tube connected before the mass flow controller and additional needle valves were added to allow purging of the system with dry filtered air which will be needed to perform adsorption and desorption tests and to dry the system in preparation for low frost points. When the generator was tested at -40 °C fp it was found that the dead volume of the pressure measurement tube to the final saturator caused instability of the output frost point. An additional valve was added to allow the pressure measurement tube to be purged in a controlled manner minimizing the disturbance to the flow through rest of the system. The additional valves also allow the input dew point to the pre-saturator to be measured which is useful for performing tests of the effect of changing the latent heating within the generator. Tubing was added to the outputs of the chilled mirror hygrometers to reduce back diffusion of water vapour from ambient air into the measuring instruments and valves were attached to the outputs to allow the system to be operated at a slightly elevated pressure in order to reduce back diffusion of water vapour through leaks in the system.

7. Uncertainty analysis of the new NML primary dew point generator for the calibration of chilled mirror hygrometers

The uncertainty analysis in this thesis will be a preliminary analysis of the uncertainties of the system at 90 °C dp. This set point is chosen as it is the most challenging dew point in the high calibration range of the chilled mirror hygrometers that the system will be tested with. Some of the tests which are expected to vary significantly at low frost points will be repeated at -40 °C frost point (the lowest and most challenging frost point in the calibration range of the chilled mirrors in use) to give an indication of how the system will perform over the initial range of use. It must be stressed that this is a preliminary uncertainty budget based on limited measurements and measurements will continue over a number of years before the evaluated uncertainties become reliable. As the system is used over time and the history and performance of the system becomes well known, many of these uncertainties may be reduced. Since the long term performance of the system is not currently known many of the uncertainties evaluated in this section will be overestimated in order to give a conservative result.

Wherever the chilled mirror hygrometer reading is stated this refers to the instrument reading with a calibration correction added to it. The correction was estimated by a third party from a calibration of the hygrometer against a primary humidity standard. The uncertainty associated with the calibration correction or the hygrometer itself is not stated as all of the measurements taken are within this uncertainty. The uncertainties evaluated in this section are measured using the sensitivity of the measuring hygrometer to detect changes in the output and not on the absolute reading of the hygrometer.

7.1. Propagation of uncertainty

If a parameter is measured and used to calculate dew point or another quantity whose uncertainty is to be determined then the output quantity α is given by,

$$\alpha = f(x_1, \dots, x_N) , \quad (7.1)$$

where $f(x_1, x_2, x_N)$ is a function of the parameters x_1 to x_N .

The error in the output quantity due to the error in one of the input quantities $u_\alpha(u_{x_i})$ can be found from,

$$u_\alpha(u_{x_i}) = u_{x_i} \frac{\partial f}{\partial x_i} , \quad (7.2)$$

where u_{x_i} is the error in the input quantity x_i .

If the function cannot be differentiated or if the differentiation is long and complex, the uncertainty in the output quantity due to an input quantity is calculated as follows,

$$u_\alpha(u_{x_i}) = \frac{f(x_i + u_{x_i}, \dots, x_N) - f(x_i - u_{x_i}, \dots, x_N)}{2} , \quad (7.3)$$

This is a first order approximation of the derivative by finite differences. This method will be used for most calculations in this section to avoid solving complicated or impossible derivatives.

The combined standard uncertainty u_c of α due to the standard uncertainties of a number of input quantities which could reasonably be attributed to the value of the α is given by [39],

$$u_c^2(\alpha) = \sum_{i=1}^N u_{x_i}^2 \left(\frac{\partial f}{\partial x_i} \right)^2 . \quad (7.4)$$

Equation 7.4 will be used to calculate the combined standard uncertainty of the generated dew/frost point.

7.2. Uncertainty due to formulations

The uncertainty in the empirical reference functions used to calculate the saturated vapour pressure at the final saturator temperature has an uncertainty which is given in table 2.2. This uncertainty will be propagated through Eq. 3.5 and the iterative solution method described in section 3.4.1 to give the uncertainty in the output dew point due to the uncertainty in the Sonntag equation. This will also be performed for the uncertainty in the enhancement factor formulation given by Eq. 2.16.

When the result of Eq. 3.5 is solved (in order to correct for pressure drop) and the output dew point is solved by the backward iterative solution of the vapour pressure and enhancement factor formulations, the uncertainties associated with the formulations are still present. Since these uncertainties are given as the vapour pressure and enhancement factor uncertainties, they will be found at the calculated output dew point and pressure at the measuring head, and then propagated backwards through the vapour pressure and enhancement factor formulations using the iterative calculation method. Since the dew point and pressure in the saturator are similar to the dew point and pressure in the measuring head it is possible that the majority of the error in the formulations will cancel since the vapour pressure is first estimated from the saturator temperature and pressure, and then the output saturation temperature is estimated from the calculated vapour pressure and total pressure in the measuring head. However this will not be investigated in this thesis.

The uncertainty due to the iterative solution method will be taken as the resolution of the iterations or in other words the value of the smallest iteration.

7.3. Saturator efficiency

The uncertainty relating to the saturator efficiency is the uncertainty due to the non-ideality of the saturation of the gas, since the gas is flowing through the system and the system is not closed as it is in the definition of the saturated vapour pressure over water. The saturation efficiency depends on the flow rate of gas through the saturator. Assuming that the rate of evaporation is sufficient to saturate the output gas at the output flow rate, this dependence is due to the increased mass transport and latent heating caused by the evaporation of H_2O , as well as vapour pressure gradients caused by lack of mixing within the saturator. Figure 7.1 is a graph showing the dependency of the output of the generator with respect to the flow rate through the generator.

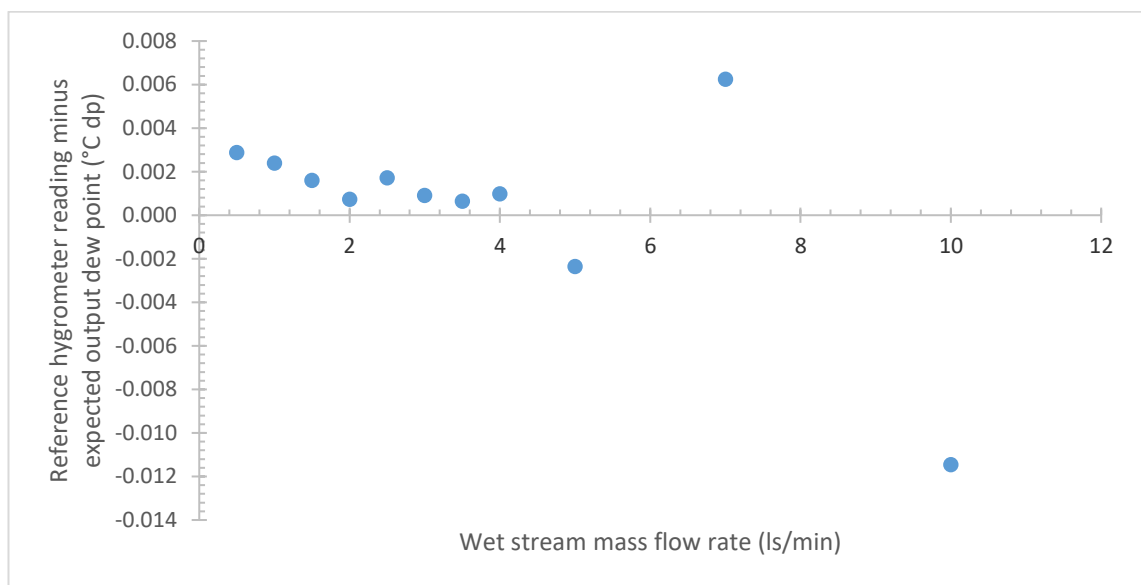


Figure 7.1: Flow rate dependency.

Figure 7.1 shows that the output dew point has little variation below 4 ls/min after which the output becomes more random and drops off at higher flow rates. The measurements were made by keeping the flow rate through the reference hygrometer constant while varying the flow rate through the generator. The measurements were made using the full system including the pre-humidifier at 90 °C.

As discussed in section 4.2, the amount of mixing of dry gas and water vapour depends on the flow rate and will affect the efficiency of the saturator. The highest flow rate before mixing reduces and flow becomes laminar was estimated using CFD simulation in 4.2. This effect will be confirmed by varying the flow rate while keeping the mass transport constant by varying the input dew point, using Eq. 4.3 to find the mass transport for various input and output dew points. Figure 7.2 is a graph showing the effect of reduced mixing due to increased flow rate.

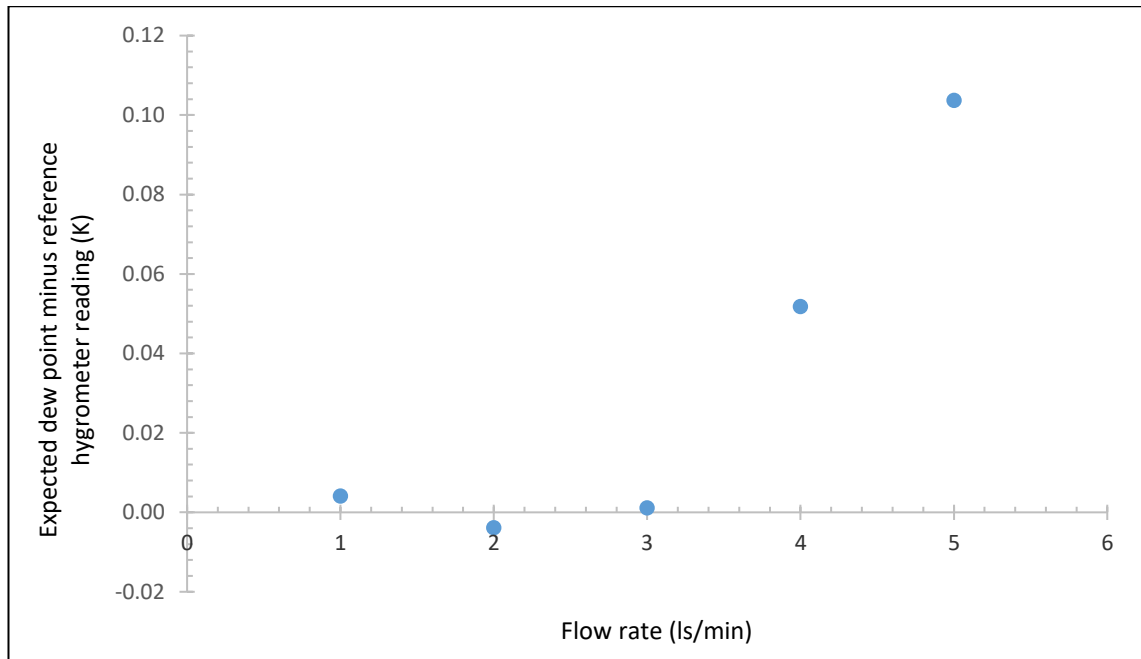


Figure 7.2: Effect of varying flow rate while latent heating is kept constant at approximately 10.38 W.

Figure 7.2 shows that the output remains approximately constant at flow rates below 3 ls/min above which the saturator efficiency drops off, which is in good agreement with the simulation results shown in figure 4.23. The measurements were made with an approximately constant latent heating throughout the pre-saturator and the final saturator of 10.38 W which is the latent heating for a flow of 0.5 ls/min at 90 °C. The latent heating in normal operation will be reduced due to the effect of the pre-humidifier. The latent heating is exaggerated here as the purpose of the test is to see the change in the efficiency due to reduced mixing and the elevated latent heating makes the drop off in efficiency larger. The elevated latent heating may reduce mixing due to the air at the bottom of the saturator being cooled and reducing convective mixing.

It was later found that before this experiment the final saturator was condensing and the water level in the saturator was elevated causing decreased mixing. If this test is re-evaluated with the correct water level the range in which the saturator is efficient will likely be increased.

The saturation efficiency due to latent heating will be estimated by varying the latent heating from approximately 0 W to 20 W by varying the input dew point (from the pre-humidifier) at 1 ls/min flow rate through the generator. The latent heating resulting from the change in dew point from input to output will be estimated using Eq. 4.4. Figure 7.3 is a graph showing the relationship between the correction to be applied to the reference hygrometer based on the expected output dew point and the latent heating within the pre-saturator and final saturator.

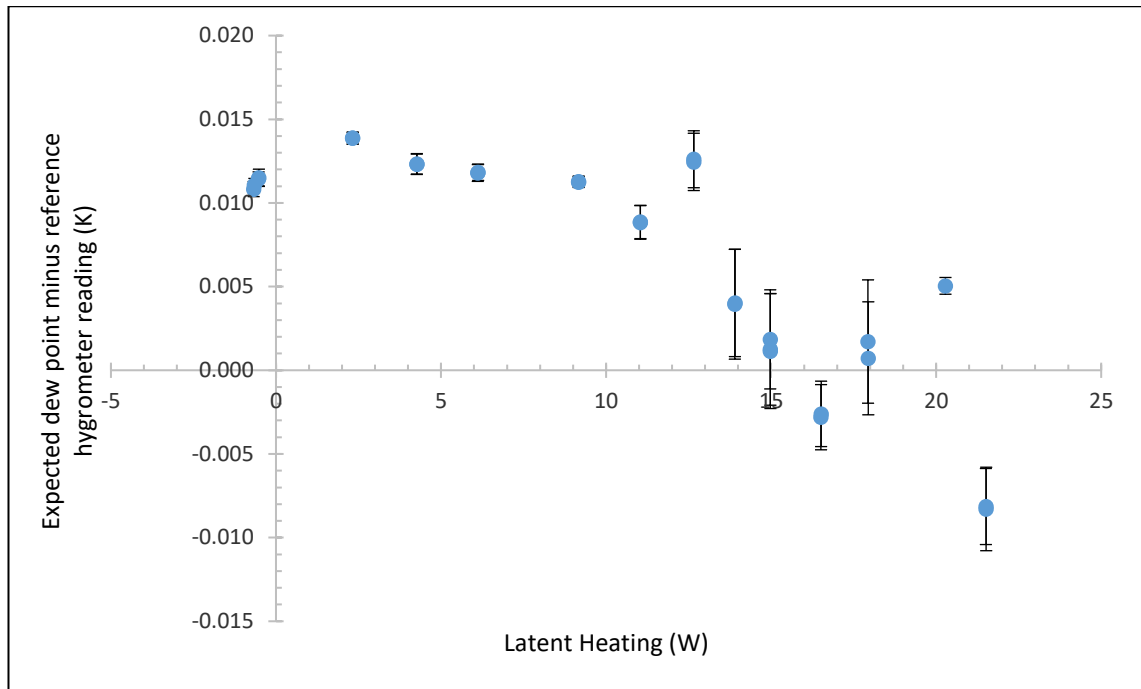


Figure 7.3: Graph of reference hygrometer correction against latent heating within the pre-saturator and final saturator with error bars representing the standard deviation.

Figure 7.3 shows no large variation (less than 4 mK) of the output dew point below 10 W after which the output begins to change. The output as measured by the reference hygrometer increases relative to the expected output. This is due to the increased latent heating, cooling the PRTs measuring the saturation temperature and creating larger gradients between the SPRT and PRTs increasing the range over which the output dew point is expected to lie. The error bars in figure 7.3 represent the standard deviation of the monitoring hygrometer reading, not the uncertainty of measurement. The error bars show the difference in variance of the results to indicate the quality of measurements. The standard deviation may vary due to the variation of the stabilization times needed for different set points which were substantially long for all set points taken. The standard deviation and instability of the results is seen to increase for set points with high latent heating. Figure 7.4 shows temperature differences between different measurement points in the final saturator.

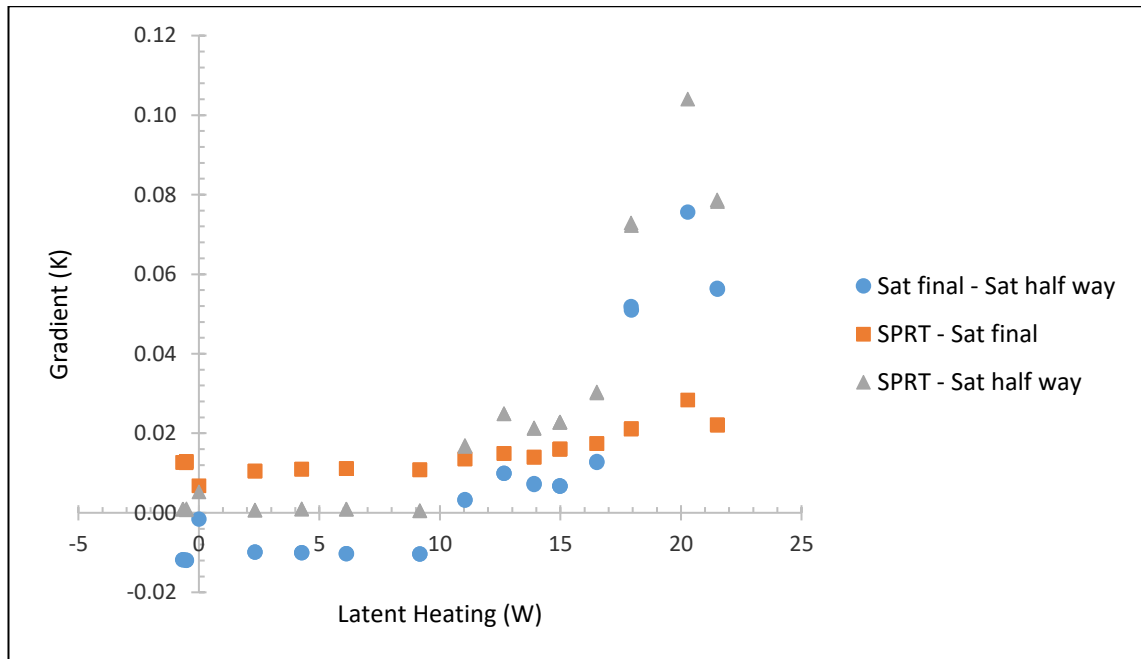


Figure 7.4: Temperature gradients across the final saturator against latent heating in pre-saturator and final saturator.

This graph shows that the difference between the PRT at the end of the saturation path and the PRT half way along the saturation path is small when the latent heating is below 9 W. This indicates that the gradient along the saturation path is low and the gas is near full saturation before the end of the path. Above 9 W the difference increases and by 20 W can be as high as 75 mK. Figure 7.4 shows that the PRTs measure the effect of the latent heating better than the SPRT which is immersed in the bath liquid near the outlet of the saturator. Based on the gradients shown in figure 7.4 the latent heating in the pre-saturator and final saturator will be kept between 0 and 5 W to ensure that the saturator remains reasonably efficient and to ensure that condensation does not occur causing the water level in the saturators to rise, reducing their efficiencies. The latent heating in the system will be approximated during use by measuring the difference in temperature between the pre-saturator and final saturator. A high temperature difference indicates incomplete saturation at the outlet of the pre-saturator and high latent heating in the system overall. Figure 7.5 shows the relationship between the temperature difference from the pre-saturator to the final saturator and the latent heating in both units.

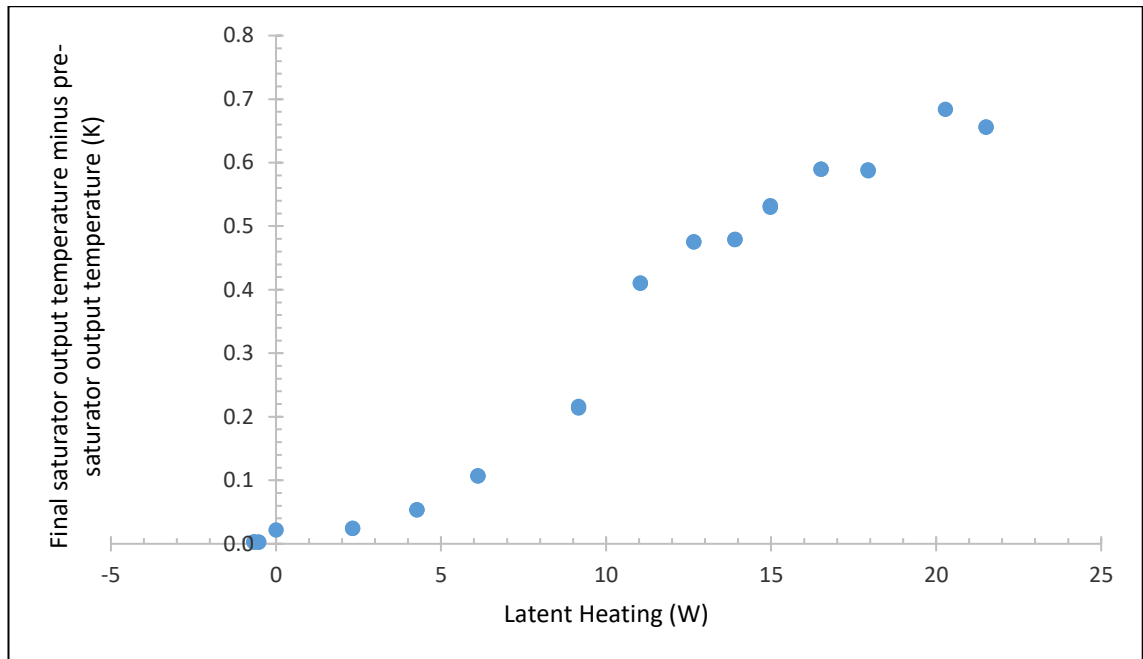


Figure 7.5: Graph of the temperature difference between the output of the final saturator and the output of the pre-saturator against the latent heating in both units.

Figure 7.5 shows that if the pre-saturator is maintained at less than 0.05 K below the final saturator then the latent heating will not exceed 5 W. The pre-saturator will therefore be maintained at slightly less than 0.05 K below the final saturator (by the operation of the pre-humidifier bypass) to ensure that net evaporation is occurring, and the latent heating is below 5 W.

Having determined the range in which the generator is efficient, the uncertainty associated with the saturation efficiency can now be estimated as the temperature difference between the measurement point near the end of the saturation path and the temperature of the bath liquid near the outlet of the final saturator. This is because, in the range where the generator is efficient; the output gas will have a higher dew point than the temperature measured near the end of the saturation path due to latent heating cooling the PRT and surroundings and the gas continuing to increase in humidity after this point. The output will be lower than the temperature of the surrounding bath liquid, since the generator is operating in an evaporative mode and the dew point is approaching the liquid bath temperature. Figure 7.6 shows a graph of the difference in temperature of the surrounding bath liquid and both the PRT at the end of the saturation path and the PRT half way along the saturation path. The temperature differences are normalized to remove the effect of gradients which do not arise from latent heating or air flow effects (the uncertainty due to these effects will be included elsewhere).

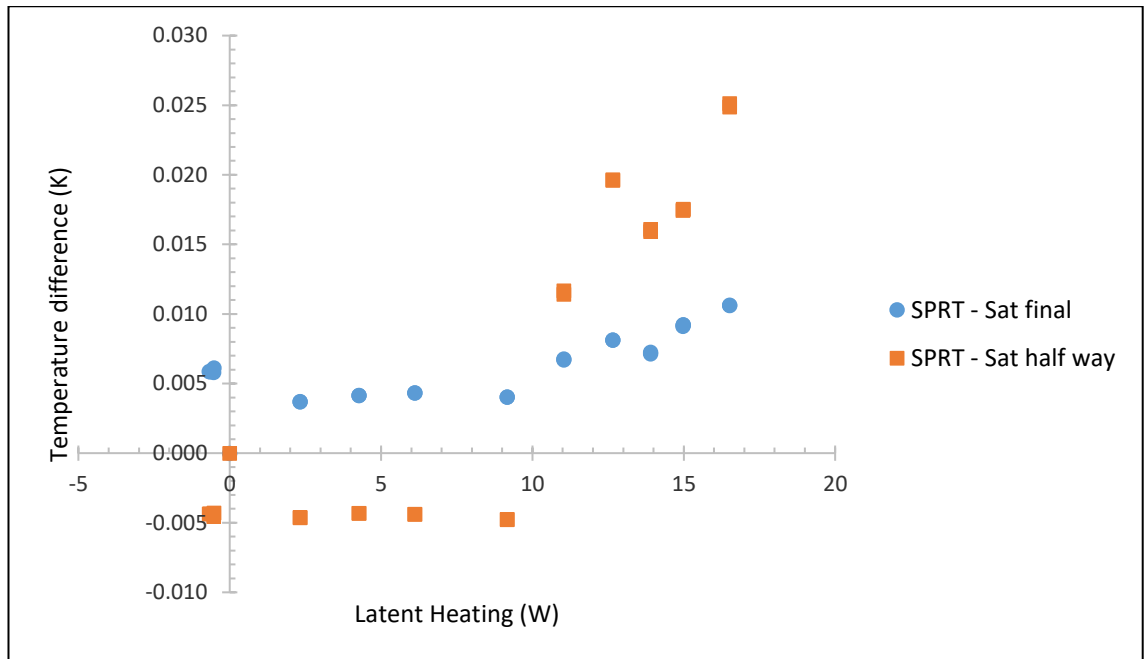


Figure 7.6: Graph of the temperature difference between two points in the final saturator and the surrounding bath liquid normalized to remove bath gradients plotted against latent heating in the system.

It can be seen in figure 7.6 that the maximum difference between the PRT near the end of the saturation path and the surrounding bath liquid is below 5 mK in the range of interest. This is therefore the halfwidth of the rectangular distribution of values attributed to the uncertainty of the saturation efficiency. The value found will be divided by $\sqrt{3}$ as described in [39] to give a standard uncertainty of ± 3 mK dp. This agrees with the initial test of the flow rate dependency shown in figure 7.1 as none of the values in figure 7.1 within the appropriate range differed by as much as ± 3 mK.

7.4. Adsorption and desorption effects

Adsorption and desorption effects can cause an offset in the output dew point by lowering or raising the output, respectively. The magnitude of the offset that it may cause under normal conditions will be estimated by comparing the output when the system is relatively dry to when the system is relatively wet. The true value should lie somewhere between these points so the uncertainty will be taken as the difference between these points and will have a rectangular distribution. Table 7.1 gives the data used to determine the uncertainty due to absorption/desorption effects.

Table 7.1: Data used to determine the uncertainty due to adsorption/desorption effects

State of the system	Expectation of dew point (°C)	Reference hygrometer reading (°C)	Correction (°C)	Variance (°C)
System dried and given long stabilization time	90.031	90.038	-0.007	0.001
System relatively wet	89.031	89.050	-0.019	0.002
Hygrometer dried	89.032	89.042	-0.010	0.002
Outlet tube dried	89.033	89.039	-0.006	0.001

The system was initially dried and given a long stabilization time (over a number of days) in order to give a reference point of what is usually considered as stable. In order to dry the system the reference hygrometer was forward purged while the rest of the system was back purged with air at approximately -55 °C fp. The system is then made relatively wet compared to its output dew point by lowering the output to 89 °C dp. Changing the set point from the calibration point of the reference hygrometer could cause linearity errors but since the calibration corrections to the mirror in the high range are small this should be insignificant. The system could also be wetted by increasing the dew point to 91 °C but since this is outside of the current range of the system it could cause other errors and since it is approaching the critical point of the water vapour pressure curve it could overestimate the uncertainty at 90 °C dp. After a stable set point is recorded with the system relatively wet compared to the output dew point, the reference hygrometer is dried and allowed to stabilize. Comparing the output when the chilled mirror hygrometer is relatively wet to when the mirror is relatively dry gives an uncertainty due to adsorption and desorption effects in the reference hygrometer of

± 9 mK. This is the uncertainty due to adsorption and desorption effects in the hygrometer. Since this is an uncertainty that affects the UUT and not the reference output of the generator it will not be included in the uncertainty budget. The outlet tube was then dried by back purging it with dry air and it was allowed to stabilize. Comparing this to the previous measurement when only the reference hygrometer was dry shows that the true value must lie somewhere within this 4 mK range. The half width of the rectangular distribution is ± 2 mK but will be expanded to ± 4 mK to give a conservative estimate. This corresponds to a standard uncertainty of ± 2 mK associated with adsorption/desorption in the outlet tube. This also agrees with the initial value where the system had a long stabilization time to within ± 1 mK. It has been seen that adsorption occurs at a higher rate than desorption and the system stabilizes much quicker if it is dried before use. The system will therefore always be thoroughly dried before use and calibrations will be performed from lowest set point to highest. This is particularly important for frost points which will be discussed in a later section.

7.5. Leaks

The system from the valves above the pre-saturator to the final point of the outlet tube where the hygrometers are usually connected was pressure tested over a number of days. The temperature of the system was maintained by the thermostatic bath at 20 °C and the pressure was set to slightly above atmospheric pressure (126 kPa). The pressure was measured with a precision barometer with a tolerance of 4 Pa. The system was found to lose 1.7234 mPa/s with a standard deviation of 0.00094 mPa/s. From the ideal gas equation this equates to 0.70712 nmol/(s.l) with a standard deviation of 0.00038 nmol/(s.l). The volume of the system is estimated to be 3.30 litres giving a leak rate from the system of 2.34 nmol/s. The molar flow rate of the output gas can be found from the mass flow rate (in units of l/min) using the ideal gas equation and the standard temperature and pressure of 293.15 K and 101.325 kPa respectively. At 1 l/min the molar flow rate at the output is 0.693 mmol/s. In order to determine the uncertainty due to leaks, the system can be considered as a mixed flow generator, combining air at the output flow rate at the generated dew point with ambient air at the flow rate determined by pressure testing. Equation 3.2 can then be used to determine the output mole fraction and therefore the output dew point after mixing. This method for calculating the uncertainty due to leaks is conservative since it assumes that outward leaks when the system is above ambient pressure will be the same as the inward leaks during operation when the system is also slightly above ambient pressure. An ambient dew point of approximately 10 °C is assumed when calculating the mixed output. The measurements are

also conservative because the full system was leak tested while only the outlet tube and the pressure measurement tube are expected to cause an offset in dew point because of leaks. The value calculated for frost point offset due to leaks at $-40\text{ }^{\circ}\text{C}$ generated frost point is found to be 2.8 mK dp using the method described. However, if the leaks are outwards only, as would be expected at $90\text{ }^{\circ}\text{C}$ generated dew point with an operating pressure slightly above ambient, and the leaks are assumed to be $100\text{ \% H}_2\text{O}$ then the molar flow rate of H_2O leaving the system can be estimated to be equal or less than the molar leak rate. This results in a 0.219 mK drop in dew point at $90\text{ }^{\circ}\text{C}$ (corresponding to a standard uncertainty of $\pm 0.126\text{ mK}$ by assuming a square distribution for the uncertainty due to leaks). This is not significant in terms of the uncertainty budget at $90\text{ }^{\circ}\text{C dp}$ as would be expected for high humidities. The uncertainty calculated is conservative because the proportion of H_2O escaping through leaks should be similar to that of N_2 and other components since the molecular radii are similar, and the cracks are probably large enough so as to not be selective in filtering only larger molecules. The effect of back diffusion is not relevant to dew points higher than ambient humidity but will have to be considered for low frost points [40].

7.6. Temperature conditioning in the outlet tube and hygrometer

The heated outlet tube must be at an elevated temperature compared to the output dew point temperature to ensure no condensation occurs, changing the output dew point from its known value at the saturator. The chilled mirror hygrometer must then cool the gas back to the saturation temperature to determine the dew point of the gas. The effect of changing the outlet tube temperature to increase and decrease the heat loading on the chilled mirror hygrometer was investigated in order to determine the uncertainty due to heat loading in the reference hygrometer. The lower limit of the outlet tube temperature required to prevent condensation in the tube was also determined. Figure 7.7 is a graph showing the variation of the measured output dew point with respect to the outlet tube temperature.

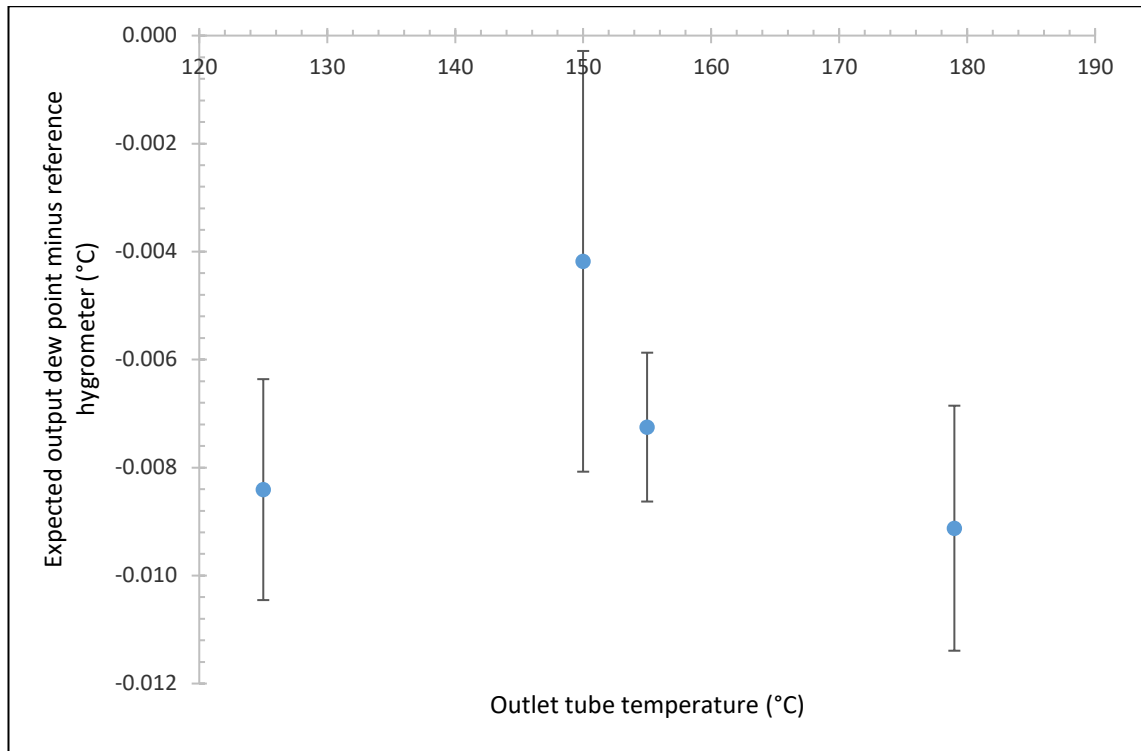


Figure 7.7: Graph of the reference hygrometer correction against outlet tube temperature with error bars representing the standard deviation.

The values in figure 7.7 were taken in the order of 155 °C, 179 °C, 125 °C and 150 °C output tube temperature, respectively. The higher standard deviation of the measurement at 150 °C could have been due to instability in the monitoring hygrometer caused by the outlet tube temperature variation or from some other unknown effect however since the variance is still below 4 mK it is acceptable for this type of measurement. The error bars represent the combined variance of the monitoring hygrometer reading and the expected output dew point but the increase in variance at 150 °C is due only to an increase in variance of the hygrometer reading.

Since the graph is not linear, the minimum to maximum value of figure 7.7 will be taken to be the halfwidth of the rectangular distribution representing the uncertainty due to temperature conditioning. This gives a value of ± 5 mK for the halfwidth which gives a standard uncertainty of ± 3 mK. Since the elevated temperature of the output gas does not affect the mole fraction of the output gas this is an uncertainty relating to the measuring instrument. When the outlet tube was brought to 120 °C (30 °C above the output dew point) the output measured by the reference hygrometer began to drop off. This is due to condensation occurring due to the large temperature inhomogeneity across the outlet tube. For example, the point at which the outlet tube leaves the liquid bath is much closer to 90 °C than the rest of the tube. Additional heat tracing is added at this point to reduce this effect. Based on figure 7.7 it is appropriate to use the generator at 90 °C with an outlet tube temperature of approximately 140 °C without

suffering from condensation in the outlet or excessive heat loading in the measuring hygrometer.

7.7. Repeatability of the generator and chilled mirror hygrometer

Repeatability is usually measured by removing the sensing element from the calibration medium and possibly by switching the instrument under test off and on. At 90 °C dp the chilled mirror hygrometer cannot be switched off as lack of measuring head heating would cause the hygrometer to flood. If the unit were dried before it is powered off and on it would introduce uncertainties other than the repeatability. For this reason, the repeatability of the chilled mirror hygrometer will be assessed by performing a mirror check and recording the difference in the measured hygrometer correction before and after. A mirror check is when the chilled mirror (the sensing element of a chilled mirror hygrometer) is heated above the measured dew point temperature, removing any condensate from the mirror after which the mirror temperature is reduced until a new condensate layer is formed and dew point measurement continues. The repeatability due to performing a mirror check was found to be 0.4 mK. This is the half width of the rectangular distribution of values due to mirror repeatability. This value will be doubled to 0.8 mK to give increased coverage, due to the limited number of measurements taken. This equates to a standard uncertainty of ± 0.5 mK.

The repeatability due to mirror cleaning will also be assessed. The sensing element of a chilled mirror hygrometer must be cleaning regularly to remove contamination that would alter the chemical potential of the condensate changing the vapour pressure at a certain temperature and encouraging condensation by providing a seed to initiate condensation. When used with the primary dew point generator discussed in this thesis it was found that the mirror could be used for a long time without been cleaned and without building up noticeable contamination. This is due to the purity of the water used in the system, the cleanliness of the system and the level of filtration of the air used in the system. When the repeatability due to mirror cleaning was carried out the mirror was used for an extended time without cleaning prior to the test. The test could be considered as measurement of the uncertainty due to mirror contamination but since the level of contamination is so small it is really a test of the repeatability of the hygrometer due to the interference with the measuring head during cleaning. The repeatability due to mirror cleaning was found to be 3.4 mK which will be taken as the half width of the square probability distribution for the associated uncertainty. This will be doubled to provide additional coverage to account for the limited number of measurements taken. This corresponds to a standard uncertainty of ± 3.9 mK.

In order to measure the repeatability of the dew point generator the output will be measured before and after the flow through the generator is stopped and then restarted. Another method to measure the repeatability of the generator is to increase the flow rate so that the efficiency drops off and the output dew point decreases before returning to an efficient flow rate and measuring the change. At 90 °C dp this increase in flow rate would cause a large temperature disturbance in the system due to the significant increase in latent heating and would require a long stabilization time to return to the set point, therefore interfering with the repeatability measurement. By stopping the flow completely the temperature and equilibrium of the system is still disturbed but to a lesser extent than if a high flow rate is used. Using this method, the uncertainty due to repeatability of the generator was found to be 0.95 mK which is taken as the halfwidth of the square distribution of values associated to this uncertainty. This will be doubled to provide additional coverage and corresponds to a standard uncertainty of ± 1.1 mK.

7.8. Effect of varying the bath water level

At 90 °C there is a large amount of evaporation from the thermostatic bath. Insulation with low water vapour permeability was used to reduce the rate of evaporation from the bath but even with insulation the bath still needs to have water added to it approximately once every one to two hours. It was also noticed that when the bath level decreased the gradients within the bath increased and the output dew point changes significantly. This was thought to be due to a combination of the increased gradients and possibly due to the temperature of the outlet tube changing near the surface of the bath liquid due to the change in the water level. This could be due in part to evaporation at the wet part of the tubing that was previously submersed. If the bath gradients are large enough they could also cause condensation in the section of the outlet tube that is submersed in the bath and is not independently heated.

The uncertainty due to the variation in bath water level was determined by first measuring the humidity output when the bath level is slightly lower than it should be, making it unfit to take measurements. This can be seen by the operator as decreased stability, increased gradient from the pre-saturator to the final saturator and by visually observing the upwelling flow of the bath liquid. The humidity output is then measured after the bath is filled with water near its set point temperature and allowed to stabilize. This gives the optimum result and the least optimum result and the uncertainty is taken as the difference between the two.

The uncertainty was found to be ± 12 mK (halfwidth of a rectangular distribution) corresponding to a standard uncertainty of ± 6.9 mK. Since this value was found by allowing the

water level to drop below the level at which it is normally used, it will not be doubled as was done with previous uncertainties. If the bath level is lower than the levels tested, the gradient from the saturator to the pre-saturator will be noticeably increased and the chilled mirror reading will drop off. The bath level will also be visibly lower than it needs to be for sufficient upwelling.

This relatively large uncertainty of 12 mK could be reduced to 0 mK by continually filling the bath with water. If the added water is approximately 90 °C, the flow rate is just high enough to maintain a minimum amount of overflow and the flow is directed into the area of the bath where the water is passed over heat exchangers before re-entering the working volume then the disturbance to the stability of the bath would be small and possibly negligible. This would also allow the system to be operated at 90 °C continuously for long time periods enabling better characterizations of the generator's performance to be achieved. However for typical calibrations where just one set point will be performed at the upper limit of 90 °C the current system allows convenient and practical operation.

7.9. Water Contamination

The result of containing pure water in copper, stainless steel, glass and plastic vessels for a period of 13 months is found to cause a maximum drop in dew point of 0.1 mK over the water surface [41]. Since the dew point generator that is the subject of this thesis will have the water changed and be flushed with pure water more frequently than 13 months and the surface of the final saturator is non-porous and unreactive it is conservative to apply an uncertainty of ± 0.1 mK (halfwidth of rectangular distribution) to the effect of contamination of the water used in the generator. This corresponds to a standard uncertainty of ± 0.06 mK. The water used in the generator is filtered and deionized using an Elga MEDICA-R 7BP water purifier to CLSI grade or better.

7.10. Other uncertainties related to the UUT

The standard deviation of 50 measurements taken from the chilled mirror hygrometer representing a typical calibration point at 90 °C dp has been measured to be below 0.5 mK, however for the sake of this uncertainty budget a value of ± 4.0 mK with Gaussian distribution will be used to cover all possible values when the system is reasonably stable. This value will be measured for each calibration set point and the exact value during calibration can be used

to generate an uncertainty specific for that calibration point. The standard deviation is taken instead of the standard deviation of the mean to give additional uncertainty coverage due to the stability of the UUT.

The resolution of the chilled mirror hygrometer is 0.1 mK when the instrument is sampled by a computer via serial communication. This gives an uncertainty contribution of ± 0.1 mK with a rectangular distribution corresponding to a standard uncertainty of ± 0.06 mK. This uncertainty is valid regardless of whether the instrument rounds or truncates additional decimal places.

7.11. Uncertainties relating to the measurement of the saturator temperature

This section gives the uncertainties expected to contribute to the uncertainty of the measured final saturator temperature. The uncertainties will be propagated through Eq. 3.5 using Eq. 7.3 to give the uncertainties in terms of the output dew point.

7.11.1. Standard deviation of the measured saturator temperature

The uncertainty due to the variance of the measurement of saturation temperature is equal to the standard deviation of the mean of (usually 50) measurements taken to estimate the temperature of the final saturator. This value can be as low as 0.01 mK but for this uncertainty budget it will be expanded to ± 0.10 mK with Gaussian distribution to cover situations with reduced but acceptable stability. The actual standard deviation of the mean during a calibration can be used to give an uncertainty specific to that calibration point.

7.11.2. Calibration uncertainty of the PRT

The uncertainty associated with the calibration of the PRTs is ± 2.5 mK with a Gaussian probability distribution. If the SPRT is used to measure the final saturator temperature this will be reduced to ± 1.0 mK or lower depending on the calibration of that specific SPRT.

7.11.3. Repeatability and hysteresis of the PRT

The hysteresis of the PRTs was measured during calibration by measuring from the lowest set point to the highest and returning to the midpoint of the calibration to record the difference

due to hysteresis effects. Since this measurement will also be affected by the repeatability of the PRTs the result will be taken as the uncertainty due to repeatability and hysteresis of the PRTs. During this test the maximum change of all the PRTs was 1.6 mK which will be taken as the halfwidth of the rectangular distribution representing this uncertainty. This corresponds to a standard uncertainty of ± 0.92 mK.

7.11.4. Drift of PRTs

The drift of the PRTs used with the dew point generator reported in this thesis is based on limited measurements and measurements must continue over time to determine a reasonable drift rate for the PRTs. During the testing of the dew point generator the PRTs used in the final saturator were found to drift less than 10 mK which will be taken as the halfwidth of the rectangular distribution representing this uncertainty. This corresponds to a standard uncertainty of ± 5.8 mK. Other PRTs from the same manufacturer were found to drift significantly more and were replaced or used for less sensitive measurements. It is therefore very important to monitor the long term drift of the PRTs over time and record the drift throughout the calibration to ensure that they continue to meet the required tolerance.

7.11.5. Uncertainty due to PRT self-heating

A sensing current of 1 mA is used to measure the resistance of the PRTs causing an error due to self-heating. The measured temperature when the current is 0 mA can be estimated by measuring the temperature using two different sensing currents and extrapolating to the temperature measurement at 0 mA. The self-heating offset ΔR_{sh} is given by [42],

$$\Delta R_{sh} = R_1 - \frac{R_2 i_1^2 - R_1 i_2^2}{i_1^2 - i_2^2}, \quad (7.5)$$

where R_1 and R_2 are resistances and i_1 and i_2 are the corresponding sensing currents.

Usually i_1 is chosen to be 1 mA and i_2 is chosen to be $\sqrt{2}$ mA. The uncertainty in the self-heating correction is found by propagating the uncertainty of the sensing currents and the uncertainty of R_2 through Eq. 7.5. The uncertainty of R_1 is not included as this is the resistance measurement to be corrected for self-heating and its uncertainty is included elsewhere in the uncertainty budget.

The self-heating at 90 °C was found to be as high as 8 mK with an uncertainty of ± 4 mK.

Considering the uncertainty of the measured self-heating effect an uncertainty of ± 16 mK with

rectangular distribution will be applied to the uncertainty of the measured final saturator temperature due to PRT self-heating. This corresponds to a standard uncertainty of ± 9.2 mK. If the SPRT is used instead of the PRT then the self-heating uncertainty could be reduced to ± 3 mK standard uncertainty but it is not expected that the SPRT will be used for the final saturator temperature measurement at 90 °C due to the difference in temperature between the bath liquid and the interior of the saturator at high dew points.

7.11.6. Non-linearity of the resistance measurement bridge

If a 100 Ω standard resistor is used then the maximum non-linearity throughout the range used is 0.2 ppm of the measured resistance ratio. The maximum resistance ratio that will be measured is 1.4 when measuring a Pt-100 Ω PRT at 100 °C. This corresponds to an uncertainty of $\pm 2.8 \times 10^{-7}$ Ω in the measured resistance ratio. For a 100 Ω reference resistor this propagates to an uncertainty of $\pm 2.8 \times 10^{-5}$ Ω in the measured PRT resistance. By propagating this uncertainty through ITS-90 it is found that this equates to a temperature uncertainty of ± 0.072 mK which is negligible compared to other uncertainties in this analysis.

7.11.7. Resistance measurement bridge resolution

The resolution of the temperature measurements sampled from the resistance bridge is 0.001 mK giving an uncertainty of ± 0.001 mK with rectangular distribution, which is negligible when combined with the other uncertainties.

7.11.8. Standard resistor calibration

The uncertainty associated with the calibration of the reference resistor is ± 35 $\mu\Omega$ with Gaussian probability distribution. Propagating this uncertainty through ITS-90 results in a temperature uncertainty of ± 0.13 mK or less throughout the range of use.

7.11.9. Standard resistor drift

Based on the calibration history of a number of standard resistors used in the temperature and humidity laboratory, the maximum yearly drift observed over a number of decades was 3.7×10^{-5} Ω . This is an outlier and is much larger than the typical yearly drift so including it

gives a conservative estimate of the drift of the standard resistor. By propagating this uncertainty through the bridge resistance ratio calculation and ITS-90 it is found that this corresponds to a temperature uncertainty of ± 0.14 mK which will be taken as the halfwidth of the rectangular distribution representing this uncertainty. This corresponds to a standard uncertainty of ± 0.081 mK.

7.11.10. Standard resistor temperature coefficient

The standard resistor manufacturer gives a temperature coefficient of 2 ppm/ $^{\circ}\text{C}$ for the standard resistor. For a $100\ \Omega$ standard resistor this corresponds to a change in resistance of $2 \times 10^{-4}\ \Omega/^{\circ}\text{C}$. The temperature at which the standard resistor is calibrated is $20\ ^{\circ}\text{C}$ ($\pm 0.01\ ^{\circ}\text{C}$) and the temperature of the laboratory in which it is used is $20\ ^{\circ}\text{C}$ ($\pm 3\ ^{\circ}\text{C}$). Therefore, for a $3\ ^{\circ}\text{C}$ temperature change, the standard resistor may change by $6 \times 10^{-4}\ \Omega$. By propagating this uncertainty through the bridge resistance ratio calculation and ITS-90 it is found that this corresponds to a temperature uncertainty of ± 2.2 mK which is assumed to be the halfwidth of the rectangular distribution representing this uncertainty. Due to the lack of knowledge of the true temperature coefficient of the standard resistor, this value will be doubled to ± 4.4 mK. This corresponds to a standard uncertainty of ± 2.5 mK.

7.11.11. Temperature gradients in the final saturator

Since temperature gradients in the final saturator are dependent on latent heating the data displayed in figure 7.4 will be used to determine the maximum temperature difference around the point of measurement in the final saturator. The highest temperature difference between any two measurement points is 11 mK for latent heating between 0 and 10 W, giving a rectangular distribution of 11 mK halfwidth for the uncertainty due to temperature inhomogeneity around the point of measurement in the final saturator. This corresponds to a standard uncertainty of ± 6.4 mK. This does not need to be expanded further as the generator will only be operated with a latent heating of less than 5 W.

7.11.12. Bath stability

The uncertainty in the measured final saturator temperature will be taken as the standard deviation of the temperature measured by the SPRT during the measurement interval. The SPRT is used for this measurement as it is immersed directly in the bath liquid and responds

faster to changes in the temperature of the liquid surrounding the saturator. This uncertainty is typically less than ± 2 mK so an uncertainty of ± 3 mK with Gaussian distribution will be applied to the uncertainty due to bath stability to give a conservative estimate. It may be overly conservative to include this as an uncertainty as the stability of the output dew point should depend more on the temperature stability inside the saturator than the stability of the bath liquid outside it which is less stable due to the high thermal mass and thermal conductivity of the saturator.

7.12. Uncertainty of the measured final saturator pressure

This section describes the uncertainties related to the measured final saturator pressure. The saturator pressure is measured by a precision digital pressure meter connected to the saturator via a $\frac{1}{4}$ inch electropolished stainless steel tube.

7.12.1. Standard deviation of the measured final saturator pressure

The standard deviation of 50 measurements of the final saturator pressure could be as low as 1 Pa. This will be expanded to an uncertainty of ± 5 Pa with Gaussian distribution to cover all cases where reasonable stability is met. This corresponds to a standard deviation of the mean of 0.7 Pa. The uncertainty in the output dew point is found from the pressure uncertainty using the method described in section 7.1. By propagating the pressure uncertainty through Eq. 3.5 and the iterative solution method described in chapter 3.4.1 it is found that this corresponds to a standard uncertainty of ± 0.2 mK dp.

7.12.2. Tolerance of the pressure transducer

The manufacturer of the digital pressure meter gives a tolerance of ± 0.01 % of the full range of the instrument including non-linearity, hysteresis, repeatability and temperature effects from 10 °C to 40 °C. The instrument has a range from 75000 Pa to 115000 Pa giving a tolerance of ± 4 Pa which will be taken as the halfwidth of the rectangular distribution representing this uncertainty. This corresponds to a standard uncertainty of ± 2 Pa which can be propagated through Eq. 3.5 to give a standard uncertainty in the output dew point of ± 0.6 mK dp.

7.12.3. Drift of the pressure transducer

The drift of the pressure transducer between yearly calibrations was determined by analysing the calibration results over the past decade. It was found that the maximum drift between calibrations over the past ten years, at any set point over the pressure range, was 4 Pa which corresponds exactly with the manufacturer's specification for yearly drift. This will be taken as the halfwidth of the rectangular distribution representing this uncertainty which corresponds to a standard uncertainty of ± 2 Pa. This results in a standard uncertainty in the output dew point of ± 0.6 mK dp.

7.12.4. Hydrostatic head correction

This is the uncertainty associated with the correction applied to the measured saturator pressure to correct for the difference in altitude of the saturator and the digital pressure instrument. Equation 3.16 is the equation used to determine the pressure correction and the uncertainty in the pressure correction is found by propagating the uncertainty of the height difference through this equation. The height difference is approximately 30 cm and its uncertainty will be estimated conservatively as 20 cm. Since the uncertainty of the height difference is large the other uncertainties relating to the correction are negligible and the correction is found to be 3 Pa (± 2 Pa with rectangular distribution). This corresponds to a standard uncertainty of ± 1 Pa, corresponding to a dew point temperature uncertainty of ± 0.3 mK.

7.12.5. Resolution of the digital pressure meter

The resolution of the digital pressure meter is 1 Pa resulting in an uncertainty of ± 1 Pa with rectangular probability distribution. This corresponds to a standard uncertainty of ± 0.6 Pa which propagates to a dew point temperature uncertainty of ± 0.1 mK dp.

7.12.6. Repeatability and hysteresis of the pressure transducer

The calibration set points that the pressure meter is calibrated at are performed in ascending and descending order. The repeatability and hysteresis of the transducer will be taken as the maximum change at any one set point of the ascending and descending results over the history of the instrument. It was found that the maximum repeatability/hysteresis of the

instrument during calibration was 2 Pa which will be taken as a the halfwidth of the rectangular distribution representing this uncertainty. This corresponds to a standard uncertainty of ± 1 Pa which can be propagated to a dew point temperature uncertainty of ± 0.3 mK dp. It is conservative to include this as an uncertainty as the manufacture's tolerance for the instrument includes repeatability and hysteresis.

7.12.7. Pressure stability in the final saturator

The uncertainty due to the pressure stability in the final saturator will be estimated as half of the peak to peak spread of measurements of the saturator pressure taken over the period of a typical measurement. This is typically below 4 Pa but will be expanded to 10 Pa to ensure that all situations with reasonable stability fall within these limits. This corresponds to the halfwidth of the rectangular distribution representing this uncertainty, and therefore corresponds to a standard uncertainty of ± 5.8 Pa, propagating to a standard uncertainty in the output dew point of ± 1.5 mK dp.

7.13. Uncertainty of the hygrometer measuring head pressure

The uncertainties relating to measured pressure of the chilled mirror hygrometer measuring head will be given in this section. The hygrometer head pressure is measured by an integrated pressure transducer connected to the flow path just after the measuring head. The temperature of this transducer is affected by the head temperature so the instrument applies a correction to compensate for the temperature dependence. This makes calibration of the integrated transducer complicated and time-consuming. Instead of calibrating the integrated transducer it will be compared with the calibrated reference pressure meter for each set point where the head temperature differs. The reference pressure meter that measures the saturator pressure can be switched to measure the hygrometer head pressure directly via a connection on the hygrometer head in which an endoscope is usually connected. If the hygrometer being calibrated does not have this connection an alternative head can be used to correct the integrated transducer before replacing the original head to perform dew point measurements.

7.13.1. Standard deviation of the measured head pressure

The standard deviation of the mean of the head pressure measured by the hygrometer's integrated transducer is found to be below 2 Pa giving an uncertainty of ± 2 Pa with Gaussian distribution corresponding to ± 0.5 mK dp.

7.13.2. Tolerance associated with the calibration correction

The reference pressure meter used to correct the integrated transducer has a manufacturer stated tolerance of 4 Pa corresponding to an uncertainty of ± 4 Pa. This corresponds to the halfwidth of the rectangular distribution representing this uncertainty, and therefore corresponds to a standard uncertainty of ± 2 Pa, propagating to a standard uncertainty in the output dew point of ± 0.6 mK dp.

7.13.3. Drift associated with the calibration correction

The reference pressure meter used to correct the integrated transducer has a yearly drift uncertainty of ± 4 Pa with rectangular distribution, corresponding to a standard uncertainty of ± 2 Pa, propagating to a standard uncertainty in the output dew point of ± 0.6 mK dp.

7.13.4. Drift of the integrated head pressure transducer

During the characterization the correction to the integrated pressure transducer was measured before and after tests were performed to assess the drift during use. The drift was also observed over a number of weeks of taking measurements at the same set point and the transducer correction was found to change by no more than 20 Pa. Due to the limited measurements and assessment of the drift, this will be expanded to give an uncertainty of ± 50 Pa, corresponding to a standard uncertainty of ± 29 Pa, which propagates to ± 7.4 mK dp. The integrated transducer correction can be measured before and after a dew point calibration point is taken in order minimize the drift uncertainty which can be as low as 1 Pa.

7.13.5. Hydrostatic head pressure difference associated with the correction

The hygrometer measuring head and the reference pressure meter have less than a 20 cm difference of vertical height. From Eq. 3.16 it is found that this height difference corresponds

to a pressure difference of 2 Pa, which is taken as the halfwidth of the rectangular distribution of values attributed to this uncertainty, corresponding to a standard uncertainty of ± 1 Pa, which propagates to ± 0.3 mK dp.

7.13.6. Resolution of the correction

The resolution of the reference digital pressure meter used to determine the correction is 1 Pa giving an uncertainty contribution to the correction of ± 1 Pa with rectangular probability distribution. This corresponds to a standard uncertainty of ± 0.6 Pa which propagates to a dew point temperature uncertainty of ± 0.1 mK dp.

7.13.7. Resolution of the measured hygrometer head pressure

The resolution of the pressure measured by the hygrometer is 1 Pa giving an uncertainty contribution of ± 1 Pa with rectangular probability distribution. This corresponds to a standard uncertainty of ± 0.6 Pa which propagates to a dew point temperature uncertainty of ± 0.1 mK dp.

7.13.8. Non-linearity, repeatability and hysteresis of the hygrometer head pressure transducer

The repeatability and hysteresis of the integrated transducer were found by varying the flow through the mirror thus varying the pressure measured by the transducer. The flow was varied by an amount larger than it would be expected to vary in normal operation to get a conservative estimate of the effect that non-linearity will have on measurements. Figure 7.8 is a graph showing the results of the pressure variation.

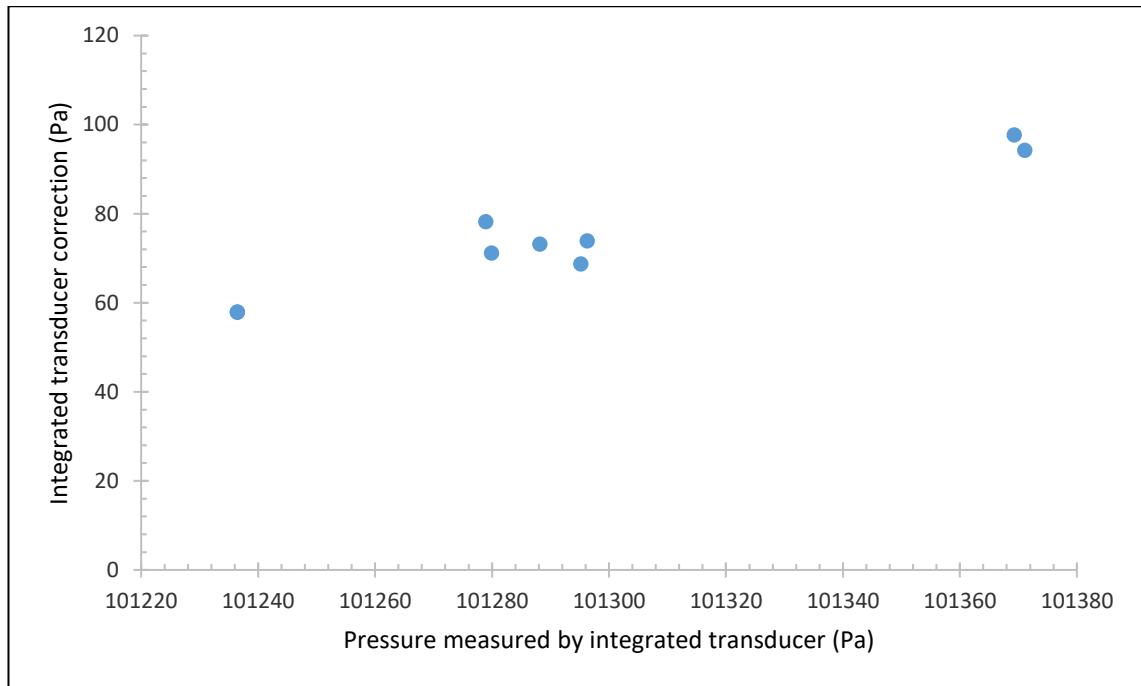


Figure 7.8: Graph showing the integrated transducer correction against the measuring head pressure.

The nonlinearity was estimated as the peak to peak value of the data divided by two, giving an uncertainty due to non-linearity of the sensor of ± 20 Pa, with rectangular distribution. This corresponds to a standard uncertainty of ± 12 Pa which propagates to a dew point temperature uncertainty of ± 3.0 mK dp. The peak to peak value is divided by two since the values are spread approximately evenly around the midpoint.

The correction was measured at 0.5 ls/min, 1 ls/min, 0.5 ls/min, 0 ls/min and 0.5 ls/min respectively. The repeatability/hysteresis was estimated as the peak to peak value of the points taken at 0.5 ls/min. This gives an uncertainty of ± 9 Pa with rectangular probability distribution. This corresponds to a standard uncertainty of ± 5 Pa which propagates to a dew point temperature uncertainty of ± 1.3 mK dp.

7.13.9. Temperature coefficient of the integrated transducer

The pressure read from the integrated transducer is automatically corrected for changes in temperature of the transducer so this test is analysing the deviation from the true value of the pressure measured and corrected by the hygrometer. When measuring a dew point of 90°C the hygrometer head is already at its maximum temperature of 105°C so the hygrometer head transducer correction will be measured at 105°C , 104°C , 103°C and 105°C again. Figure 7.9 shows a graph of the results.

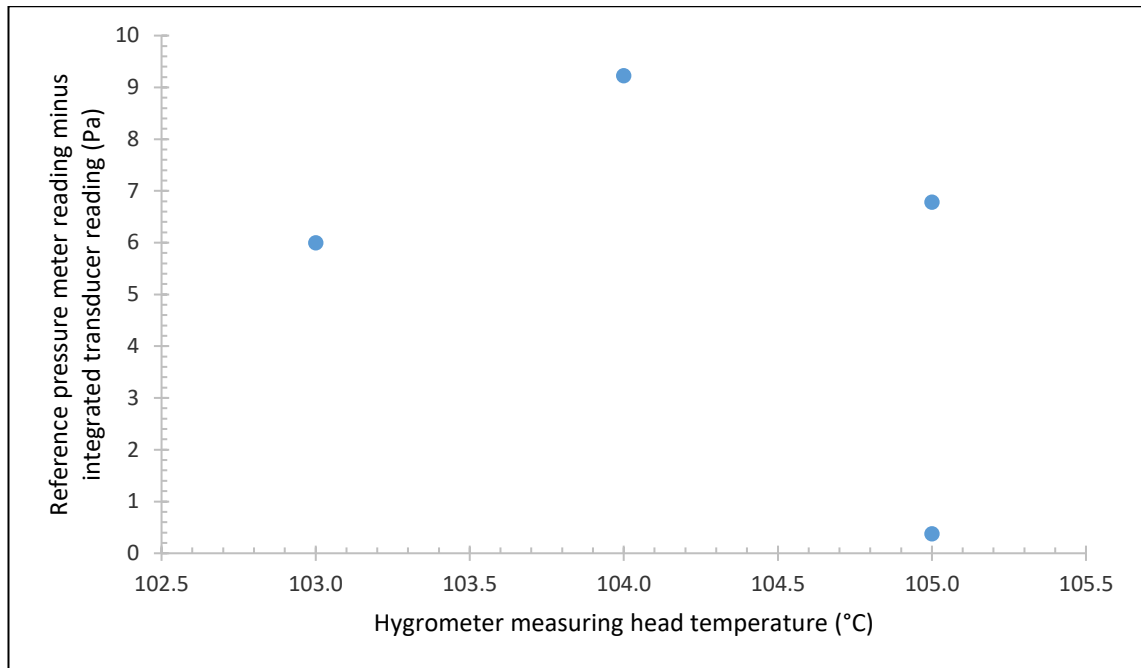


Figure 7.9: Graph of the integrated measuring head transducer correction against the measuring head temperature.

The uncertainty of the measured head pressure due to the variation of the head temperature is taken as the peak to peak value of figure 7.9 divided by two. This results in an uncertainty of ± 5 Pa with rectangular distribution. This corresponds to a standard uncertainty of ± 3 Pa which propagates to a dew point temperature uncertainty of ± 0.7 mK dp. This uncertainty may be conservative due to the fact that the head temperature will not vary by 1°C during measurement and will likely vary by less than 0.1°C . The repeatability observed in figure 7.9 when the head is returned to the original set point fits the previous estimate of repeatability of ± 16 mK.

7.13.10. Stability of the hygrometer head pressure transducer

The uncertainty due to the pressure stability in the hygrometer measuring head will be estimated as half of the peak to peak spread of measurements of the head pressure taken over the period of a typical measurement. This gives an uncertainty of less than ± 20 Pa with rectangular distribution corresponding to a standard uncertainty of ± 12 Pa which propagates to a dew point temperature uncertainty of ± 3.0 mK dp.

7.14. The complete uncertainty budget

The uncertainty budget is evaluated in accordance with the Guide to Expression of Uncertainty of Measurement (GUM) [39]. It lists the results of all uncertainties evaluated. If the uncertainty has a rectangular probability distribution it is divided by $\sqrt{3}$ to give the standard error as described in [39]. If the uncertainty has a Gaussian distribution it is divided by the coverage factor of the given uncertainty in order to give the standard error as described in [39]. Each uncertainty is propagated through Eq. 3.5 and the iterative solution method described in 3.4.1 to give the uncertainty contribution to the estimated output dew point, unless the output dew point is directly affected by the uncertainty in question. The combined standard error and the expanded uncertainty are calculated in accordance with [39]. Table 7.2 is the complete uncertainty budget for the calibration of chilled mirror hygrometers at 90 °C dp.

Table 7.2: Uncertainty budget for the NML primary humidity standard at 90 °C dp:

Description of uncertainty	Value determined	Unit	Divisor	Standard Error	Propagated standard error	Unit
Uncertainties directly affecting the estimate of the output dew point or saturation temperature:						
Saturator efficiency	0.005	K dp	1.73	0.003	0.003	K dp
Leaks	-2.34E-09	mol/s	1.73	-1.35E-09	0.000126	K dp
Adsorption/desorption in output tubing	0.004	K dp	1.73	0.002	0.002	K dp
Water contamination	0.0001	K dp	1.73	0.00006	0.00006	K dp
Temperature conditioning (outlet and hygrometer)	0.005	K dp	1.73	0.003	0.003	K dp
Repeatability of generator	0.0019	K dp	1.73	0.0011	0.0011	K dp
Effect of varying bath water level	0.012	K dp	1.73	0.0069	0.0069	K dp
Uncertainty associated with the measurement of the final saturator temperature:						
Standard deviation of measurand	0.00010	K	1	0.00010	0.00010	K dp
Calibration of PRT	0.0050	K	2	0.0025	0.0025	K dp
Repeatability/Hysteresis of PRT	0.0016	K	1.73	0.00092	0.00092	K dp
Drift of PRT	0.010	K	1.73	0.0058	0.0058	K dp
Uncertainty due to self-heating	0.016	K	1.73	0.0092	0.0092	K dp
Resistance bridge non-linearity	0.000072	K	1.73	0.000042	0.000042	K dp
Resistance bridge resolution	0.000001	K	1.73	0.0000006	0.0000006	K dp
Std. Resistor calibration	0.00013	K	1	0.00013	0.00013	K dp
Std. Resistor drift	0.00014	K	1.73	0.000081	0.000081	K dp
Std. resistor temp coefficient	0.0044	K	1.73	0.0025	0.0025	K dp
Final gradients in saturator	0.011	K	1.73	0.0064	0.0063	K dp
Bath stability	0.003	K	1	0.003	0.003	K dp
Uncertainty associated with the measurement of the final saturator pressure:						
Standard deviation of measurand	0.7	Pa	1	0.7	-0.0002	K dp
Manufacturer's stated tolerance	4	Pa	1.73	2	-0.0006	K dp
Drift of pressure transducer	4	Pa	1.73	2	-0.0006	K dp
Hydrostatic head correction	2	Pa	1.73	1	-0.0003	K dp
Resolution	1	Pa	1.73	0.6	-0.0001	K dp
Repeatability/hysteresis	2	Pa	1.73	1	-0.0003	K dp
Stability	10	Pa	1.73	5.8	-0.0015	K dp
Uncertainty associated with the measurement of the pressure in the measuring head of the UUT:						
Standard deviation of measurand	2	Pa	1	2	0.0005	K dp
Tolerance associated with correction	4	Pa	1.73	2	0.0006	K dp
Drift associated with correction	4	Pa	1.73	2	0.0006	K dp
Temperature coefficient of integrated transducer	5	Pa	1.73	3	0.0007	K dp
Drift of integrated transducer	50	Pa	1.73	29	0.0074	K dp
Hydrostatic head (of correction)	2	Pa	1.73	1	0.0003	K dp
Resolution (of correction)	1	Pa	1.73	0.6	0.0001	
Resolution	1	Pa	1.73	0.6	0.0001	K dp
Repeatability/hysteresis	9	Pa	1.73	5	0.0013	K dp
Linearity	20	Pa	1.73	12	0.0030	K dp
Stability	20	Pa	1.73	12	0.0030	K dp
Uncertainty associated with formulations:						
Vapour pressure formulation	0.001	K dp	1	0.001	0.001	K dp
Enhancement factor	-0.000013	K dp	1	-0.000013	-0.000013	K dp
Dew point calculated from vapour pressure	0.001	K dp	1	0.001	0.001	K dp
Iterative solution resolution	6.E-09	K dp	1	6.E-09	6.E-09	K dp
Uncertainty associated with the UUT:						
Variance	0.0040	K dp	1	0.0040	0.0040	K dp
Resolution	0.0001	K dp	1.73	0.00006	0.00006	K dp
Repeatability due to mirror check	0.0008	K dp	1.73	0.0005	0.0005	K dp
Repeatability due to mirror cleaning	0.0068	K dp	1.73	0.0039	0.0039	K dp
Combined standard error					0.019	K dp
Expanded uncertainty (k=2, 95% coverage interval)					0.038	K dp

8. Changes to the uncertainty budget at -40 °C frost point

This chapter covers the re-evaluation of uncertainties that are expected to differ significantly at -40 °C fp, the lowest humidity in the calibrated range of the chilled mirror hygrometers currently in use at NML. The previous uncertainty analysis concerned air that is made up of more than 70 % water vapour whereas at -40 °C fp air is made up of 0.01 % water. This makes the effect of leaks and adsorption/desorption effects significant. Long drying times are required to prevent instability and an offset due to desorption. Stabilization times are much longer after any change to the system is made. Any dead volumes will need to be purged in order to achieve stabilization and may be affected by leaks due to the fact that there is no flow and any leaks that occur will build up over time. The chilled mirror hygrometers currently in use with the generator are designed primarily for high dew points and -50 °C fp is the lower limit of their specified range. The design of chilled mirror hygrometers intended for use at lower frost points differ significantly. The latent heat of vaporization at low frost points is negligible and saturation is readily obtained. The gradients across the saturator are expected to be reduced due to the absence of latent heating effects.

8.1. Saturation efficiency

At $-40\text{ }^{\circ}\text{C}$ fp latent heating is negligible so varying the flow rate mainly varies the flow regime and the degree of mixing. Figure 8.1 shows the flow rate dependency of the generator.

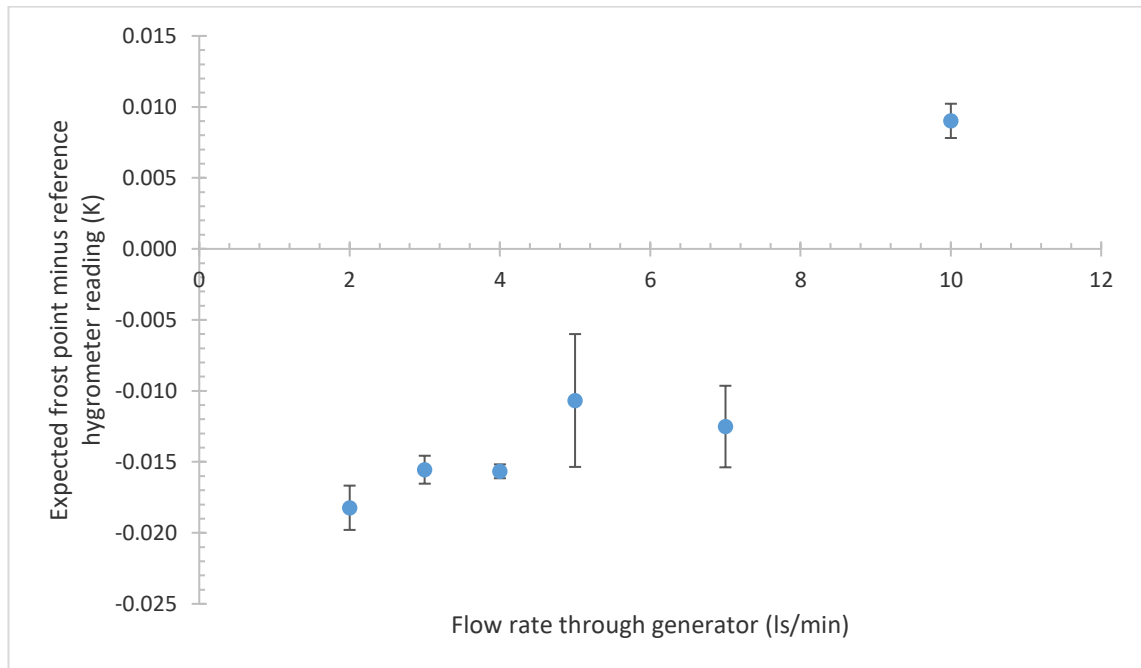


Figure 8.1: Hygrometer correction against flow rate through generator at $-40\text{ }^{\circ}\text{C}$ fp.

Figure 8.1 shows that the output frost point stays relatively constant below 4 ls/min after which the variance of the output increases, and the output frost point as read by the hygrometer decreases. This approximately agrees with simulation results and the results given in figure 7.2. One reason for the increased flow rate range in figure 8.1 is the elevated water level in the saturator during the measurements in figure 7.2 causing an increase in the flow speed and decreased mixing. In figure 8.1, below 4 ls/min, the measured output frost point varies by less than 3 mK peak to peak. Because of this, 4 ls/min will be taken as the maximum operating flow rate of the generator at $-40\text{ }^{\circ}\text{C}$ fp.

Since latent heating is negligible the effect of variation of latent heating will not be investigated. The saturation efficiency will be taken as the difference in temperature between the PRT near the end of the saturation path and the surrounding bath liquid under normal flow conditions. This is because the air should be more saturated than the temperature near the end of the saturation path and should be approaching the temperature of the surrounding bath liquid. The PRTs used suffer more from drift and are less accurate at temperatures below $0\text{ }^{\circ}\text{C}$ so to overcome the reduced accuracy, after a gradient is measured; the position of the two PRTs will be switched, the gradient will be re-measured and an average of the two measurements will be found, cancelling any offsets that the PRTs have. A gradient of less than

1 mK was measured from the PRT half way along the saturation path and the PRT near the end of the saturation path. A gradient of less than 4 mK was measured from the PRT near the end of the path and the position in the bath liquid where the SPRT is usually located. The temperature increases from the location half way along the path, to the final section of the path, to the bath liquid near the outlet. This gives an uncertainty of ± 4 mK dp with rectangular distribution corresponding to a standard uncertainty of ± 2 mK dp relating to the saturation efficiency at -40 °C fp.

8.2. Adsorption and desorption

The uncertainty due to adsorption and desorption effects was determined by drying the tubing and chilled mirror hygrometer and allowing the system to stabilize before recording the difference between the hygrometer reading and the expected output frost point. The system was then wetted by increasing the frost point by one degree Celsius and allowing the system to stabilize. The system was then returned to the original frost point and allowed to stabilize before measuring the correction when the system is relatively wet. For both wet and dry measurements the corrections were measured when stable conditions were first met and after a longer period of stabilization for comparison. In both cases the frost point rose by approximately 5 mK in the period of longer stabilization. The uncertainty due to adsorption and desorption in the outlet tube and the chilled mirror hygrometer was found to be less than ± 14 mK fp with rectangular distribution. The uncertainty due to adsorption and desorption in the chilled mirror hygrometer alone could be as high as ± 9 mK. The adsorption and desorption effect might be measured more accurately by purging the dead volume of the pressure measurement tube between measurements and performing a mirror check before the start of the measurements. However, the long stabilization times at -40 °C fp make it difficult to measure the effect accurately. The uncertainty due to adsorption/desorption in the hygrometer will not be removed from the overall uncertainty. Due to the difficulty in measuring the effect it is safer to use the more conservative estimate of ± 14 mK fp until more measurements are taken, further characterizing the effect. The standard uncertainty of this effect is ± 8.1 mK fp assuming a rectangular distribution.

8.3. Effect of varying the bath liquid level

Since there is negligible evaporation at -40 °C the level of the bath liquid does not change and this uncertainty can be removed.

8.4. The effect of leaks

If the output frost point is below the ambient humidity then back diffusion of water vapour through leaks can affect the output frost point even if the system is over pressure and the leaks are outward due to the fact that the water vapour pressure in system is lower than the ambient water vapour pressure [40]. In [40] the effect of back diffusion through leaks is investigated by creating holes of various diameters in a sampling line and comparing the frost point of a precisely metered flow before and after the leak. It was found that for sufficiently high leak flow rate back diffusion of water vapour is prevented and a slightly elevated pressure is sufficient to achieve the critical leak flow rate. However [40] states that tiny leaks can be potential routes for diffusing water vapour. Back diffusion also occurs through the output of the hygrometer under test and is prevented by attaching a length of stainless steel tubing to the output and a needle valve is placed at the end of the tubing to control the system pressure. In order to prevent back diffusion of water vapour the system will be kept approximately 10 kPa above atmospheric pressure. Figure 8.2 shows the effect of the system pressure on the output frost point (presumably due to back diffusion of H_2O) at $-50\text{ }^{\circ}\text{C}$ output frost point.

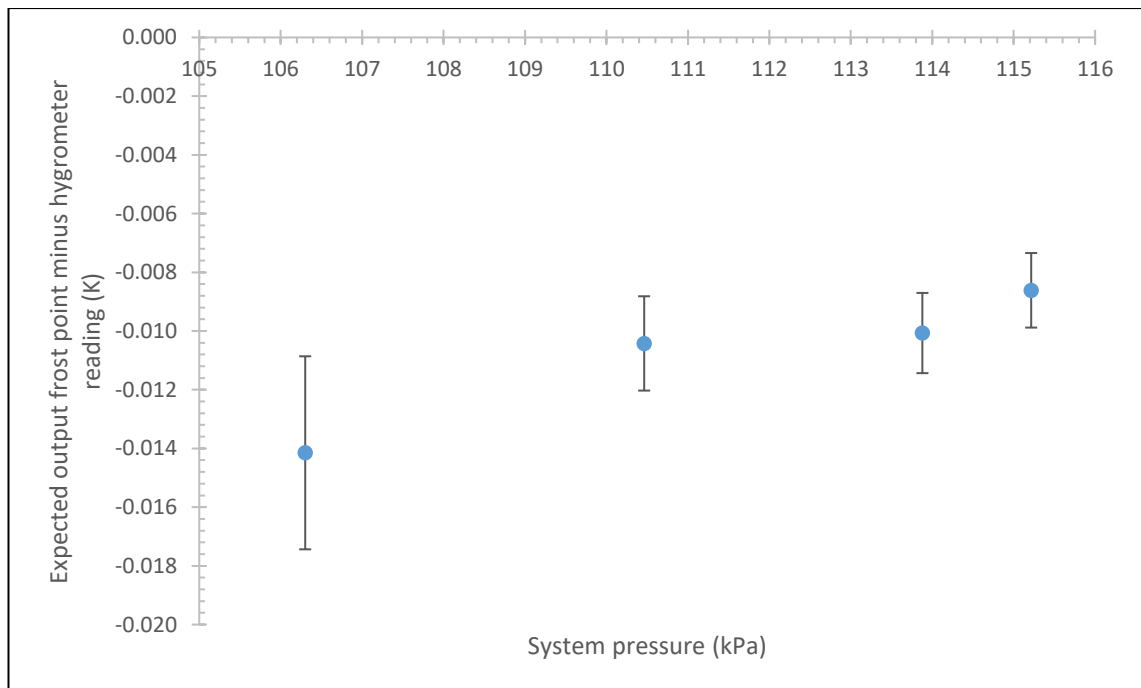


Figure 8.2: Effect of system pressure on the output frost point with error bars representing the standard deviation of the hygrometer reading.

Figure 8.2 shows that the output frost point increases for low gauge pressure in the system. This agrees with what is expected due to the decreased leak flow speed and therefore increased rate of back diffusion of water vapour. The uncertainty in the output frost point due

to back diffusion of water vapour will be taken as the peak to peak value of figure 8.2, giving an uncertainty of ± 5.5 mK fp with rectangular distribution, corresponding to ± 3.2 mK fp. This is reasonably conservative as in reality the system will not be used under 10 kPa gauge pressure for frost points and it is not expected that the effect of back diffusion will reduce significantly at pressures above those in figure 8.2. This method of calculating the effect of back diffusion of water vapour does not account for diffusion through hygroscopic materials in the system and is reliant on no hygroscopic materials such as PTFE being used. At present the only place in the system (excluding the UUT) where such materials are found is in the connection to the digital pressure meter where PTFE tape is used to create the seal between the threads of the connection. Since this is not in the flow path of the generator it is assumed that its effect is negligible however it may improve the water vapour leak tightness of the system and reduce the need for purging of the pressure measurement tube if a metal to metal seal is used.

8.5. Temperature conditioning in the outlet tube and hygrometer

Since the temperature conditioning tests at 90 °C dp covered a temperature change as high as 90 °C from the outlet tube to the measuring head and the temperature conditioning required of the measuring head at -40 °C fp requires a change of approximately 60 °C from ambient to the frost point temperature, it will be assumed that the temperature conditioning uncertainty at 90 °C dp is still valid. However, the mechanics of how the temperature change is brought about is different at -40 °C fp (due to the different head and tube temperatures) so the uncertainty due to the effect of temperature conditioning in the chilled mirror hygrometer should be tested in the future. It may be conservative to include this as an uncertainty as it relates more to the UUT than the generated reference frost point.

8.6. Effect of purging the pressure measurement tube

The ¼ inch diameter electropolished stainless steel tube that connects the digital pressure meter to the final saturator must be dried and purged with air of equal humidity to the air in the final saturator. If the system is in operation for an extended time without purging the pressure measurement tube the effect of leaks in the tube could build up, becoming significant and the generator output becomes unstable. The effect of any frost point offset due to the dead volume of the pressure tube is estimated by running the system for an extended time and measuring the difference in the hygrometer correction before and after the pressure tube is purged. The uncertainty is found to be less than ± 10 mK fp with rectangular distribution,

corresponding to a standard uncertainty of ± 5.8 mK fp. This uncertainty could be reduced by better characterization and specification for the time interval over which the pressure tube should be purged and possibly by reducing leaks in the pressure tube.

8.7. UUT flow rate dependency

The flow rate dependency of the chilled mirror hygrometer was found to be significant at -40 °C fp. Figure 8.3 is a graph showing the flow dependency of the hygrometer.

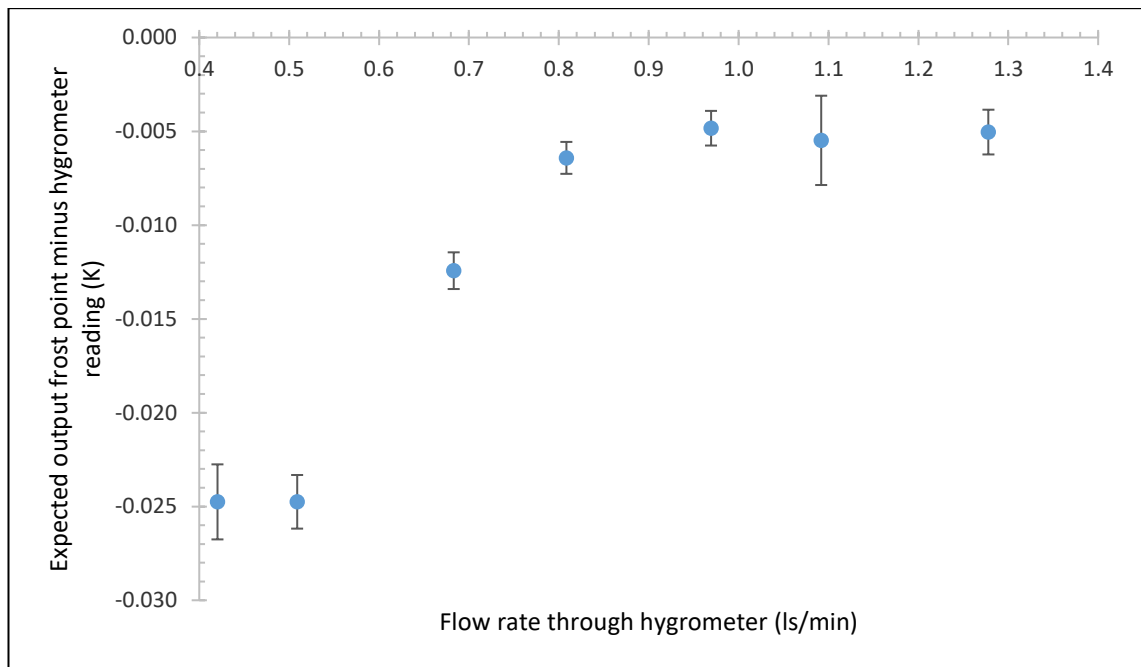


Figure 8.3: Hygrometer correction against flow rate through hygrometer with error bars representing the standard deviation.

The UUT flow rate dependency was investigated by varying the flow through the chilled mirror hygrometer while keeping the flow through the saturators constant at 2 ls/min, a flow rate known to produce efficient saturation. Figure 8.3 shows that the flow rate dependency of the hygrometer is smallest around 1 ls/min, the usual flow rate for frost points. The uncertainty due to the flow rate dependency at 1 ls/min is taken as the peak to peak variation from 0.8 ls/min to 1.2 ls/min divided by 2 giving an uncertainty of ± 2.3 mK fp with rectangular distribution, corresponding to ± 1.3 mK fp standard uncertainty. The flow rate through the hygrometer in regular operation with the dew point generator should not vary by more than 0.1 ls/min based on the resolution of the measured flow.

8.8. UUT measuring head temperature dependency

At $-40\text{ }^{\circ}\text{C}$ fp the measuring head is not temperature controlled resulting in a head temperature slightly above room temperature, usually at approximately $25\text{ }^{\circ}\text{C}$. This means that the Peltier cooler controlling the temperature of the chilled mirror must cool the mirror $65\text{ }^{\circ}\text{C}$ below the surrounding head temperature. The head could reach a temperature slightly above $30\text{ }^{\circ}\text{C}$ due to fluctuations in the laboratory temperature. Figure 8.4 is a graph showing the effect of the head temperature on the measured frost point.

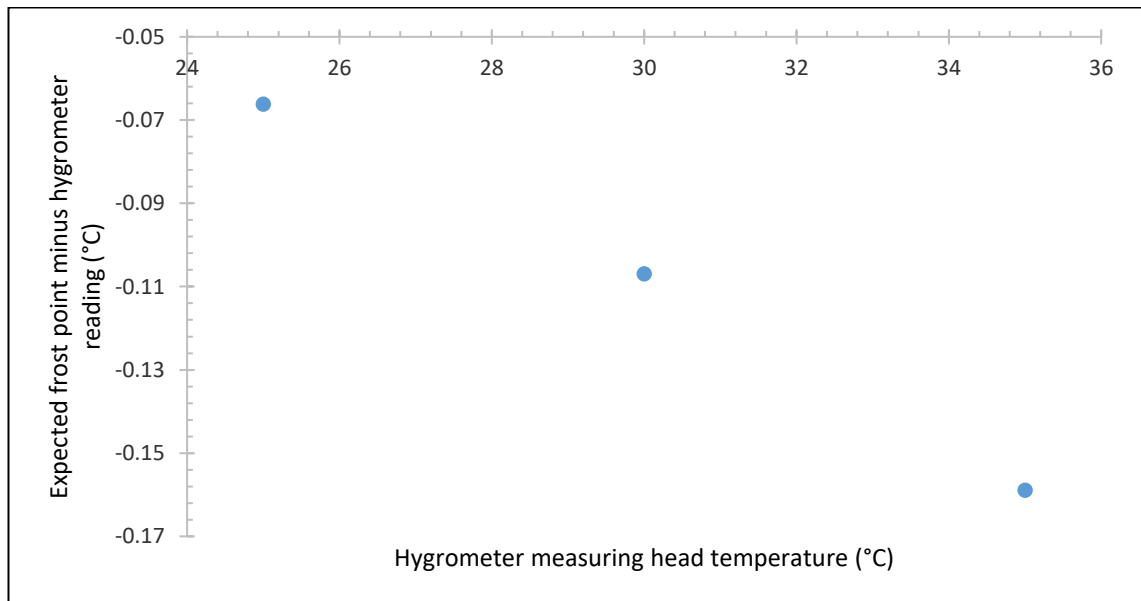


Figure 8.4: Hygrometer correction against the measuring head temperature.

Figure 8.4 shows a large head temperature dependence on the output frost point at $25\text{ }^{\circ}\text{C}$ head temperature giving an uncertainty of at least $\pm 0.05\text{ K}$, making it by far the most dominant uncertainty relating to the calibration of chilled mirror hygrometers using the dew point generator. This uncertainty is only valid if the hygrometer is used only at $25\text{ }^{\circ}\text{C}$ ($\pm 5\text{ }^{\circ}\text{C}$) to match the calibration conditions. If the chilled mirror is to be used at $20\text{ }^{\circ}\text{C}$ (which is common) this uncertainty would have to be expanded to at least $\pm 0.1\text{ K}$. In an attempt to reduce this uncertainty, the measuring head will be cooled by pumping water from a temperature controlled bath through the measuring instrument. This brought the measuring head to approximately $6\text{ }^{\circ}\text{C}$. Figure 8.5 is a graph showing the dependence of the measured frost point on the head temperature with head cooling used.

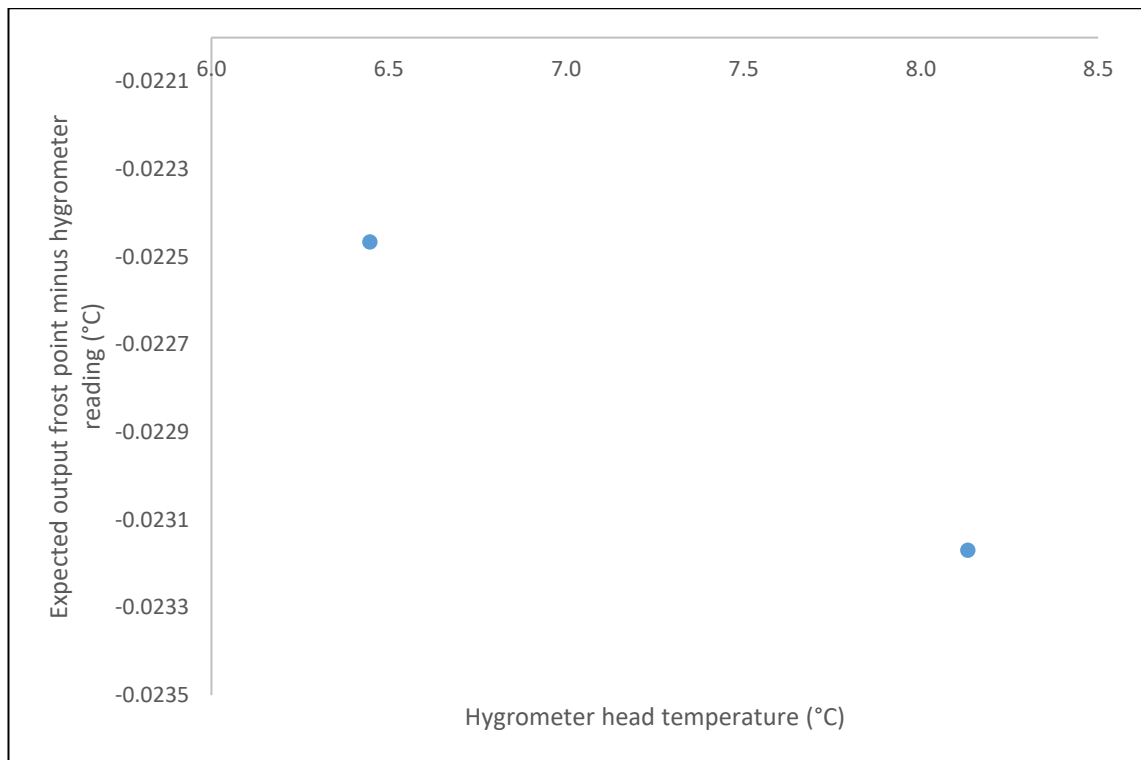


Figure 8.5: Hygrometer correction against hygrometer head temperature with head cooling used.

Figure 8.5 shows that the measured frost point changes by 0.7 mK when the head temperature is changed by approximately 1.5 °C, giving an uncertainty due to variation of the head temperature of ± 0.7 mK with rectangular distribution corresponding to ± 0.4 mK standard uncertainty. This is negligible and the change in the measurement is probability due to the stability and repeatability of the measuring instrument and unrelated to the head temperature. When cooling was used the standard deviation of the head temperature was always below 0.1 °C and was sometimes as low as 5 mK. The dependence of the measured dew/frost point temperature on the head temperature is not usually assessed as part of a chilled mirror calibration as it is an uncertainty that relates to the hygrometer. However, as a user of an instrument it is important to assess its dependence on such variables and the validity of the calibration results depends on the conditions of use matching the calibration conditions. As such, the hygrometer will be used with head cooling at low frost points for future measurements, otherwise a larger uncertainty component for the head temperature variation should be used.

8.9. UUT repeatability

The repeatability of the hygrometer under test was found by performing a mirror check as described in section 7.7. The measurements before and after the mirror check differed by 4.0 mK giving an uncertainty of ± 4.0 mK rectangular distribution. This value will be doubled to ± 8.0 mK to increase confidence despite the limited number of measurements taken. This corresponds to a standard uncertainty of ± 4.6 mK.

The uncertainty due to repeatability before and after mirror cleaning will not be tested at frost points due to the large drying times needed. It will be assumed that it has the same value as was found previously at 90 °C dp. It may be unnecessary to include this as an uncertainty and it may be removed in the future.

8.10. Uncertainties relating to the measurement of the final saturator temperature

The uncertainties relating to the measured final saturator temperature are calculated in the same manner as in section 7.9 except that due to the increased drift of the PRTs at low temperatures the SPRT will be used to estimate the final saturator temperature. This will have a minimal effect on the accuracy of the result since latent heating at -40 °C fp is negligible so the temperature inside the saturator is closer to the surrounding bath temperature than it is at high dew points. The use of the SPRT instead of the PRT reduces the uncertainty associated with calibration, drift and self-heating, and the uncertainty due to hysteresis is removed, as can be seen in the full uncertainty budget at -40 °C fp.

The uncertainty associated with the resistance measurement of the SPRT will remain unchanged as it is an estimate of the maximum resistance measurement uncertainty across the range of the generator and recalculating the uncertainty for a -40 °C measurement would produce a reduction in uncertainty that would be negligible in terms of the total uncertainty of the generated frost point.

The uncertainty in the measured saturator temperature due to bath gradients was measured using the same method that was used to measure the gradients across the saturator in section 8.1 except the uncertainty is taken as the maximum temperature difference across all three temperature sensor locations giving an uncertainty of ± 4.7 mK with rectangular distribution corresponding to ± 2.7 mK standard uncertainty. The uncertainty due to the bath stability is

taken as the standard deviation of the temperature of the liquid surrounding the saturator over a period of 12 hours giving an uncertainty of ± 0.40 mK with Gaussian distribution.

8.11. Uncertainties relating to the measurement of the final saturator pressure

The standard deviation of the mean of the final saturator pressure is usually below 0.7 Pa but will be expanded to give an uncertainty of ± 1.4 Pa with Gaussian distribution to ensure that all reasonably stable conditions are covered by the uncertainty. The stability is usually below 20 Pa from peak to peak so the stability uncertainty will be assumed to be ± 20 Pa (halfwidth of the rectangular distribution associated with the uncertainty) effectively doubling the uncertainty to add confidence despite the limited number of measurements taken. This corresponds to a standard uncertainty of ± 12 Pa

The hydrostatic head correction is calculated using the same method as described in 7.10.4 and was found to be equal to 3.6 Pa with an uncertainty of ± 2.4 Pa with rectangular distribution corresponding to ± 1.4 Pa standard uncertainty. All other saturator pressure uncertainties remain unchanged.

8.12. Uncertainties relating to the measurement of the UUT head pressure

The standard deviation of the mean head pressure is usually under 1.4 Pa but will be expanded to give an uncertainty of ± 2.1 Pa with Gaussian distribution due to the lack of data for the integrated pressure transducer. The stability can be as high as 31 Pa from peak to peak with reasonable overall system stability so the halfwidth of the rectangular distribution representing this uncertainty will be taken as ± 31 Pa, effectively doubling the uncertainty. This corresponds to a standard uncertainty of ± 18 Pa.

The integrated transducer was found to drift by 21 Pa over two weeks of taking measurements. The uncertainty due to drift of the transducer during calibration will remain unchanged at 50 Pa due to the limited data.

The uncertainty due to temperature variation of the integrated head transducer was found at room temperature without head cooling. The test should be repeated with head cooling in the future. It is expected to yield a smaller uncertainty with cooling due to the reduced variation of

head temperature. Figure 8.6 is a graph showing the variation of the integrated transducer reading with respect to the head temperature.

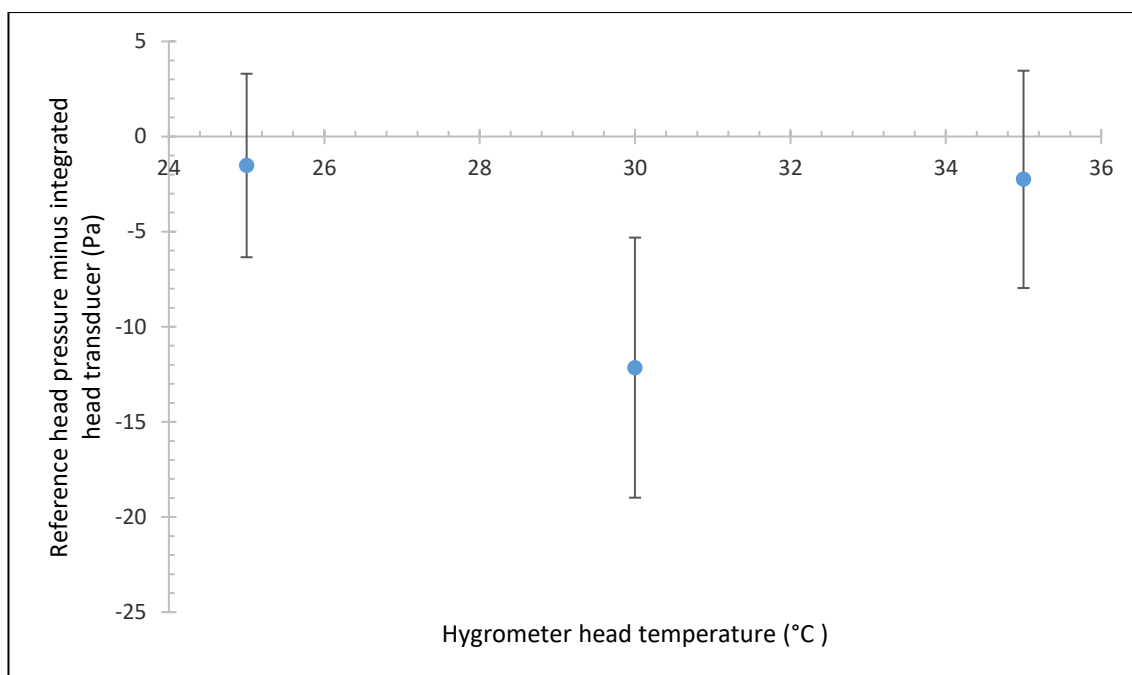


Figure 8.6: Graph of the head transducer correction against the hygrometer head temperature.

The uncertainty in the measured head pressure due to the variation of the head temperature will be taken as the peak to peak value of figure 8.6 giving an uncertainty of ± 11 Pa with rectangular distribution, corresponding to a standard uncertainty of ± 6.4 Pa.

8.13. Full uncertainty budget at -40 °C fp

The combined uncertainty at -40 °C fp was calculated in the same manner described in section 7.14 with the changes described in this chapter. Table 7.3 shows the results of the uncertainty budget.

Table 8.1: Uncertainty budget for the NML primary humidity standard at -40 °C fp:

Description of uncertainty	Value determined	Unit	Divisor	Standard Error	Propagated standard error	Unit
Uncertainties directly affecting the estimate of the output dew point or saturation temperature:						
Saturator efficiency	0.004	K dp	1.73	0.002	0.002	K fp
Leaks	0.0055	K dp	1.73	0.0032	0.0032	K fp
Adsorption/desorption in output tubing	0.014	K dp	1.73	0.0081	0.0081	K fp
Water contamination	0.0001	K dp	1.73	0.00006	0.00006	K fp
Temperature conditioning (outlet/hygrometer)	0.005	K dp	1.73	0.003	0.003	K fp
Repeatability of generator	0.0019	K dp	1.73	0.0011	0.0011	K fp
Effect of purging pressure tube	0.010	K dp	1.73	0.0058	0.0058	K fp
Uncertainty associated with the measurement of the final saturator temperature:						
Standard deviation of measurand	0.000071	K	1	0.000071	0.000071	K fp
Calibration of SPRT	0.0020	K	2	0.0010	0.0010	K fp
Drift of SPRT	0.0030	K	1.73	0.0017	0.0017	K fp
Uncertainty due to self-heating	0.0005	K	1.73	0.0003	0.0003	K fp
Resistance bridge non-linearity	0.000072	K	1	0.00007	0.00007	K fp
Resistance bridge resolution	0.000001	K	1.73	0.0000006	0.0000006	K fp
Std. Resistor calibration	0.00013	K	1	0.00013	0.00013	K fp
Std. Resistor drift	0.00014	K	1.73	0.000081	0.000081	K fp
Std. resistor temp coefficient	0.0044	K	1.73	0.0025	0.0025	K fp
Final gradients in saturator	0.0047	K	1.73	0.0027	0.0027	K fp
Bath stability	0.00040	K	1	0.00040	0.00040	K fp
Uncertainty associated with the measurement of the final saturator pressure:						
Standard deviation of measurand	1.4	Pa	1	1.4	-0.00011	K fp
Manufacturer's stated tolerance	4	Pa	1.73	2	-0.00019	K fp
Drift of pressure transducer	4	Pa	1.73	2	-0.00019	K fp
Hydrostatic head correction	2.4	Pa	1.73	1.4	-0.00011	K fp
Resolution	1	Pa	1.73	0.6	-0.00005	K fp
Repeatability/hysteresis	2	Pa	1.73	1	-0.00009	K fp
Stability	20	Pa	1.73	12	-0.00093	K fp
Uncertainty associated with the measurement of the pressure in the measuring head of the UUT:						
Standard deviation of measurand	2.1	Pa	1	2.1	0.00017	K fp
Tolerance associated with correction	4	Pa	1.73	2	0.00019	K fp
Drift associated with correction	4	Pa	1.73	2	0.00019	K fp
Temperature coefficient of integrated	11	Pa	1.73	6.4	0.00051	K fp
Drift of integrated transducer	50	Pa	1.73	29	0.00233	K fp
Hydrostatic head (of correction)	3	Pa	1.73	2	0.00014	K fp
Resolution (of correction)	1	Pa	1.73	0.6	0.00005	K fp
Resolution	1	Pa	1.73	0.6	0.00005	K fp
Repeatability/hysteresis	9	Pa	1.73	5.2	0.00042	K fp
Linearity	20	Pa	1.73	12	0.00093	K fp
Stability	31	Pa	1.73	18	0.00145	K fp
Uncertainty associated with formulations:						
Vapour pressure formulation	0.019	K fp	1	0.019	0.019	K fp
Enhancement factor	-0.000026	K fp	1	-0.000026	-0.000026	K fp
Dew point calculated from vapour pressure	0.019	K fp	1	0.019	0.019	K fp
Iterative solution resolution	6.E-09	K fp	1	6.E-09	6.E-09	K fp
Uncertainty associated with the UUT:						
Variance	0.0060	K dp	1	0.0060	0.0060	K dp
Resolution	0.0001	K dp	1.73	0.00006	0.00006	K dp
Repeatability due to mirror check	0.0080	K dp	1.73	0.0046	0.0046	K dp
Repeatability due to mirror cleaning	0.0068	K dp	1.73	0.0039	0.0039	K dp
Flow rate dependency	0.0023	K dp	1.73	0.0013	0.0013	K dp
Head temperature dependency	0.0007	K dp	1.73	0.0004	0.0004	K dp
Combined standard error					0.030	K fp
Expanded uncertainty (k=2, 95% coverage interval)					0.060	K fp

9. Calibration of a chilled mirror hygrometer

A chilled mirror hygrometer was calibrated using the newly developed system and the hygrometer was then sent to an external laboratory to be calibrated against a primary humidity generator in order to compare the newly developed system to one already in operation and internationally validated. The results from the external calibration are still pending and will be compared to the results obtained at NML when received. Figure 9.1 shows the results obtained by NML and the results obtained one year previously by the same external calibration laboratory.

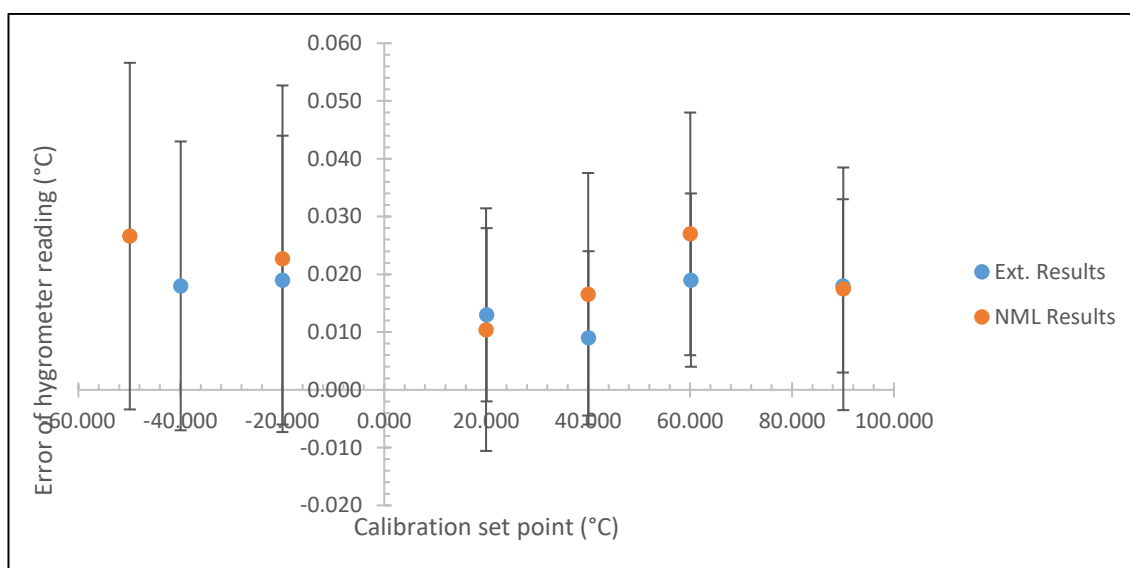


Figure 9.1: NML primary calibration results compared to that obtained by an external laboratory one year previously with error bars representing the combined uncertainty of the primary standard with 68% confidence interval.

Figure 9.1 shows agreement between the calibration results of NML and the external laboratory within the calibration uncertainties of both laboratories. The error bars represent the combined standard uncertainty of the primary standard used to calibrate the hygrometer and does not include uncertainties relating to the UUT, such as drift and linearity, that do not affect the calibration result. The maximum difference between any two results is 9 mK at -50 °C frost point which is well within the uncertainties of both systems. The yearly drift is not accounted for and a better comparison will be obtained when the pending calibration in the external laboratory is completed. The calibration point at -50 °C fp was taken instead of -40 °C fp in order to extend the calibrated range of the instrument to its lowest operating limit. Since the external calibration result only varies by 1 mK fp between -20 °C fp and -40 °C fp it is expected not to vary significantly at -50 °C fp. This will be verified when the ongoing calibration is completed. For the purpose of the comparison it is assumed that the

uncertainty determined at $-40\text{ }^{\circ}\text{C}$ fp is equal to the uncertainty at $-50\text{ }^{\circ}\text{C}$ fp which is yet to be determined. The uncertainty calculated at $-40\text{ }^{\circ}\text{C}$ fp is used for all frost points and the uncertainty calculated at $90\text{ }^{\circ}\text{C}$ dp is used for all dew points. This is assumed to give a conservative estimate and the uncertainty analysis will be conducted at intermediate set points in the future.

10. Conclusion and further work

The fundamentals of humidity metrology and primary humidity generation were discussed. The designs of a number of primary dew point generators used in different laboratories were given. Several designs for saturators to be used with a new dew point generator were proposed and compared on the basis of computational fluid dynamics. A final design of the full system for a new primary dew point generator was completed. The components of the design were fabricated by a number of specialist engineering workshops. The new generator was completed and tested. A number of modifications were made on the basis of the initial testing. A preliminary characterization and evaluation of the uncertainty associated with the system as a primary humidity standard was conducted at $-40\text{ }^{\circ}\text{C}$ fp and $90\text{ }^{\circ}\text{C}$ dp, the extremes of the calibrated range of the chilled mirror hygrometers in use at NML. The system was found to perform well and it is intended that measurements to characterize the uncertainty will continue. A calibration of a chilled mirror hygrometer was performed and the results will be compared to the calibration results obtained in an external laboratory.

A number of further modifications could be made to the system. It was observed that at low frost points occasionally peaks are visible that could be caused by tiny frost crystals formed by condensation breaking away and becoming suspended in the airstream. This could be prevented by bypassing the pre-saturator at low frost points in order to prevent condensation occurring in the final saturator.

It was observed that the input air supply is at approximately $-55\text{ }^{\circ}\text{C}$ fp. This makes it very difficult to bring the system to $-55\text{ }^{\circ}\text{C}$ fp or below as the outlet tube needs to be back purged with gas drier than the target set point while the system is decreasing in temperature in order to prevent condensation forming in the outlet tube. Dry air is also necessary to speed up the drying time of the chilled mirror hygrometer and the tubing. A heat exchanger made from $\frac{1}{4}$ inch diameter tubing could be inserted into the bath and used to dry the air used for back purging so that the purge gas is never at a frost point higher than the temperature of the outlet tube. Alternatively, dry nitrogen gas could be used for back purging.

As discussed, the bath had to be refilled frequently while operating at $90\text{ }^{\circ}\text{C}$. This disturbs the temperature and limits the amount of time that the generator can be operated continuously at $90\text{ }^{\circ}\text{C}$ dp. It also results in a 12 mK uncertainty due to the variation of the bath water level causing reduced stability of the system. This uncertainty could be made negligible and the operation could be made more convenient by directing a constant flow of water into the bath. If the flow rate is just enough so that the bath is overflowing to a minimum amount, the temperature of the fill water is controlled to be very near $90\text{ }^{\circ}\text{C}$ and the flow is directed to the

area of the bath where the water passes heat exchangers before being redirected to the upwelling working volume of the bath then the disturbance to the bath temperature should be small to negligible.

The only parts of the system that are not controlled by a computer and cannot be automated and operated remotely are the heated input and output tubes and the valves. The valves and the voltage control for the heated tubes could be controlled using stepping motors to allow full remote operation and automation of the system.

Fill and drain tubes could be added to the pre-saturator and final saturator to allow the units to be filled and flushed with water without being removed from the bath. This could be accomplished by using one of the free connections to the units and using blank stainless steel gaskets to feed narrow tubing to the bottom of the saturator without compromising leak tightness or alternatively, a length of tubing could be welded to one of the VCR connections on the underside of the lid. The connections contain sockets where 6 mm diameter tubing can fit. The unit can then be emptied by increasing the pressure in the system with the fill/drain tube open. It is important that the system can be flushed in order to reduce the build-up of impurities in the water.

The use of synthetic liquids could be investigated in order to achieve a wide temperature range with just one thermostatic bath liquid. Some liquids exist that could cover the range from $-40\text{ }^{\circ}\text{C}$ to $130\text{ }^{\circ}\text{C}$, the current calibrated range of the chilled mirror hygrometers in use in NML. The ability of the liquid to be used above $100\text{ }^{\circ}\text{C}$ would reduce evaporation and increase stability at $90\text{ }^{\circ}\text{C}$ dp. The viscosity of the fluid at $-40\text{ }^{\circ}\text{C}$ and its effect on the stability should be investigated.

The system could be leak tested at elevated pressures to determine an appropriate operating pressure range. An expansion valve could then be used to operate the system as a two-pressure generator for faster change in set points and extended low frost point range. The system already calculates the dew point based on the measured pressure drop automatically and the calculations are only limited by the range over which the empirical reference functions are valid.

The effect of back diffusion of water vapour through leaks at low frost points could be further characterized. Modifications could be made in an attempt to extend the range of the instrument to lower frost points. Helium leak testing could also be performed in order to give a more conservative estimate of the uncertainty due to leaks in the high range.

Further experiments could be conducted to evaluate the saturation efficiency. The temperature gradient along the saturation path could be mapped and the effect of shortening

the saturation path could be tested. The effect of purging the pressure measurement tube could be studied in more detail and improved operation at low frost points could be determined. A low range chilled mirror hygrometer could be purchased in order to extend the working range of the system and to improve the capabilities and validation at frost points.

Computational fluid dynamics proved to be a very useful tool in the design of the generator and in understating its operation and setting limits on its mass flow rate range. The use of a multiphase CHT model could be investigated to simulate the evaporation in the saturator and compare the humidity output to what would be expected based on normal measurements. The results of these simulations could be compared to measurements made with the generator.

When the performance of the system becomes well known it will take part in an inter-comparison among other national metrology institutes with primary humidity capabilities. This involves a number of laboratories calibrating a reference hygrometer whose calibration is unknown and comparing the results from the different institutes. If a full inter-comparison cannot be organised then a reference hygrometer that was previously used in an inter-comparison can be sought and calibrated to give a comparison of the dew point generator at NML to the other participants. This may be enough to establish traceability to international standards and the SI until the next time an official inter-comparison is held. A bilateral comparison between NML and an NMI with a validated primary humidity generator may also be performed to obtain traceability and validate the uncertainty claims of the new system.

11. References

- [1] D. Batchelor, "Humidification in pharmaceutical manufacturing | Knowledge Hub." [Online]. Available: <https://www.condair.ie/knowledge-hub/humidification-in-pharmaceutical-manufacturing>. [Accessed: 06-Jun-2017].
- [2] R. P. Donovan, "Why control humidity in a cleanroom? | Solid State Technology." [Online]. Available: <http://electroiq.com/blog/2003/10/why-control-humidity-in-a-cleanroom/>. [Accessed: 06-Jun-2017].
- [3] C. D. Ahrens, *Meteorology Today, AN INTRODUCTION TO WEATHER, CLIMATE, AND THE ENVIRONMENT*, vol. 53, no. 9. 2013.
- [4] M. Scott *et al.*, "A Guide to the Measurement of Humidity." 1996.
- [5] G. N. Lewis and M. Randall, *Thermodynamics*, Second Edi. McGraw-Hill Book Company, 1961.
- [6] L. Wexler, A; Greenspan, "Vapor pressure equation for water in the range 0 to 100 C," *J. Res. Natl. Bur. Stand. Sect. A Phys. Chem.*, vol. 75A, no. 3, pp. 213–245, 1971.
- [7] D. SONNTAG, "Important new values of the physical constants of 1986, vapour pressure formulations based on the ITS-90, and psychrometer formulae.," *Z Meteorol*, vol. 40, no. 5, pp. 340–344, 1990.
- [8] J. Lovell-Smith, "The propagation of uncertainty for humidity calculations," *Metrologia*, vol. 46, no. 6, pp. 607–615, 2009.
- [9] S. Boyes and S. A. Bell, "Assessment of fundamental data used in humidity metrology," *NPL Publ.*, 1999.
- [10] J. Nielsen, J. Lovell-smith, M. De Groot, and S. Bell, "Uncertainty in the generation of humidity .," *Measurement*, pp. 1–33.
- [11] M. Heinonen, "Uncertainty in humidity measurements," 2006.
- [12] "MSL Technical Guide 24 Dew-Frost Error and the Chilled-Mirror Hygrometer," vol. 64, no. 0, pp. 2–5.
- [13] B. Schirmer *et al.*, "High precision trace humidity measurements with a fibre-coupled diode laser absorption spectrometer at atmospheric pressure," *Meas. Sci. Technol.*, vol. 11, no. 4, p. 382, 2000.
- [14] an number of Rotronic Instrument Corp staff, "The Rotronic Humidity Handbook,"

Rotronic Humidity Handb., 2005.

- [15] R. Kaarls and T. J. Quinn, "The Comite Consultatif pour la Quantite de Matiere: A brief review of its origin and present activities," *Metrologia*, vol. 34, no. 1, pp. 1–5, 1997.
- [16] P. De Bièvre, "The 2012 International Vocabulary of Metrology: 'VIM,'" *Accredit. Qual. Assur.*, vol. 17, no. 2, pp. 231–232, 2012.
- [17] D. Hudoklin, J. Bojkovski, J. Nielsen, and J. Drnovšek, "Design and validation of a new primary standard for calibration of the top-end humidity sensors," *Meas. J. Int. Meas. Confed.*, vol. 41, no. 9, pp. 950–959, 2008.
- [18] D. Hudoklin and J. Drnovšek, "The new lmk primary standard for dew-point sensor calibration: Evaluation of the high-range saturator efficiency," *Int. J. Thermophys.*, vol. 29, no. 5, pp. 1652–1659, 2008.
- [19] J. Nielsen and M. J. De Groot, "Revision and uncertainty evaluation of a primary dewpoint generator," *Metrologia*, vol. 41, no. 3, pp. 167–172, 2004.
- [20] B. Hardy, "Trust But Verify---Practical Approaches to Humidity Generation and Measurement," *RH Syst. White Pap.*, no. 1, p. 10, 2004.
- [21] C. W. Meyer *et al.*, "Calibration of Hygrometers with the Hybrid Humidity Generator," no. December, 2008.
- [22] M. Stevens and S. A. Bell, "The NPL standard humidity generator: an analysis of uncertainty by validation of individual component performance," *Meas. Sci. Technol.*, vol. 3, no. 10, p. 943, 1992.
- [23] M. Heinonen, "The CMA humidity standard," *Meas. J. Int. Meas. Confed.*, vol. 17, no. 3, pp. 183–188, 1996.
- [24] R. Bosma and J. N. A. Peruzzi, "Development of the High-Temperature Dew-Point Generator Over the Past 15 Years," *Int. J. Thermophys.*, vol. 38, no. 10, pp. 1–14, 2017.
- [25] C. Paper, H. Mitter, and H. Mitter, "THE BEV / E + E ELEKTRONIK STANDARD," no. May 2006, 2015.
- [26] D. Zvizdic, M. Heinonen, and D. Sestan, "New Primary Dew-Point Generators at HMI / FSB-LPM in the Range from -70°C to $+60^{\circ}\text{C}$," vol. 33, pp. 1536–1549, 2012.
- [27] "Reynolds Number." [Online]. Available: http://www.engineeringtoolbox.com/reynolds-number-d_237.html. [Accessed: 02-Aug-2017].

- [28] "Dry Air Properties." [Online]. Available: https://www.engineeringtoolbox.com/dry-air-properties-d_973.html. [Accessed: 08-Nov-2017].
- [29] "Determination of the critical Rayleigh number." [Online]. Available: <http://hmf.enseeiht.fr/travaux/CD9900/travaux/optmfn/gpfmho/99-00/grp13/chap2.htm>. [Accessed: 08-Nov-2017].
- [30] J. F. Wendt, *Computational Fluid Dynamics: An Introduction*, vol. 7. 1992.
- [31] Nicolas Huc, "Conjugate Heat Transfer | COMSOL Blog," 2014. [Online]. Available: <https://www.comsol.com/blogs/conjugate-heat-transfer/>. [Accessed: 15-Jun-2018].
- [32] George Sidebotham, "Heat Transfer Modeling," *Article*, p. 37, 2006.
- [33] "Overall Heat Transfer Coefficients for Fluids - Heat Exchanger Surface Combinations." [Online]. Available: https://www.engineeringtoolbox.com/overall-heat-transfer-coefficients-d_284.html. [Accessed: 19-Apr-2018].
- [34] "Thermal Conductivities of Heat Exchanger Materials." [Online]. Available: https://www.engineeringtoolbox.com/heat-exchanger-material-thermal-conductivities-d_1488.html. [Accessed: 19-Apr-2018].
- [35] "Electroless Nickel Data for Corrosion Resistance | Electro Coatings." [Online]. Available: <http://www.electro-coatings.com/electroless-nickel-data.php>. [Accessed: 20-Apr-2018].
- [36] "CORROSION RESISTANCE OF ELECTROLESS NICKEL COATINGS."
- [37] R. Taheri, "Evaluation of Electroless Nickel-Phosphorus (EN) Coatings," 2003.
- [38] D. C. Giancoli, *Physics: Principles with Applications*, vol. 1. 2004.
- [39] J. C. F. G. I. M. Jcgm, "Evaluation of measurement data — Guide to the expression of uncertainty in measurement," *Int. Organ. Stand. Geneva ISBN*, 2008.
- [40] M. Heinonen and M. Vilbaste, "Frost-point measurement error due to a leak in a sampling line," *Int. J. Thermophys.*, vol. 29, no. 5, pp. 1589–1597, 2008.
- [41] M. Vilbaste, M. Heinonen, O. Saks, and I. Leito, "The effect of water contamination on the dew-point temperature scale realization with humidity generators," *Metrologia*, vol. 50, no. 4, pp. 329–336, 2013.
- [42] P. R. Thermometry, "Guide to the Realization of the ITS-90."